Periventricular white matter damage in the postnatal brain in hypoxic conditions

DENG YIYU, MD

A THESIS SUBMITTED FOR THE DEGREE OF

DOCTOR OF PHILOSOPHY

DEPARTMENT OF ANATOMY

YONG LOO LIN SCHOOL OF MEDICINE

NATIONAL UNIVERSITY OF SINGAPORE

2010

ACKNOWLEDGMENTS

I am deeply indebted to my supervisors, **Dr Charanjit Kaur**, Associate Professor, Department of Anatomy, National University of Singapore, and **Dr Lu Jia**, Associate Professor, Defence Medical and Environmental Research Institute, DSO National Laboratories, Singapore, for their constant encouragement, invaluable guidance and infinite patience throughout this study.

I am very grateful to **Professor Ling Eng Ang**, former Head of Anatomy Department, National University of Singapore, and **Professor Bay Boon Huat**, Head of Anatomy Department, National University of Singapore for their constant support and encouragement to me as well as their valuable suggestions to my project, and also for their full support in using the excellent working facilities.

I would like to acknowledge my gratitude to **Dr Viswanathan Sivakumar**, **Mrs. Ng Geok Lan** and **Mrs Yong Eng Siang** for their excellent technical assistance; **Mr. Yick Tuck Yong** for his constant assistance in computer work and **Mrs. Carolyne Wong, Ms Violet Teo** and **Mdm. Diljit Kour** for their secretarial assistance.

I also wish to thank all staff members and my fellow postgraduate students at Department of Anatomy, National University of Singapore for their assistane one way or another.

Certainly, without the financial support from the National University of Singapore, in terms of Research Scholarship and National Medical Research Council in terms of a research grant (181-000-65-112 and 181-000-98-112 from NUS) to A/P

Charanjit Kaur, this work would not have been brought to a reality.

Finally, I am greatly indebted to my wife, **Mrs Zhou Yan** for her constant encouragement, patience and help during my study.

This thesis is dedicated to

my beloved family

PUBLICATIONS

Various portions of the present study have been published or submitted for publication.

International Journals:

1. **Deng Y**, Lu J, Sivakumar V, Ling EA, Kaur C. Amoeboid microglia in the periventricular white matter induce oligodendrocyte damage through expression of proinflammatory cytokines via MAP kinase signaling pathway in hypoxic neonatal rats. **Brain Pathol**. 2008 Jul;18(3):387-400.

2. **Deng Y**, Lu J, Ling EA, Kaur C. Monocyte chemoattractant protein-1 (MCP-1) produced via NF-kappaB signaling pathway mediates of amoeboid microglia in the periventricular white matter in hypoxic neonatal rats. **Glia.** 2009 Apr 15; 57(6):604-21.

3. Lu J, Goh SJ, Tng PY, **Deng YY**, Ling EA, Moochhala S. Systemic inflammatory response following acute traumatic brain injury. **Front Biosci.** 2009 Jan 1; 14: 3795-813

4. **Deng Y**, Lu J, Ling EA, Kaur C. Microglia-derived macrophage colony stimulating factor promotes generation of proinflammatory cytokines by astrocytes in the periventricular white matter in the hypoxic neonatal brain. **Brain Pathol.** 2010 Mar 9.

5. **Deng Y**, Lu J, Ling EA, Kaur C. Microglia and inflammation in the hypoxic developing brain. Revised paper submited to **Front Biosci.**

Conference Abstracts:

1. 38th Annual Meeting of the Society for Neuroscience**,** held on Nov. 15 to 19, 2008 in Washington**,** DC**.**

Deng Y, Lu J, Ling EA, Kaur C. Monocyte chemoattractant protein-1 (MCP-1) produced via NF-kappa B signaling pathway mediates of amoeboid microglia in the periventricular white matter in hypoxic neonatal rats.

2. International Anatomical Sciences and Cell Biology Conference, held on May 26-29, 2010 in Singapore.

Deng Y, Lu J, Ling EA, Kaur C. Microglia-derived macrophage colony stimulating factor promotes generation of proinflammatory cytokines by astrocytes in the periventricular white matter in the hypoxic neonatal brain.

TABLE OF CONTENTS

ABBREVIATIONS

AD, Alzheimer’s disease

AMC, amoeboid microglial cells

AP-1, activating protein-1

APC, antigen-presentation cell

BBB, blood-brain barrier

BrdU, Bromodeoxyuridine

BSA, bovine serum albumin

CCR2, chemokine (C-C motif) receptor 2

CNS, central nervous system

CuZn, CopperZinc

CSF-1R, colony stimulating factor-1 receptor

DAPI, 4’, 6- diamidino-2-phenylindole dihydrochloride

dNTP, Deoxyribonucleotide triphosphate

DMEM, Dulbecco's Modified Eagle Medium

EAE, experimental autoimmune encephalomyelitis

EDTA, ethylenediaminetetraacetic acid

ERK1/2, extracellular-signal-regulated kinases

eNOS, endothelial nitric oxide synthase

FADD, Fas-associated death domain

FBS, Fetal bovine serum

GFAP, glial fibrillary acidic protein

GW, gestational weeks

GM-CSF, Grannulocyte-Macrophage colony stimulating factor

IL-1β, interleukin-1β

IL-1R_1, IL-1 receptor 1

IL-6, interleukin-6

IL-2, interleukin-2

IL-3, interleukin-3

IHC, Immunohistochemistry

iNOS, inducible nitric oxide synthase

IFN- ɣ , interferon-gamma

ICAM-1, intercellular adhesion molecule-1

JNKs, c-jun N-terminal kinases/stress-activated protein kinases

LPS, lipopolysaccharide

Mn, manganese

MAP kinase signaling pathway, mitogen-activated protein kinase signaling pathway

MBP, myelin basic protein

MCP-1, monocyte chemoattractant protein-1

M-CSF, macrophage-colony stimulating factor

MHC, major histocompatibility complex

MS, multiple sclerosis

NADPH , nicotinamide adenine dinucleotide phosphate

NF-κB, nuclear factor-κB

NMDA, N-methyl-D-aspartic acid

nNOS, neuronal nitric oxide synthase

NO, nitric oxide

NUS, National University of Singapore

OLs, oligodendrocytes

O2A, oligodendrocyte-type 2 astrocyte

PI3k, phosphatidylinositol-3 kinase

PLP, proteolipid protein

Pre-OL, late OL progenitors

PWM, periventricular white matter

PWMD, periventricular white matter damage

RIP-1, receptor interacting protein-1

ROS, reactive oxygen species

RT-PCR, reverse transcription-polymerase chain reaction

SVZ, subventricular zone

SODD, silencer of death domain

SMase, sphingomyelinase

TNF-α, tumor necrosis factor-α

TNF-R_1, TNF receptor 1

TRADD, TNF-R-associated death domain

TRAF-2, TNF-R-associated factor-2

TGF-β, transforming growth factor-beta

VCAM-1, vascular cell adhesion molecule-1

VEGF, vascular endothelial growth factor

VLBW, very low birth weight

Hypoxia-ischemia in the perinatal period is an important factor affecting the proper development of the brain. Although different regions of the developing brain are affected by hypoxia, the periventricular white matter (PWM) is highly vulnerable to damage. The pathogenesis of PWM damage (PWMD) has been reported to be multifactorial, inflammation being recognized as a major factor. Amoeboid microglial cells (AMC), the nascent form of microglia, are active macrophages and are present in large numbers in the developing PWM. It is well documented that microglial cells play a crucial role in the modulation of inflammatory response in the central nervous system (CNS). Astrocytes are also implicated in inflammatory response in the CNS under pathological conditions. However, the role of AMC and astrocytes in PWMD in neonatal brain under hypoxic conditions has not been fully elucidated. The present study was undertaken to investigate their role in PWMD in hypoxic conditions. The potential mechanisms and signaling pathways by which AMC and astrocytes induce oligodendrocytes and axon damage in hypoxic conditions were also examined. To address these, both *in vivo* & *in vitro* studies were carried out.

For the *in vivo* experiments, Wistar rats (1-day old) were subjected to hypoxia (5% oxygen and 95% nitrogen), following which upregulated mRNA and protein expression of tumor necrosis factor-α (TNF-α), interleukin-1β (IL-1β), TNF receptor 1 ($TNF\text{-}R_1$) and IL-1 receptor 1 ($IL\text{-}1R_1$), monocyte chemoattractant protein-1 (MCP-1) and its receptor (CCR_2), macrophage-colony stimulating factor (M-CSF) and CSF-1 receptor (CSF-1R) in the PWM was observed. Immunofluorescence labeling of TNF-α, IL-1β, MCP-1, CCR_2, and M-CSF expression was specifically

colocalized in AMC from 24h-7d after hypoxic exposure. However, at a late stage of injury i.e 7 and 14d following hypoxic exposure, CSF-1R, TNF-α and IL-1β immunoexpression was detected in the astrocytes in the same area. TNF-R_1 and IL-$1R_1$ immunoexpression was localized in the oligodendrocytes and axons of the PWM. This was coupled with apoptosis and reduction in the number of oligodendrocytes and swelling and disruption of axons. Another striking feature in hypoxic rats was a marked increase in cell numbers of AMC in the PWM. BrdU immunostaining showed that there was no significant change in the proliferation rate of AMC after hypoxic exposure suggesting that the increase in numbers may be due to migration of AMC from the nearby regions such as the cerebral cortex. When MCP-1 (100ug/mL) was injected intracerebrally into the PWM of 7-day old postnatal rats, it induced the chemotactic migration of AMC to the injection site.

For the *in vitro* studies, primary cultured microglial cells were subjected to hypoxia (3% oxygen, 5% CO_2 and 92% nitrogen). They showed enhanced expression of TNF-α, IL-1β, MCP-1 and M-CSF. MAP kinase signaling pathway was implicated in the expression of TNF-α and IL-1β in microglia subjected to hypoxia. Furthermore, NF-kappaB signaling pathway was involved in release of MCP-1 from microglia subjected to hypoxia. Primary cultured astrocytes treated with M-CSF exhibited increased expression of CSF-1R, TNF-α and IL-1β. In addition, it was also shown that MAP kinase signaling pathway was involved in TNF-α and IL-1 β expression in astrocytes which were subjected to M-CSF treatment. In the *in vitro* chemotaxis assay, the medium derived from hypoxia-treated microglial cultures attracted more

migratory microglial cells than that from the control microglial culture.

This study has revealed that in the early phase of injury following hypoxic exposure, microglial cells in the PWM in the neonatal brain produce inflammatory cytokines such as TNF-α and IL-1β *via* MAP kinase signaling pathway. An increase in MCP-1 production via NF-kappaB signaling pathway in AMC following hypoxic exposure induces the migration of AMC from the neighboring areas to the PWM. Undoubtedly, this would augment the inflammatory response in the PWM of the hypoxic neonatal rats and aggravate PWMD. M-CSF produced by AMC in the early phase of injury interacts with its receptor, CSF-1R, which was located on the astrocytes. The possible interaction between AMC and astrocytes via M-CSF and its receptor would lead to release of proinflammatory cytokines such as TNF-α and IL-1β from the latter cell type via the JNK kinase signaling pathway at the late phase of injury following hypoxic exposure. Therefore, in the course of the inflammatory response in the PWM of the neonatal rats following a hypoxic injury, AMC might contribute to inflammation at the early phase and astrocytes at the late phase. Concomitantly, TNF-α and IL-1β interact with their respective receptors expressed on the oligodendrocytes and axons. This would lead to apoptosis and reduction in the number of oligodendrocytes, degeneration of the axons as well as delay in their myelination. Therefore, these inflammatory cytokines and chemokines are detrimental to oligodendrocytes and axons resulting in PWM lesion in hypoxic injury.

Chapter 1

Introduction

Cerebral white matter is located in the deep parts of the brain and occupies nearly one half of the brain volume (Zhang and Sejnowski 2000; Filley 2005). It is made up of axons and glial cells, including oligodendrocytes, astrocytes and microglia (Filley 2005). The axons are arranged regularly and form neural fiber tracts, which play a crucial role in neural information transmission (Dougherty *et al.* 2005). Oligodendrocyte processes contact and repeatedly envelope a stretch of axon to form multispiral myelin sheath. Axons in the neonatal brain are not myelinated. Myelination of axons in the periventricular white matter (PWM) of developing rat brain was first observed at the end of the first postnatal week and progresses rapidly over the next 2-3 weeks (Sturrock 1980). In the course of rat brain development the process of axonal myelination is divided into three phases: (i) premyelinating before postnatal 7 day (P1-7), (ii) early myelinating which is present around 10 days (P10), and (iii) late myelinating which appears around postnatal 21 day (P21) (McCarran and Goldberg 2007). The disruption of these axons and myelin sheath cause disorders of neural networks function resulting in some neurobehavioural abnormalities (Mulhern *et al.* 2001; Filley 2005).

Hypoxia-ischemia and inflammation occurring in the perinatal period result in the white matter injury which is one of the major causes of neonatal mortality and neurological defects such as cerebral palsy, impaired vision, hearing impairments and mental retardation in premature newborns (Volpe 2003; Vannucci 2005). The PWM, peripheral to the lateral ventricles (**Fig.1**), is vulnerable to damage in the perinatal period (Folkerth 2006). The vulnerability may be attributable to the existence of

widespread oligodendrocyte progenitors and lack of anastomoses of blood vessels in this area (Folkerth 2006).

The pathogenesis of PWM damage (PWMD) is complex and is not fully elucidated. Studies have shown that a common feature of PWMD is injury to the axons and developing oligodendrocytes before myelination occurs (Dammann *et al.* 2001). Activated immune cells are believed to play a crucial role in damaging axons and oligodendrocytes through producing inflammatory mediators (Yamasaki *et al.* 1996). It has also been found that excess extracellular glutamate causes death of oligodendrocyte progenitors through glutamate receptor-regulated excitotoxicity leading to PWMD (Volpe 2001; Folkerth *et al.* 2004).

1.1 Etiology and risk factors associated with PWMD

There are several possible perinatal risk factors that have been reported to be associated with PWMD.

1.1.1 Immaturity

The immaturity of the fetus is the most common risk factor related to PWMD (De Vries *et al.* 1988). When the subjects are born prematurely before 34 gestational weeks, they are vulnerable to PWM lesions (Jacobson *et al.* 2006). White matter damage of immaturity may affect visual, motor and cognitive functions (Jacobson *et al.* 2006). Neuroimaging studies of very low birth weight (VLBW) survivors suggest that the cerebral palsy, cognitive/behavioral deficits correlate with the focal or diffuse cerebral white matter injury (Perlman *et al.* 1997).

1.1.2 Hypoxia/ischemia

Hypoxia/ischemia is another important factor affecting the normal development and maturation of the CNS. Many maternal causes such as diabetes, asthma, anemia and smoking and intrapartum events such as prolonged labor are associated with fetal hypoxia/ischemia (Sugai *et al.* 2006). In the neonates, pulmonary or cardiac dysfunction and neonatal stroke result in hypoxia/ischemia (Mu *et al.* 2003).

1.1.3 Infection

Apart from cerebral hypoxia-ischemia, another important prenatal risk factor is most likely to be intrauterine infection, which causes premature delivery and increases fetal morbidity in preterm infants (Vigneswaran 2000). Infections of the amniotic fluid, decidua or placenta and overproduction of inflammatory cytokines are believed to be important contributing factors which promote spontaneous rupture of the membranes and preterm labor prior to 30 gestational weeks (GW) (Baud *et al.* 1998). In particular, asymptomatic bacterial vaginosis in the mother is ranked No.1 among the pathogen-induced infections related to premature delivery (Baud *et al.* 1998). Several epidemiological studies have reported that chorioamnionitis is a primary causative factor for fetal neurological disturbance and cerebral palsy (Baud *et al.* 1998). Chorioamniotic infection leads to the fetal brain and lung tissue injuries through overproduction of pro-inflammatory cytokines as well as the activation of macrophages (Baud *et al.* 1998).

1.1.4 Inflammation

In the past decades, the fetal and neonatal inflammatory responses under various pathological conditions have been found to contribute to PWMD (Rezaie and Dean 2002). Overproduction of inflammatory mediators including TNF-α, IL-1β and interleukin-2 (IL-2), interleukin-6 (IL-6) as well as adhesion molecules such as vascular cell adhesion molecule-1 (VCAM-1), intercellular adhesion molecule-1 (ICAM-1) has been involved in the pathogenesis of PWMD (Kadhim *et al.* 2001). Free radicals and excitotoxic-mediated damage associated with inflammatory response have also been considered to be implicated in PWMD (Rezaie and Dean 2002).

1.1.5 Vascular factors

It has been shown that due to the relatively low vascularity of white matter in comparison with the gray matter, hypoxia/ischemia is likely to facilitate the pathogenesis of PWMD (Ballabh *et al.* 2004). The astrocyte end-feet contacts play a pivotal role in the maintenance of the structural integrity of the cerebral blood vessels (El-Khoury *et al.* 2006). The blood vessels in the PWM of neonatal rats are thin walled and many of them are lack of the astrocyte end-feet contacts (El-Khoury *et al.* 2006). It has been reported that the permeability of the cerebral blood vessels is upregulated in hypoxic conditions (Kaur *et al.* 2010). This was coupled with increased expression of VEGF in astrocytes and endothelial nitric oxide synthase (eNOS) in the blood vessel endothelium (Kaur *et al.* 2006b). Moreover, clinical and experimental data demonstrated that cerebrovascular autoregulation disturbance in the premature

infants is associated with a high likelihood of occurrence of PWMD (Tsuji *et al.* 2000).

1.1.6 Other risk factors

Other proposed factors that are implicated in the PWMD in the neonate include genetic factors, multiple pregnancy, bradycardia, pre-eclampsia, bilirubin toxicity, intrauterine growth retardation, deficiencies in trophic factors as well as hyaline membrane disease (Resch *et al.* 2000; Saliba and Marret 2001).

1.2 Pathological changes in the PWMD

PWM lesions range from cystic necrosis of the PWM to myelination disorders (Skoff *et al.* 2001). Axonal swelling, microglial activation, astrocytosis and oligodendroglial injury have been reported in the PWMD (Skoff *et al.* 2001). Swollen and degenerating axons in the PWM in the neonatal rat brain after hypoxic exposure have been found (Kaur *et al.* 2006a). Along with the above, necrotic and apoptotic cells were observed at different time points in hypoxic neonatal rats (Kaur and You, 2000). Concomitantly, it has also been found that AMC phagocytosed the degenerating axons, necrotic and apoptotic cells (Kaur and You, 2000). The necrotic cystic cavities were formed in the PWM in later stages (Cai *et al.* 2001). This is also accompanied by impaired or delayed myelination (Cai *et al.* 2001). Reduced myelin basic protein (MBP) after hypoxic exposure suggested that myelination process was altered in the PWM (Biran *et al.* 2006; Kaur *et al.* 2006a). Several studies have shown edema in the PWM as a common histological feature (Sridhar *et al.* 2001).

1.3 Oligodendrocytes development, maturity, myelination and injury in the PWMD

Oligodendrocytes are the myelin-forming cells in the CNS which originate from neuroepithelial cells of the ventricular zones in the very early period of embryonic life (Thomas *et al.* 2000). The subventricular zone (SVZ), which appears in late gestational and early postnatal mammalian brain, is the main source of oligodendrocytes and astrocytes (Thomas *et al.* 2000). Oligodendrocyte progenitors migrate to developing white matter tracts and undergo substantial proliferation before their final differentiation into myelin-forming cells (Thomas *et al.* 2000). Different developmental stages of the oligodendrocyte lineage can be identified by a panel of cell specific antibodies, which are regarded as the sequential expression of oligodendrocyte developmental markers such as A2B5, O4, O1, MBP, and myelin proteolipid protein (PLP) (Back *et al.* 2001). Some researchers have defined four successive development stages of oligodendrocytes during gestation as follows: (i) early oligodendrocyte progenitors ($A2B5^+$); (ii) late oligodendrocyte progenitors (pre-OL), which are present from ~18 GW, specifically express platelet-derived growth factor-α (PDGF-α) receptor and are positive for the antibody O4 as well as the proteoglycan NG-2; (iii) immature oligodendrocytes (adenomatus polyposis coli (CC_1^+), $O1^+$) appear between 18 and 27 weeks; and (iv) mature oligodendrocytes (MBP) which are present around 30 GW (Back *et al.* 2001).

Myelination is a complex physiological process which consists of the spiraling of the oligodendrocyte process around the axon. The mechanism of myelination or the

signals that modulate this complex process have not been elucidated. The steps involved in the process are as follows: 1) Oligodendrocytes migrate to the vicinity of the axons that are to be myelinated; 2) The oligodendrocyte process adheres to the axon; and 3) The process spirals around the axon with the formation of a large number of myelin sheaths and some unmyelinated space is recognized as the node of Ranvier (Baumann and Pham-Dinh 2001).

The hallmark of PWMD occurring primarily in preterm infants is oligodendrocyte progenitor injury. The period of the greatest risk for PWMD is approximately to 23-32 weeks postconception in humans (Pang *et al.* 2000). In this period, oligodendrocyte precursors dominate in the PWM and myelin sheaths are not synthesized (Pang *et al.* 2000). Some researchers have demonstrated that immature oligodendrocytes during the specific prenatal window were vulnerable because of lack of the antioxidant enzymes such as Manganese (Mn) and CopperZinc (CuZn) superoxide dismutases as compared to mature oligodendrocytes (Mitrovic *et al.* 1994; Ludwin 1997; Kinney and Back 1998; Folkerth *et al.* 2004). In addition, premyelinating oligodendrocytes express cytokine interferon- γ receptor and α-amino-3-hydroxy 5-methyl-4-isoxazolepropionic acid (AMPA) recptor (Folkerth and Haynes *et al.* 2004;Talos *et al.* 2006). Therefore, developing oligodendrocytes are susceptible to free radical injury, inflammatory mediators and excitotoxicity.

At present the specific mechanisms responsible for developing oligodendrocyte injury have not been fully elucidated. But, glutamate excitotoxicity, free radical and cytokine-induced injury under pathological conditions are believed to be the major

contributors.

Glutamate is the predominant excitatory neurotransmitter in the CNS. Actions of glutamate are modulated by activated metabotropic glutamate receptors (mGluRs) and ionotropic receptors such as [N-methyl-d-aspartate (NMDA), AMPA and kainite receptors (KA)]. It is well known that oligodendrocytes express both ionotropic and metabotropic glutamate receptors (Káradóttir *et al.* 2005; Deng W *et al.* 2004). Therefore, excessive glutamate released from disrupted axons in hypoxic-ischemic brain results in excitotoxicity towards oligodendrocytes (Oka *et al.* 1993). Activation of glutamate receptors mediates Ca^{2+} increase and initiates a cascade of biochemical effects in immature oligodendrocytes leading to PWMD (Cai *et al.* 1995; Micu *et al.* 2006).

Hypoxia/ischemia is well documented to induce free radical reactions, leading to overproduction of reactive oxygen species (ROS) (Sum *et al.* 1998). Excess production of ROS has been described to be harmful to immature oligodendrocytes (Haynes *et al.* 2005). ROS preferentially injure vulnerable premyelinating ($O4^+$ and $O1^+$) oligodendrocytes, resulting in their loss, subsequent decreased numbers of mature oligodendrocytes, and hypomyelination (Haynes *et al.* 2003). Activated microglia have been considered as the main source of ROS (Domercq *et al.* 2007). *In vitro* studies have reported that increased level of ROS was produced by microglia in hypoxic conditions (Kaur *et al.* 2009).

It has been reported that the activated cytokine receptors were involved in oligodendroglial necrosis or apoptosis not only in the pathogenesis of adult

demyelinating disorders but also during development (Casaccia-Bonnefil 2000). The activation of cytokine receptors on the surface of oligodendrocytes can cause the necrosis or apoptosis of these cells through cross-talk between ligand and receptors, which activates intracellular signaling pathways related to apoptosis and energy metabolism disruption (Casaccia-Bonnefil 2000). Some *in vitro* studies have demonstrated that the proinflammatory cytokines such as TNF-α and interferon-gamma (IFN-γ) induce apoptosis of cultured oligodendrocytes through the activation of 'death' receptors including Fas and TNF-R_1 expressed on their surface (Pouly *et al.* 2000; Torres *et al.* 1995).

While under physiological conditions, microglia and astrocytes have been proven to contribute to the survival, differentiation and maturity of oligodendrocyte progenitors, activated microglia and astrocytes under pathological conditions can lead to oligodendroglial damage through release of various proinflammatory cytokines (Ohno and Aotani 2000; Pang *et al.* 2000). *In vitro* studies have shown that bacterial lipopolysaccharide (LPS) alone has no direct toxic effect on oligodendrocyte progenitors (Pang *et al.* 2000). However, oligodendroglial apoptosis is induced by conditioned medium which originated from microglia or astrocyte cultures administered with LPS (Pang *et al.* 2000). So the toxic effects of LPS on oligodendrocyte progenitors are due to activation of microglia and astrocytes (Pang *et al.* 2000). The extent of oligodendrocyte precursor damage *in vivo* has been thought to depend on the property of the stimuli and the state of activation of microglia (Cai *et al.* 2001).

1.4 Axon injury in the PWMD

The axon is the elongated fiber that extends from the neuronal body to the terminal endings and transmits information. The larger the axon, the faster it transmits the neural signal (Baumann and Pham-Dinh 2001). Most axons are covered with a fatty substance called myelin that acts as an insulator (Baumann and Pham-Dinh 2001). These myelinated axons transmit the neural signal much faster than the non-myelinated ones. In normal myelinated axons, Na^+ channels are concentrated at nodes of Ranvier, which accelerate signal transduction through allowing the action potential to rapidly jump from node to node (Baumann and Pham-Dinh 2001). The axons are not myelinated in the neonatal animals. In hypoxic rats, the swollen and degenerating axons observed under the electron microscope were described as the most conspicuous feature between 3 h and 7 days after the hypoxic exposure (Kaur *et al.* 2006a). Quantification of the degenerating axons in the PWM showed a significantly higher number of degenerating axons in the hypoxic neonatal brain (Kaur *et al.* 2006a). Many of the degenerating axons in the hypoxic rats appeared to have lost the axoplasm and appeared to be empty (Kaur *et al.* 2006a). Very few axons were found to be myelinated in the hypoxic 7-day-old rats, and the myelin sheaths of these axons appeared completely distorted (Kaur *et al.* 2006a). Moreover, the degenerating axons were predominantly found in the vicinity of the cerebral blood vessels in the hypoxic rats (Kaur *et al.* 2006a).

Mechanisms of axon injury are complex and remain unclear. Some studies have demonstrated that premyelinated white matter axons in isolated rodent optic nerve

were highly resistant to hypoxic-ischemic injury, whereas early and late myelinating white matter axons were increasingly vulnerable (Fern *et al.* 1998). Several mechanisms of hypoxic-ischemic axonal injury have been proposed. Energy depletion during hypoxia-ischemia leads to failure of energy-dependent extracellular and intracellular ionic balance, resulting in axonal Ca^{2+} overload, conduction damage, and structural injury (Stys 2005). Excessive glutamate receptor activation, or excitotoxicity, results in ischemic white matter axon injury, as shown by intracerebral injection of AMPA (Cuthill *et al.* 2006). AMPA/kainite receptors participate in ischemic injury to myelinated white matter axons *in vivo*, but not to isolated axons. Studies have shown that ionotropic glutamate receptor agonists did not damage isolated axons, nor did glutamate receptors antagonists protected isolated axons from oxygen-glucose deprivation (McCarran and Goldberg 2007). Therefore, excess glutamate may induce white matter axon injury by causing damage to myelinating oligodendrocytes. It has been reported in some studies that axonal injury in myelinated white matter results from oligodendrocyte excitotoxicity and can be prevented by blockade of oligodendrocyte AMPA/kainate receptors (McCarran and Goldberg 2007). The mechanisms linking oligodendrocyte injury to axon damage might include release of toxic substances from injured oligodendrocytes, loss of trophic support to axons, or loss of glial homeostatic functions (Fowler *et al.* 2006). Attenuation of oligodendrocyte-myelin-axon interactions in myelinated white matter decreases axonal injury after AMPA injection (Fowler *et al.* 2006). However, interaction between axons and immature oligodendrocytes is weak in premyelinated

white matter. Some studies have reported that prevention of oligodendrocyte excitotoxicity does not decrease premyelinated axonal damage (Fowler *et al.* 2006). Therefore, oligodendrocyte excitotoxicity does not result in axonal damage in premyelinated white matter (McCarran and Goldberg 2007). Axons in premyelinated white matter suffer from hypoxic/ischemic injury through a non-excitotoxic way (McCarran and Goldberg 2007). The mechanism of axonal injury likely includes failure of ionic homeostasis and intra-axonal Ca^{2+} overload, as mentioned above (McCarran and Goldberg 2007). The downstream pathways of Ca^{2+}-induced axonal injury remain unclear.

In addition, activation of cytokine receptors has also been involved in axonal injury. The activation of cytokine receptors on the surface of axons can result in their damage by interaction between ligand and receptors, which triggers intracellular signaling pathways associated with apoptosis and energy metabolism depletion (Tezel, 2008).

1.5 Role of astrocytes in the PWMD

Astrocytes, the primary glial cell type in mammalian CNS, have been found to execute some critical functions including generation of nutrient and growth factors, scavenging free radicals, maintenance of blood brain barrier (BBB) integrity, ionic homeostasis and uptake of neurotransmitter (Panickar and Norenberg 2005; Nedergaard *et al.* 2003). Astrocytic end-feet form an envelope around the blood vessels and astrocytic processes extend to beneath the pial membrane and ependymal surface, thereby separating the CNS parenchyma from the external environment

(Panickar and Norenberg 2005). Astrocytes can uptake the excitatory amino acid glutamate from extracellular fluid surrounding the synaptic cleft, which is critical for optical glutamatergic neurotransmission and for preventing cellular excitotoxicity (Danbolt 1994). Furthermore, astrocytes also can take up and buffer excess extracellular K^+ released from neurons which prevents the accumulation of extracellular K^+ during neuronal depolarization (Panickar and Norenberg 2005). Another important physiological role of astrocytes is their ability to supply neurons with substrates of glycogen metabolism that might be pivotal in states of energy stress (Dringen *et al.* 1993). Thus it is clear that the physiological functions of astrocytes are multifaceted and complex.

Cerebral white matter astrocytosis is one of the characteristic pathological changes in the PWMD (Hirayama *et al.* 2001). It occurs in approximately 15-40% of neonates who had suffered from hypoxia-ischemia (Rezaie and Dean 2002). The main feature of astrogliosis is described as cellular hyperplasia, hypertrophy and upregulated expression of glial fibrillary acidic protein (GFAP) (Zhu *et al.* 2006). Astrocytic responses may be helpful to the repair of the PWMD. However, excessive astrogliosis may be harmful and contribute to axonal or oligodendroglial injury (Zawadzka and Kaminska 2003). Astrogliosis along with extracellular matrix results in scar-formation at the injury site (Di *et al.* 2005). The scar comprising reactive astrocytes can prevent axonal regeneration and reestablishment of synapse after injury in the CNS through forming a local biochemical and physiological barrier (Di *et al.* 2005). Furthermore, excessive astrogliosis may be another source of proinflammatory

cytokine production in the PWM besides microglia. Therefore, early inhibition of astrogliosis would help to alleviate the white matter injury (Di *et al.* 2005).

Vascular endothelial growth factor (VEGF) is not only an angiogenic growth factor whose expression induces vasculogenesis, but it is also described as a vascular permeability enhancing factor (Croll *et al.* 2004). Some studies have shown that up-regulated VEGF expression is located in astrocytes in the vicinity of the foci of necrosis in PWMD, and may participate in white matter lesion (Ment *et al.* 1997). The expression of VEGF is increased after hypoxic exposure, which plays a pivotal role in the pathogenesis of vascular leakage in the hypoxic brain leading to the formation of cerebral edema (Kaur *et al.* 2006). Many VEGF positive astrocytes were found to be present around the blood vessels in the PWM in hypoxic neonatal brains (Kaur *et al.* 2006). The precise mechanism by which VEGF results in vascular hyperpermeability is still not clear. It has been reported that VEGF-mediated zonula occludens-1 expression at the tight junctions of the endothelial cells were involved in hypoxia-induced hyperpermeability of the cerebral blood vessels (Dobrogowska *et al.* 1998). VEGF is also well-known to induce changes such as fragmentation of the endothelium, fenestration of the endothelial cells, appearance of interendothelial gaps and degenerative changes in endothelial basement membrane in microvascular segments which disrupt the structural integrity of the cerebral microvessels and causes extravasation of blood plasma proteins such as albumin (Dobrogowska *et al.* 1998). VEGF expression was located in both astrocytes and endothelial cells in vessels that comprised neovascularization in the vicinity of necrotic foci in brains with PWMD

(Arai *et al.* 1998). Besides modulating the vascular permeability, VEGF may also participate in inducing inflammatory responses in the PWM (Arai *et al.* 1998). Therefore, VEGF has been regarded as a proinflammatory mediator which exacerbates inflammatory responses observed in cerebral ischemia. VEGF regulates immune responses in the CNS by potentiating vascular permeability and inducing BBB breakdown. This leads to occurrence of cross-talks between normally sequestered CNS antigens and blood-borne immune mediators, and hence, the immune privileged status of the brain is altered (Proescholdt *et al.* 1999). Because of its proinflammatory functions, VEGF induces the adhesion of leukocytes to vascular walls and enhances ICAM-1 and VCAM-1 expression (Min *et al.* 2005). Overexposure of normal brain to VEGF has been observed to increase ICAM-1 and major histocompatibility complex (MHC) class Ⅰ and Ⅱ expression (Min *et al.* 2005). It is speculated that VEGF may induce inflammatory response in the hypoxic neonatal brain leading to PWMD (Min *et al.* 2005).

1.6 Role of microglia in the PWMD

AMC, present in large numbers in the developing PWM (Ling and Wong 1993), are resident immune cells in the CNS. Although microglial cells are necessary for normal functions, their overactivation can result in bystander damage to other CNS cells. Activated microglia have direct toxic effects on oligodendrocytes in culture through release of NO (Mitrovic *et al.* 1996). Some studies have found that TNF-α secreted by activate microglia was capable of killing oligodendrocytes (Zajicek *et al.* 1992). Based on these findings, it appears that NO and TNF-α produced by activated

microglia are involved in oligodendroglial death. Furthermore, activated microglia may induce oligodendrocyte injury through complement-induced phagocytosis and direct cell-cell contact (Rezaie and Dean 2002). There are ample evidences to suggest that microglia not only trigger PWMD, but also contribute to the development of lesions in the PWM (Rezaie and Dean 2002).

1.6.1 Origin and morphology of microglia

Microglia constitute 5-20% of all glial cells in the CNS. The developmental origin of microglia has been controversial for many years since Rio-Hortega described for the first time microglia as a cellular "third element" besides the neurons and neuroglia in the CNS (Kaur *et al.* 2001). At present, three main schools of thought are associated with the origin of microglia: (1) mesodermal, (2) neuroectodermal, and (3) monocytic (Ling, 1977; Kaur *et al.* 2001). Most researchers support the hypothesis that microglia are derived from blood monocytes and/or their hematopoietic precursors (Ling, 1977, 1980; Kaur *et al.* 2001). Immigration of microglial precursors into the developing CNS occurs during the late embryonic and early postnatal periods (Dalmau *et al.* 1998), and this influx of cells, which gradually increases in number and transform into mature ramified cells, is considered the basis for acquisition of the adult microglial cell population (Dalmau *et al.* 2003).

Two microglial phenotypes have been described: AMC and ramified microglial cells (Kaur et al., 2001). In the developing brain, the preponderant AMC exhibit a round cell body with some processes (Kaur et al., 2001). These cells transform into ramified microglial cells with the development and maturity of brain (Kaur et al.,

2001); the latter exist as the resting form under normal conditions. However, under pathological conditions such as trauma, infection and hypoxia/ischemia, ramified microglia retract their processes and assume an amoeboidic form (Ling et al., 2001; Dheen et al., 2007).

1.6.2 Properties of microglia

AMC, which are multifunctional immune cells in the developing brain, play a key role in the cerebral innate immunity. Previous studies have reported that AMC are active macrophages in the developing CNS, scavenging cellular debris in pathological conditions and during normal development (Kaur *et al.* 2007). On the other hand, AMC in the developing brain may also execute a cytotoxic effect by the release of some toxic factors, including inflammatory mediators and NO in pathological conditions (Kaur *et al.* 2007). In addition to their predominant role in phagocytosis, recent studies have reported additional properties of AMC in the developmental period.

1.6.2.1 Phagocytosis

The phagocytic property of microglial cells has been proven by a large number of observations under various experimental methods such as uptake of exogenous substances, activated surface receptors and antigens associated with phagocytosis as well as the localization of hydrolytic enzymes (Kaur *et al.* 2007). Ultrastructural studies have shown the phagocytic nature of AMC in the normal neonatal brains or following *Escheria coli (E coli)* injection or hypoxic injury (Kaur and You, 2000; Kaur *et al.* 2004). The AMC in the PWM of the hypoxic developing brain participated

in the phagocytosis of apoptotic cells and degenerating axons (Kaur *et al.* 1985; Kaur and You, 2000; Kaur *et al.* 2006). In the fetal or neonatal rat brains, AMC were observed to devour apoptotic and necrotic cells following transient maternal hypoxia (Li, 1997). Further direct evidence of the phagocytic nature of AMC comes from their engagement in the phagocytosis of *E coli* injected directly into the postnatal rat brains (Kaur *et al.* 2004). Many *E. coli* were ingested by AMC in less than 3 h (Kaur *et al.* 2004). Therefore, it appears from the above mentioned observations that a protective barrier formed by AMC is indispensable during the early development when the BBB is not fully functional.

1.6.2.2 Antigen presentation

Although the brain has been regarded as an 'immune privileged' organ for a long time, some studies showed that MHC I antigen expression was found on AMC (Ling *et al.* 1991). MHC antigens, which are cell surface molecules, are required for macrophages to activate T lymphocytes through presenting certain antigens to them. MHC I antigens serve as restriction elements for cytotoxic/suppressor lymphocytes. The expression of MHC I antigens on AMC also indicates that these cells are ready to interact with extravasating T lymphocytes when the BBB is deficient during the development (Kaur *et al.* 2007).

The expression of MHC II antigens, which is required for macrophages to interact with helper/inducer T lymphocytes, is not found on AMC under physiological conditions. However, it is induced under experimental and pathological conditions (Kaur *et al.* 2004). For instance, the expression of these antigens is upregulated when

AMC are administered with interferon-γ (IFN-γ) or with lipopolysaccharide (LPS) (Xu *et al.* 1994, 1994). The AMC in the vicinity of injected live *E coli* are found to express MHC II antigens (Kaur *et al.* 2004; Kaur *et al.* 2007). The MHC II expression on AMC under pathological conditions demonstrates that AMC are able to interact with helper/inducer T lymphocytes to initiate an immune reaction.

1.6.2.3 Proliferation

One of the common features of microglial cell population is their remarkable capacity to increase their numbers when CNS injury or neurological disease processes occur (Ladeby *et al.* 2005). This expansion has been attributed predominantly to proliferation of activated microglia and, to a lesser extent, believed to be due to migration of microglia from neighboring brain areas (Ladeby *et al.* 2005). Proliferating microglia have been reported to be involved in the onset and/or progression of various CNS pathologies such as trauma (Urrea *et al.* 2007), hypoxia/ischemia (Denes *et al.* 2007), degenerative CNS diseases such as Parkinson's disease (Henze *et al.* 2005) as well as Alzheimer's disease (AD) (Remington *et al.* 2007). Micoglial proliferation induced by injury may also contribute to brain repair and functional recovery through phagocytosing the debris. However, excessive proliferation may also result in glial scar formation and produce cytotoxic factors (Byrnes and Faden 2007)

Several molecules such as M-CSF, grannulocyte-macrophage colony stimulating factor (GM-CSF), interleukin-6 (IL-6) and, interleukin-3 (IL-3) have been demonstrated to be potent stimuli for microglia proliferation *in vitro* (Sawada *et al.*

1990). For all of these cytokines, microglia can express the corresponding receptors (Sawada *et al.* 1990). In addition, all of the cytokines mentioned above can be produced locally in the CNS (Schobitz *et al.* 1993). Therefore, under pathological conditions, microglia proliferation is induced by the cytokines mentioned above in an autocrine and/or paracrine fashion. Several *in vivo* studies using proliferating cell nuclear antigens such as Ki67, Bromodeoxyuridine (BrdU) and autoradiography have confirmed the hypothesis that microglia can proliferate in the developing brain (Schobitz *et al.* 1993).

1.6.2.4 Migration

It is well-known that microglia are capable of migrating toward damaged neural tissue to clear the debris at the injured site when necessary. Some researchers have reported that a rapid increase in number of microglial cells at injury sites is partly due to recruitment from blood monocytes or migration from other CNS regions (Brockhaus *et al.* 1996). The mechanism involving microglia migration to the injury sites is complex and poorly understood. The migration of microglia may be modulated by chemokines, which are released by microglia in an autocrine or paracrine manner during injury and infection (Zhou *et al.* 2007). Chemokine receptors may be redistributed to the cellular edge when microglia acquire a migratory phenotype (Zhou *et al.* 2007). The actin and tubulin, known as cytoskeleton proteins, are closely related with cellular morphology and migration. Under resting conditions *in vitro*, they are confined in the perinuclear region (Eugenin *et al.* 2005). However, when microglia are treated with a chemotactic stimulus, actin and tubulin are

rearranged to facilitate the process of attachment, protrusion and extension that contributes to migration of microglia (Eugenin *et al.* 2005). Chemokine orchestrated chemotaxis is regarded as a protective response to injury. However, the overmigration of microglia can also have harmful consequences by promoting toxicity (Eugenin *et al.* 2005).

1.6.2.5 Generation of reactive oxygen species (ROS) and nitrogen intermediates

Microglia can generate ROS when activated by various stimuli such as hypoxia and LPS. Nicotinamide adenine dinucleotide phosphate (NADPH) oxidase, which is involved in the production of microglial-derived extracellular ROS (Babior 2000), is a pivotal enzyme which catalyses the generation of superoxide from oxygen. Except for the release of extracellular ROS, NADPH oxidase is also associated with microglial signaling pathway related to inflammatory response (Block and Hong 2007). NADPH oxidase-derived intracellular ROS may act as a second messenger to augment the inflammatory response through executing effects on transcription factor activation and kinase cascades (Block and Hong 2007). ROS can also strengthen the phagocytosis of microglia by supporting the degradation of ingested antigens and cellular debris (Block and Hong 2007). However, excessive intracellular ROS might cause microglial apoptosis. The overactivation of NADPH oxidase and the dysregulation of intracellular ROS in microglia have been reported to be associated with the pathogenesis of some CNS diseases, including AD (Shimohama *et al.* 2000) and PWMD (Haynes *et al.* 2005).

NO, an important free radical, is released from L-arginine which is catalyzed by

nitric oxide synthase (NOS). NOS comprises of nNOS, eNOS and inducible NOS (iNOS). Both nNOS and eNOS belong to constitutively expressed enzymes, which are activated by upregulated intracellular calcium. However, iNOS is calcium-independent, and NO produced by this enzyme is well documented to modulate immune activities. NO executes a large amount of physiologic functions, such as muscle relaxation, blood vessel dilatation, immune modulation as well as neuronal activity. NO directly interacts with guanylate cyclase, cytochrome P450, cyclooxygenase, and hemoglobin, to regulate their functions. In addition, NO can react with membrane lipids and induce lipid peroxidation. Indirectly, the combination of NO and superoxide can produce highly reactive intermediates, such as peroxynitrite, that can cause DNA strand breaks, lipid peroxidation, and protein nitration. In the postnatal brain, iNOS expression is not normally detected but can be found in activated microglia after inflammatory or hypoxic stimuli (Kaur *et al.* 2006a). Overproduction of NO derived from iNOS has been found to execute harmful effects on the oligodendrocytes and hence delayed myelination leading to the pathogenesis and development of PWMD in hypoxic rats (Kaur *et al.* 2006a). NO released from iNOS has also been reported to damage myelin-forming oligodendrocytes in neuropathological disorders such as multiple sclerosis (MS) and AD (Koprowski *et al.* 1993). *In vitro* studies have demonstrated that activated microglial cell-derived NO induced the oligodendrocyte lysis (Merrill *et al.* 1993). Recent studies have also shown that peroxynitrite generated by iNOS in activated microglia may play a crucial role in the pathogenesis of PWMD as it is a highly reactive oxidant which is harmful

to the immature oligodendrocytes (Haynes *et al.* 2005; Li *et al.* 2005).

1.6.2.6 Release of cytokines and chemokines

A large number of cytokines and chemokines are usually expressed or secreted by microglia under pathological conditions. These cytokines and chemokines are implicated in microglial communication and effector network system with other types of cells (Hanisch 2002). Cytokines and chemokines secreted by microglia participate in innate defense mechanisms, help the initiation of immune responses, modulate the recruitment of leukocytes into the CNS and contribute to tissue repair and recovery (Hanisch 2002).

1.6.2.6.1 TNF-α and its receptors

TNF-α is one of the most important proinflammatory mediators released by activated microglia as well as blood-derived macrophages with pleiotropic functions during CNS inflammation (Arnett *et al.* 2001). In microglia culture, synthesis and release of TNF-α is induced by pathogens or pathogen components such as LPS and IFN-γ (Arnett *et al.* 2001). TNF-α can amplify CNS inflammatory response through inducing expression of chemokines and adhesion molecules in cerebrovascular endothelial cells and astrocytes, which help in recruitment of leukocytes into the CNS (Andrews *et al.* 1998). In addition, TNF-α is a multipotent inflammatory cytokine that initiates various responses such as apoptosis in some cells and proliferation in others through the activation of its different receptors (Andrews *et al.* 1998). Therefore, it is possible that TNF-α plays a wide variety of roles in PWM damage and repair.

All known effects of TNF-α occur through binding to one of two different receptors, known as TNF-R_1 (p55) and TNF-R_2 (p75), which are differentially expressed on various cell types in physiological and pathological conditions (Nakazawa *et al.* 2006b). The extracellular ligand-binding domains of TNF receptors show sequence homology containing cysteine-rich subdomains (Ledgerwood *et al.* 1999). On the contrary, the intracellular domains of the two TNF receptors lack sequence homology, have no intrinsic enzyme activity, and transduce different biological signals through interaction with different intracellular protein complexes (Ledgerwood *et al.* 1999). The TNF-R_1 contains death domain (DD), but TNF-R_2 doesn't. The distinctions of TNF-R_1 and TNF-R_2 constitution lead to their diverse functions. In general, cell apoptosis and pro-inflammatory response are largely mediated through TNF-R_1. Therefore, the activation of TNF-R_1 is frequently associated with tissue or organ injury (Ledgerwood *et al.* 1999). The consequences of TNF-R_2 activation are not fully known, but it is known to mediate cell proliferation and promote tissue repair and angiogenesis (Ledgerwood *et al.* 1999).

TNF-R_1, a type Ⅰ transmembrane protein, has been found on most cells in the body. TNF-R_1 is mainly stored in the Golgi apparatus in resting cells, from where it may be translocated to the cell membrane (Jones *et al.* 1999). Surface-expressed TNF-R_1 contains a pre-ligand domain which locates within the cell membrane. The cytoplasmic domain of TNF-R_1 is pre-bound to a cytoplasmic protein called silencer of death domain (SODD) (Jones *et al.* 1999). SODD can prevent the signal transduction of TNF-R_1. After TNF binds to TNF-R_1, SODD is released from the

binding complex. Subsequently, TNF-R_1 binds to a distinct DD-containing cytoplasmic protein designated TNF-R-associated DD protein (TRADD) (**Fig.A**) (Jones *et al.* 1999). TRADD initiates two different signaling pathways namely programmed cell death (PCD) signaling pathway and phosphorylated c-Jun induced gene transcription by recruitment of distinct cytoplasmic adaptor proteins (**Fig.A**) (Jones *et al.* 1999).

The PCD signaling pathway is initiated when the Fas-associated DD protein (FADD) binds to TRADD (**Fig.A**). Subsequently, pro-caspase-8 is recruited by the TRADD-FADD complex (**Fig.A**) (Chan *et al.* 2000). After this, pro-caspase-8 can be activated by autocatalytic process and release activated caspase-8 that may activate and cleave pro-caspase-3. Activated caspase-3 released from pro-caspase-3 results in cell apoptosis (**Fig.A**). TRADD initiates another signaling transduction by recruitment of two additional proteins namely receptor interacting protein-1 (RIP-1) as well as TNF-R-associated factor-2 (TRAF-2) (Chan *et al.* 2000). Subsequently, the TRADD-RIP-1-TRAF2 complex is internalized and released from TNF-R_1. RIP-1 regulates the recruitment of mitogen extracellular signal-regulated kinase (MEK) kinase-3 and transforming growth factor-beta (TGF-β)-activated kinase (TAK)1, which in turn, activates the β-subunit of the inhibitor of kB (IkB) kinase (IKK) complex (**Fig.A**) (Chan *et al.* 2000). This causes the phosphorylation of IkB protein. The phosphorylated IkB is degraded immediately and NF-kB is released from IkB-NFkB complex. NF-kB is phosphorylated, then enters the nucleus and initiates corresponding gene transcription (**Fig.A**) (Chen 2005). The TRADD-RIP-1-TRAF-2

complex can also activate and phosphorylate c-Jun N-terminal kinases (JNKs) and p38 MAPKs through MEKs cascades (**Fig.A**) (Chen 2005). Subsequently, phosphorylated JNK activate and phosphorylate c-Jun, a subunit of the transcription factor activating protein 1 (AP-1) (**Fig.A**) (Ichijo *et al.* 1997). Phosphorylated c-Jun translocates to nucleus and activates gene transcription (**Fig.A**). TNF-R_1 can also activate sphingomyelinase (SMase) enzyme through interaction with FAN (factor associated with neutral SMase activation). Activated SMase can breakdown plasma membrane sphingomyelin which result in the generation of ceramide (Ichijo *et al.* 1997). Ceramide is a signal that induces cell apoptosis through the mitochondrial pathway. TNF-R_1 can also activate the phosphatidylinositol-3 kinase (PI3K) and ras-raf-MEK1-ERK1, 2 pathway, which cause Akt signaling pathway cascades (Ichijo *et al.* 1997). Akt and ERK-1,-2 are involved in cell proliferation and survival (Ichijo *et al.* 1997).

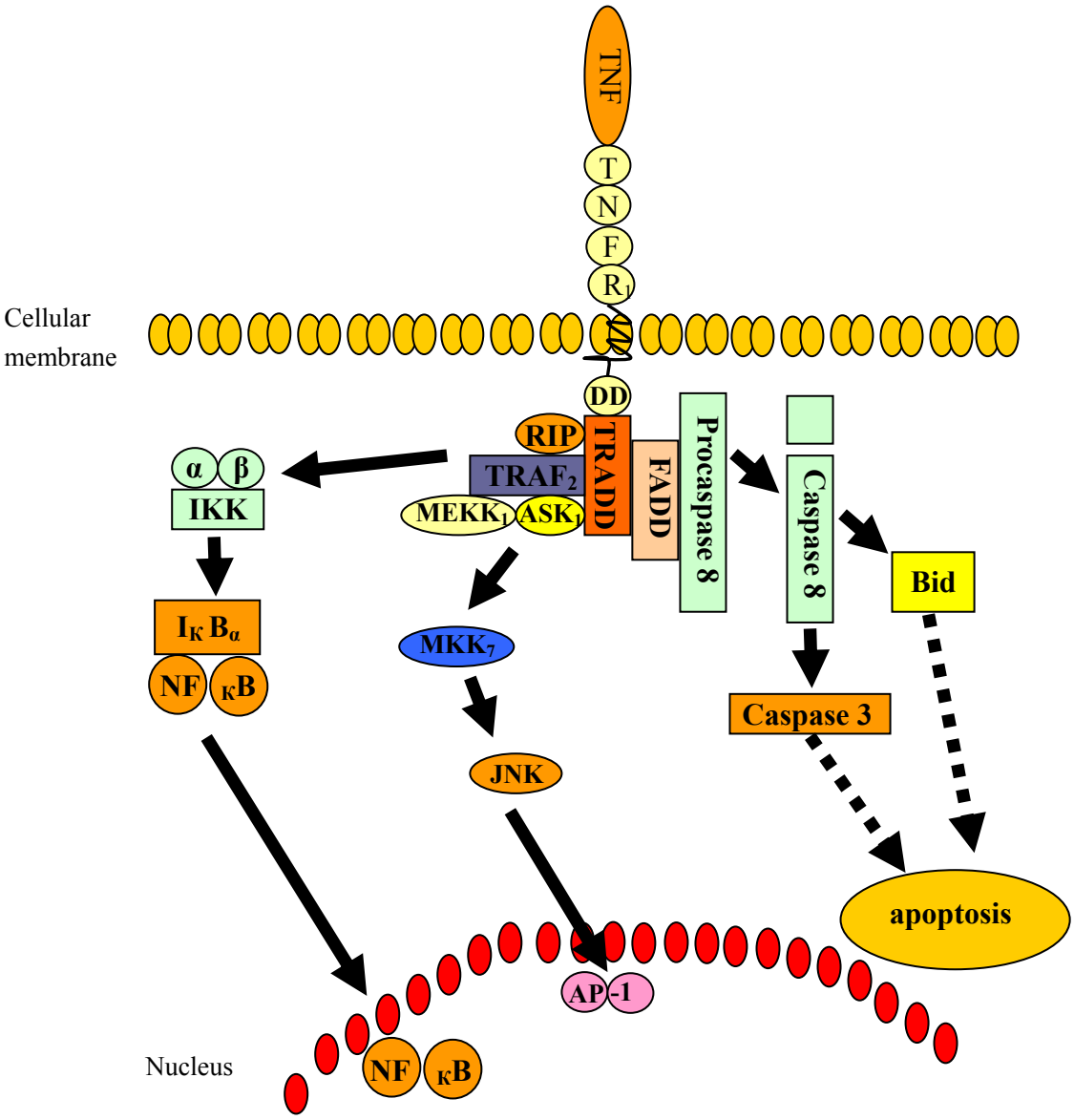

Figure A. Signaling pathways leading to the main cellular responses of TNF-α through TNF-R_1. TNF-α binds to TNF-R_1 and, hence, activates MAP kinase, NF-kB as well as cellular apoptosis signaling pathways.

The role of TNF-R_2 in physiological and pathological processes is less investigated. Unlike TNF-R_1, TNF-R_2 can not recruit apoptosis associated proteins such as TRADD and FADD because of lack of an intracellular DD (Ichijo *et al.* 1997; Rothe *et al.* 1994). Therefore, the activation of TNF-R_2 doesn't trigger cellular apoptosis. However, some research has demonstrated that expression of TNF-R_2 on

the cell potentiates TNF-R_1-induced death through the formation of p55 and p75 TNF receptors heterocomplexes (Rothe *et al.* 1994). Furthermore, TNF-α induces a conformational change in TNF-R_2 which activates endothelial/epithelial tyrosine kinase (Etk) in a TRAF2-independent manner (Rothe *et al.* 1994). The phosphorylation of Etk causes Akt activation, which contributes to TNF-induced cell proliferation (Rothe *et al.* 1994).

1.6.2.6.2 Interleukin 1 (IL-1) and its receptors

IL-1 includes two mediators, IL-1α and IL-1β, which share similar biological activities and three-dimensional structure but have less than 30% sequence homology (Grehan *et al.* 1997). The role of IL-1 is modulated through binding to distinct receptorss including a true receptor (IL-1RⅠ), a decoy (IL-1RⅡ) as well as a specific receptor antagonist (IL-1ra) (Grehan *et al.* 1997). Although IL-1α and IL-1β can bind equally to type Ⅰ and type Ⅱ IL-1R, signal transduction across the plasma membrane has been reported to be accomplished via the type Ⅰ receptor (Grehan *et al.* 1997). At present, there is no evidence that a signal can be transmitted through the type Ⅱ receptor. In the CNS, high level expression of IL-1 is found in the prenatal and postnatal period, and its expression declines gradually to low constitutive levels in the adult and increases markedly after injury (Vela *et al.* 2002). Astroglia and microglia possess IL-1 receptors and are the predominant intrinsic sources of IL-1 in the CNS, but oligodendroglial cells also produce IL-1 and express IL-1 receptors (Vela *et al.* 2002). IL-1 induces activation and secretion of multiple factors by microglia and astrocytes. It has been reported recently that remyelination is dramatically reduced in

the absence of IL-1β, but the effects of this cytokine on cells of the oligodendroglial lineage remain to be elucidated (Vela *et al.* 2002).

1.6.2.6.3 Macrophage-colony stimulating factor

The macrophage-colony stimulating factor (M-CSF), also designated as CSF-1, is a hematopoietic cytokine that induces activation, proliferation, and migration of microglia and is released mainly by macrophages, T cells, B cells and microglia (Stanley *et al.* 1997). M-CSF has also been well known as an important inflammatory mediator and may modulate the production of proinflammatory cytokines from macrophages (Hao *et al.* 2002). M-CSF executes its pleiotropic effects through binding to its high-affinity receptor CSF-1R that is encoded by the *c-Fms* proto-oncogene (Rovida *et al.* 2008).

1.6.2.6.4 Monocyte chemoattractant protein-1

Chemokines are chemotactic cytokines which act by binding to their respective G-protein-coupled receptors. Chemokines may contribute to the migration of microglia to injured CNS sites and potentiate their activation. In addition, chemokines released by microglia are likely to induce leukocyte migration and amplify the CNS inflammatory response. Together with integrins and endothelial cell-adhesion molecules, chemokines are believed to regulate the migration of macrophages, leukocytes and other immune cells (Ambrosini and Aloisi 2004). A variety of inflammatory chemokines and their respective receptors have been found in the brain during development and disease processes. Glial cells, stimulated by LPS and some proinflammatory cytokines such as TNF-α and IL-1 *in vitro* have been shown to

generate several chemokines such as Monocyte chemoattractant protein-1 (MCP-1), interleukin-8 (IL-8), macrophage inflammatory protein 1 alpha (MIP-1α) as well as macrophage inflammatory protein 1 beta (MIP-1β) (Ehrlich *et al.* 1998; Lipovsky *et al.* 1998; Lokensgard *et al.* 1997; McManus *et al.* 1998; Peterson *et al.* 1997). Microglia *in vitro* can also express chemokine receptors such as chemokine (C-X3-C motif) receptor 1 (CX3CR1) (Nishiyori *et al.* 1998), chemokine (C-C motif) receptor 3 (CCR3), chemokine (C-X-C motif) receptor 4 (CXCR4) (Lavi *et al.* 1997) and chemokine (C-C motif) receptor 5 (CCR5) (He *et al.* 1997).

Among chemokines, MCP-1, also designated as CCL2, is a member of β-chemokine subfamily, which modulates the migration of lymphocytes, microglia and monocytes to the inflammation sites in the CNS (Cross and Woodroofe 1999; Taub *et al.* 1995; Gunn *et al.* 1997; Babcock *et al.* 2003). MCP-1 exerts its effects on target cells through interaction with its receptor, chemokine (C-C motif) receptor 2 (CCR2) which is a seven-transmembrane domain G-protein coupled receptor. It is produced predominantly by microglia and astrocytes in the CNS (Hayashi *et al.* 1995). The expression of MCP-1 and CCR2 has been found to be upregulated following various CNS insults such as AD (Fenoglio *et al.* 2004), ischemia (Che *et al.* 2001; Minami and Satoh 2003; Vilhardt 2005), MS and its animal model experimental autoimmune encephalomyelitis (EAE) (Sorensen *et al.* 1999; Simpson *et al.* 1998; Glabinski *et al.* 2003), and HIV type-1-associated dementia (Conant *et al.* 1998),. In EAE animal model, MCP-1 resulted in the activation and migration of endogenous microglia and blood-derived macrophages to demyelinated sites, potentiating myelin

phagocytosis (Ambrosini and Aloisi 2004). Furthermore, the functional antagonism of MCP-1 may attenuate leukocyte extravasation and decrease the severity of CNS injury (Calvo *et al.* 1996; Muessel *et al.* 2002). In a murine stroke model, MCP-1 deficiency has been demonstrated to play a protective role in acute infarct development (Hughes *et al.* 2002). It has also been reported that MCP-1 could potentially modulate microglial activation and induce migration of blood-derived monocytes into the brain in hypoxic-ischemic neonatal rats (Ivacko *et al.* 1997).

1.7 Aims of this study

Inflammation has been recognized as a major factor leading to PWMD (Kadhim *et al.* 2002; Wu and Colford, Jr. 2000) under hypoxic conditions. It is well documented that microglial cells, the resident immune cells of the CNS, and astrocytes play a crucial role in the modulation of inflammatory response in some diseases (Dheen *et al.* 2005b; Vilhardt 2005). In the developing brain, AMC aggregate in large numbers in the PWM (Ling and Wong 1993). The activated microglia may release a lot of potentially cytotoxic molecules such as proinflammatory mediators, ROS, proteinases and complement proteins. However, the role of AMC and astrocytes in PWMD in neonatal brain under hypoxic conditions has not been fully elucidated. The main aim of this study was to determine if AMC and astrocytes contribute to PWMD under hypoxic conditions in the neonatal brain. The potential mechanisms and signaling pathways by which activated AMC and astrocytes cause the PWMD under hypoxic conditions were also investigated.

1.7.1. Role of AMC in the PWMD

A large number of proinflammatory mediators such as TNF-α, IL-1β, MCP-1 and M-CSF are usually expressed or secreted by microglia under inflammatory conditions. Activated microglial cells communicate or cross talk with other type cell through these cytokines and chemokines. As mentioned earlier, TNF-α executes different functions through binding to one of two different receptors, $TNFR_1$ (p55) and $TNFR_2$ (p75). TNF-α induces cell apoptosis and mediates pro-inflammatory response through $TNFR_1$. The action of IL-1 is modulated by two different types, IL-1RⅠ and IL-1RⅡ.

Based on these data, it is hypothesized that AMC in the PWM may induce oligodendrocyte and axon damage through expression of proinflammatory cytokines and chemokines such as,TNF-α, IL-1β, MCP-1 and M-CSF in hypoxic neonatal rats. To address this,

1). The mRNA and protein expression of cytokines such as TNF-α, IL-1β, MCP-1 and M-CSF in AMC in the PWM was examined.

2). The signaling pathway involved in production of some of the cytokines such as TNF-α and IL-1β in hypoxic conditions was also examined.

3). It was then ascertained whether developing oligodendrocytes in the PWM in hypoxic neonatal rats would be the potential target of TNF-α and IL-1β by expressing $TNF\text{-}R_1$ and $IL\text{-}1R_1$ and, if so, whether they would undergo apoptosis or necrosis and a significant reduction in the number.

4). The expression of $TNF\text{-}R_1$ and $IL\text{-}1R_1$ on the axons was also examined.

5). Changes in the axons and myelination disturbances were investigated.

1.7.2. Regulation of microglial migration in the PWM by MCP-1 production by AMC in hypoxia

In the CNS, microglia appear to be the main source for the generation of chemokines including interferon-gamma-inducible protein-10 (IP-10) and MCP-1 (Gebicke-Haerter *et al.* 2001). MCP-1 is well documented to play a significant role in the initiation and progression of acute inflammatory brain injury in the neonatal rat (Galasso *et al.* 2000). It has been reported that MCP-1 could activate and recruit macrophages within inflammatory foci to aggravate CNS injury (Galasso *et al.* 2000). It has also been found that MCP-1 and its receptor is colocalized in the microglial cells (Galasso *et al.* 2000). Therefore, it is possible that MCP-1 may activate and direct microglia recruitment to injured CNS sites in an auto- and paracrine manner and thus amplify the ongoing inflammatory response. In view of the above, MCP-1 released by AMC under hypoxic conditions may contribute to the migration of AMC from the surrounding brain areas such as the cerebral cortex or it may attract infiltration of monocytes to the PWM and aggravate PWMD. To address this,

1). Cell count of AMC and their proliferation rate in the PWM in hypoxic rats was examined.

2). The mRNA and protein expression of MCP-1 and CCR_2 in AMC in the PWM at different time points in control and hypoxic rats was observed.

3). The migration of AMC to the PWM was induced by MCP-1 injection *in vivo*.

4). MCP-1 production via activation of NF-kappaB signaling pathway in the activated microglia under hypoxic conditions *in vitro* was investigated.

5). The *in vitro* migration of microglia in response to microglia conditioned medium was also assessed.

1.7.3. Regulation of TNF-α and IL-1β generation by astrocytes in the PWM by AMC-derived M-CSF in hypoxic neonatal rats

It has been reported that besides microglial cells, astrocytes may also contribute to an inflammatory response by releasing inflammatory cytokines (Sawada *et al.* 1995). Astrocytes have been thought to be predominantly responsible for the release of inflammatory mediators in the late phase of inflammatory response in the CNS (Sawada *et al.* 1995). Therefore, it was speculated that astrocytes may also be another source of TNF-α and IL-1β production in the PWM resulting in damage to the axons and oligodendrocytes. However, the mechanism by which astrocytes are activated and release proinflammatory cytokines has not been fully elucidated. Recent studies have shown that M-CSF is an important inflammatory mediator and can also promote the release of proinflammatory cytokines from immune cells by binding to its receptor, CSF-1R (Hao *et al.* 2002; Rovida *et al.* 2008).

Arising from the above, we hypothesized that M-CSF produced by AMC in the early phase following hypoxic injury may activate astrocytes and regulate the release of TNF-α and IL-1β in the later phase by them that may sustain and exacerbate the inflammatory response in hypoxic neonatal rats. To address this,

1). The mRNA and protein expression of M-CSF in AMC in the PWM was

examined.

2). The expression of CSF-1R, TNF-α, IL-1β in astrocytes in the PWM in hypoxic rats was examined.

3). It was then ascertained whether M-CSF protein can induce the expression of CSF-1R and production of TNF-α and IL-1β from primary cultured astrocytes through MAP kinase signaling pathway *in vitro*.

This research mainly focuses on the mechanisms by which microglia and astroglia induce oligodendrocyte and axon damage in the PWM in hypoxic neonatal rats. The findings obtained may be helpful in understanding the role of these cells in the pathogenesis of PWMD in hypoxic conditions and also for development of better therapeutic strategies for the treatment of PWMD.

Chapter 2

Materials and Methods

2.1 Animals

Wistar rats (1-day old) were used in this study as the developmental stage of white matter in rats at birth has been described to be equivalent to mid-gestation in humans (Sheldon *et al.* 1996). 222 rats were subjected to hypoxia by placing them in a chamber filled with a gas mixture of 5 % oxygen and the remainder 95% nitrogen (Model: MCO 18M; Sanyo Biomedical Electrical Co, Ltd, Tokyo, Japan.). The rats were then allowed to recover under normoxic conditions for 3 and 24 h, 3, 7 or 14 days before being killed. Another group of 222 rats kept outside the chamber were used as age-matched controls (Table 1). For mixed primary glial cell culture, another 160 rat pups were used. Animal handling and experiments were approved by Institutional Animal Care and Use Committee, National University of Singapore (NUS).

Table 1. Number of rats killed at various time points after the hypoxic exposure (in brackets) and their age-matched controls for various methods (outside the brackets).

Control (hypoxia)	Double Immunohistochemistry	Real time-RT-PCR	ELISA and Western blotting	MCP-1 Injection	Electron microscopy
1 day (3h)	9 (9)	15 (15)	15 (15)		3(3)
2 days (24h)	9 (9)	15 (15)	15 (15)		3(3)
4 days (3days)	9 (9)	15 (15)	15 (15)		3(3)
8 days (7days)	9 (9)	15 (15)	15 (15)	24	3(3)
15 days (14 days)	9 (9)	15 (15)	15 (15)		3(3)

2.2 Mixed Glial Cell Culture

2.2.1. Materials

Dulbecco's Modified Eagle Medium (DMEM) (Sigma, USA, Cat. No. D1152)

Insulin (Sigma-Aldrich, USA, Cat. No. I0516)

Non-essential amino acid (Sigma, USA, Cat. No. M7145)

Antibiotic antimycotic solution (100X Sigma-Aldrich, USA, Cat.No. A5955)

Trypsin and ethylenediaminetetraacetic acid (EDTA) (10X Sigma, USA, Cat. No. T4549)

Ethylenediaminetetraacetic acid (EDTA) (10X Sigma, USA, Cat. No. E-7889)

Deoxyribonuclease Ⅰ (Sigma-Aldrich, USA, Cat.No. D4527)

Fetal bovine serum (FBS) (Invitrogen, USA, Cat. No. 10099)

70μm nylon cell strainer (BD Biosciences, USA, Cat. No. 352350)

75cm^2 tissue culture flasks (NUNC, Denmark)

Lectin (*Lycopersicon esculentum* tomato) (Sigma-Aldrich, USA, Cat. No. L0401)

4', 6- diamidino-2-phenylindole dihydrochloride (DAPI) (Sigma, USA, Cat. No. D1306)

Phosphate buffered saline (PBS; 0.1M, pH 7.4)

2.2.2. Procedure

2.2.2.1. Removal of Brain Tissue

The rat pups were deeply anesthetized with 6% sodium pentobarbital (60mg/kg) and were decapitated. The heads were wiped with 70% ethanol and washed with ice-cold PBS. The skin was incised along the midline in a caudal to rostral direction to expose the skull. The skull was penetrated with the tip of a pair of scissors and cut-opened rostrally to the nose. Further from the original point of incision, the skull was cut mediolaterally and then in a rostral direction reaching the first set of cuts. In this way, two roughly rectangular flaps of skull were removed. Underlying brain tissue was moistened with PBS. A pair of curved forceps was used to scoop the brain tissue out. Then, the brain tissue was placed onto a 100 mm diameter dish with PBS and was rinsed three times. The cortices were collected into a 50 ml tube in PBS on ice and were rinsed three times with PBS. The undesired brain regions, such as thalamus, hippocampus, basal ganglia, and, olfactory bulb, were removed first. The meninges and superficial vessels were removed subsequently. The remaining cortices were transferred to a new 60 mm diameter dish, containing cold PBS. The tissue was finely dissected further to remove the remaining meninges and vasculature. Finally, the tissue was transfered to a new 60-mm-diameter dish containing 9 ml cold DMEM medium.

2.2.2.2. Mechanical dissociation of brain tissue

A long pair of scissors was used to chop the brain tissue in the dish with gentle up-and-down motion. The tissue pieces were collected and mechanically

dissociated by pipetting in and out with a 10ml plastic pipette in a 50 ml sterile concial tube on ice.

2.2.2.3. Enzymatic digestion

One ml of Trypsin-EDTA solution (0.5mg/ml) and 100μl of Deoxyribonuclease Ⅰsolution (50μg/ml) were added into the tube, and mixed before the solution was transfered to a 75cm^2 tissue culture flask. The flask was placed in an orbital shaker at 37℃ and shaken at 200 rpm/min for 15 min. Cells were passed through a 70μm cell strainer to remove remaining clumps of tissue and then transfered to a 50ml centrifuge tube again.

Finally the cell suspension was centrifuged at 1000rpm for 5 min, then seeded in culture dish containing DMEM plus 10% FBS at a density of 1.2×10^6 cells/ml and cultured at 37℃ in humidified 5% CO_2/95% air. Medium was changed every 2-3 days and confluency was achieved after 10 to 12 days *in vitro*.

2.2.3. Microglia purification

Microglial cultures were prepared by a mild trypsinization method as described by Saura and others (Saura *et al.* 2003). The mixed glial cultures were purified after 10 to 12 days. Briefly, the cultures were washed with PBS twice and incubated with a trypsin solution (1ml of 0.25% trypsin and 20μl of 0.5M EDTA diluted in 40 ml of DMEM) for about 10 min. This resulted in the detachment of an upper layer of cells which were removed subsequently. The microglial cells remained attached to the bottom of the flask and were cultured in DMEM contained 10% FBS.

For enzyme-linked immunosorbent assay (ELISA), 2.5×10^5 cells were seeded per well in 24-well plates. For immunoblotting and RNA extraction, 1×10^6 cells were seeded per $75cm^2$ flask. For immunocytochemistry, 2.5×10^5 cells were seeded per well in a 24 multi-well plate and incubated at 37°C in a humidified incubator supplemented with 95% air and 5% CO_2 for 24h. The following day, the cells were subjected to different treatments.

The purity of microglia was determined immunohistochemically using Lectin (1:100), a marker for microglia, and DAPI (20µg/ml) a nuclear marker of all cells attached to the coverslips. The purity of microglial cultures was found to be around 96%.

2.2.4. Astrocytes purification

The mixed glial cultures were purified after 12 to 14 days. The flask containing the mixed glial cells was shaken for 15h at 200rpm. Non-astroglial cells including microglial cells and oligodendrocytes in the supernatant were removed after shaking (Kliot *et al.* 1990; McCarthy and de 1980; Rovida *et al.* 2008). The majority of the remaining cells were astrocytes. The astrocytes remained attached to the bottom of the flask and were cultured in DMEM supplemented with 10% FBS.

For immunoblotting and RNA extraction, 1×10^6 cells were seeded per $75cm^2$ flask. For immunocytochemistry, 2.5×10^5 cells were seeded per well on a 24 multi-well plate and incubated at 37°C in a humidified incubator supplemented with 95% air and 5% CO_2 for 24h.

The purity of astrocyte cultures was assessed by double immunocytochemistry analysis of cultured cells with mouse anti-GFAP (1:1000: Chemicon International, CA, USA), a widely used marker for astrocytes, and DAPI (20μg/ml; Sigma), a nuclear marker of all cells. This double-labeling analysis showed that more than 99% of the confluent cells were GFAP-positive astrocytes.

2.3 Treatment of microglial cells for expression of TNF-α, IL-1β, M-CSF and MCP-1

Microglial cell cultures were divided into seven groups: Group Ⅰ: To study the effects of hypoxia on expression of TNF-α and IL-1β in microglial cells. For this, the cells were exposed in a hypoxia chamber (Model 18M; Multi-gas incubator, Sanyo Company Pte Ltd, Japan) for 1, 2, 4 and 6h at 3% oxygen, 5% CO_2 and 37℃. Group Ⅱ: To study the effects of hypoxia on MAP kinase pathway. In this, the microglial cells were placed in a hypoxia chamber for 0.5, 1, 2 and 4h at 3% oxygen, 5% CO_2 and 37℃. Group Ⅲ: To examine the effects of MAP kinase inhibitors on hypoxia-induced TNF-α and IL-1β expression in microglial cells. Microglial cell cultures were treated with either SP600125 (1μM; Scientific, Inc, USA) or SB203580 (1 μM; MERCK, Darmstadt, Germany), inhibitors of JNK and p38, respectively, 30 min before hypoxia treatment. Group Ⅳ: To study the effects of hypoxia on expression of M-CSF in microglial cells, the cells were exposed to hypoxia in a chamber for 1, 2, 4 and 6h at 3% oxygen, 5% CO_2 at 37℃. Group Ⅴ: To study the effects of hypoxia on release of MCP-1 and expression of

MCP-1 mRNA in microglial cells. For this, the cells were exposed to hypoxia in a chamber for 1, 2, 4 and 6h at 3% oxygen and 5% CO_2 and at 37℃. Subsequently, the microglial cells were used for mRNA extraction and the medium was collected and stored at −20°C for ELISA. Group Ⅵ: To study the effects of hypoxia on NF-kappaB signaling pathway. In this, the microglial cells were placed in a hypoxia chamber for 15, 30min, 1 and 2h or hypoxia + BAY 11-7082 (10mM; Calbiochem, CA, USA) for 4h at 3% oxygen and 5% CO_2 at 37℃. Subsequently, the protein was extracted from the microglial cells and stored at −20°C for Western blotting. Group Ⅶ: To examine the effects of the medium derived from hypoxia-treated microglial cultures on chemotaxis of microglia *in vitro*. In the latter, the cells were exposed in a hypoxia chamber for 4h at 3% oxygen and 5% CO_2 at 37℃. Subsequently, the medium was collected and stored at −20°C for chemotaxis assay. In all the experiments, microglial cells in matching controls were incubated in incubator with 95% air and 5% CO_2 at 37°C.

2.4 Treatment of Astrocytes Culture

Astrocyte cultures were divided into three groups: Group Ⅰ: To study the effects of M-CSF treatment on expression of TNF-α, IL-1β and CSF-1R in the astrocytes. The cells were treated with M-CSF (Antigenix America Inc; Cat. No. RC333140; 25ng/ml) for 3, 6, 12 and 24h at 37°C in a humidified incubator supplemented with 95% air and 5% CO_2 at 37℃. Group Ⅱ: To study the effects of M-CSF treatment on MAP kinase pathway. In this, the astrocytes were treated with M-CSF (Antigenix America Inc; Cat. No. RC333140; 25ng/ml) for 15,

30min, 1 and 2h at 95% air, 5% CO_2 at 37℃. Group Ⅲ: To examine the effects of MAP kinase inhibitors on M-CSF treatment-induced TNF-α and IL-1β expression in the astrocytes. Astrocyte cultures were treated with either 1μM SP600125 (Scientific, Inc, USA) or 1 μM SB203580 (MERCK, Darmstadt, Germany), inhibitors of JNK and p38, respectively, 30 min before M-CSF administration. In all the experiments, astrocytes in matching controls were incubated in an incubator filled with 95% air and 5% CO2 at 37°C.

2.5. RNA Isolation and Real time reverse transcription-polymerase chain reaction (RT-PCR)

2.5.1. Materials

RNeasy mini kit (Qiagen, Germany, Cat. No. 74106)

Molony murine leukemia virus reverse transcriptase (M-MLV) (Promega, USA, Cat. No. M1701)

Oligo(dT) primer (Promega, USA , Cat. No. C1101)

dNTP mix (Promega, USA , Cat. No. U1240)

RNase inhibitor (Promega, USA, Cat. No. N2111,)

LightCycler FastStart DNA Master^{PLUS} SYBR Green I (Roche Applied Sciences, Germany, Cat. No. 03515885001)

TAE buffer (Invitrogen, USA, Cat. No. 15558034)

100bp DNA step ladder (Promega, USA, Cat. No. G6951)

LightCycler instrument (Roche Molecular Biochemicals)

GeneGenius (Syngene, UK)

Spectrophotometer (Eppendorf, Germany)

2.5.2 Procedure

2.5.2.1 Extraction of total RNA

The PWM was dissected under the Leica stereo microscope (MZ 6; Leica Pte Ltd, Singapore). Total RNA was extracted from the PWM or cultured microglial cells or cultured astrocytes using RNeasy mini kit (Qiagen, Valencia, CA, USA) according to the manufacturer's protocol. Approximately, 20g tissues or 1×10^6 cells were used to extract the total RNA. Tissues or cells were lysed in 650µl of RLT buffer (containing a highly denatured guanidine isothiocyanate which inactivates RNase). The cells then were scraped from the flask with the scraper. The lysate was homogenized, then centrifuged for 30s at 14000×g in a microfuge and the supernatant was mixed with 650µl of 70% ethanol to clear lysate. The sample was applied to an RNeasy mini spin column (silica-gel membrane, maximum binding capacity is 100µg of RNA longer than 200 bases) and spun for 30sec at 14000×g and then flow-through was discarded. The RNA bound to the membrane was washed with buffer RW1 and RPE sequentially. High-quality RNA was then eluted in 20µl of RNase free water. The concentration and purity of the extracted RNA was evaluated spectrophotometrically at 260 and 280 nm (Biophotometer, Eppendorf, Germany)

2.5.2.2 cDNA Synthesis

The cDNA synthesis was carried out in a total volume of 25µl containing the RNA template, Oligo(dT) Primer, M-MLV reverse transcriptase, transcription

buffer, dNTP, RNase inhibitor and RNase-free water.

2μg of RNA was added with 1μl Oligo $(dT)_{15}$ primer into a microcentrifuge tube and then heated to 70° for 5 min to melt secondary structure within the template. The tube was immediately transferred to ice. The following components were added to the annealed primer/template in the order shown.

M-MLV 5 X Reaction Buffer	5μl
10 X dNTP Mix	1.25μl
RNase inhibitor	0.675μl
M-MLV Reverse transcriptase	1μl
RNase free water to final volume	25μl

The reaction mixture was mixed gently and incubated for 1h at 42℃. Finally the reaction was terminated by heating at 95℃ for 5min. The cDNA synthesized was kept at 4℃.

2.5.2.3 Real time RT-PCR

Quantitative RT-PCR was carried out on a Light Cycler 3 instrument using a FastStart DNA Master plus SYBR Green I kit (Roche Diagnostics, GmbH, Roche Applied Science, Germany) according to the manufacturer's instructions. Briefly, a light-cycler master mix was prepared using 2 μL Light Cycler-FastStart DNA Master plus SYBR Green I with forward and reverse primers for TNF-α, IL-1β, $TNF\text{-}R_1$, $IL\text{-}1R_1$, M-CSF, CSF-1R, MCP-1, CCR_2 and β-actin (Table 2.) at a final concentration of 0.5 μM each. A 2 μL sample of the cDNA was added into 18 μL of LightCycler master mix and transferred into LightCycler glass capillaries. The

capillaries were capped, placed in a LightCycler carousel and centrifuged in a specific LightCycler centrifuge. Thermal cycling was carried out. The first segment of the amplification cycle consisted of a denaturation programme at 95°C for 10 min. The second segment was performed as follows: 35 cycles of denaturation at 95°C for 15s, annealing at 60°C (for TNF-α, IL-1β, TNF-R_1, IL-$1R_1$, M-CSF, CSF-1R, MCP-1 and CCR_2) or 62°C (for β-actin) for 5s, and elongation at 72°C for PCR product size per 25s. The third segment consisted of a melting curve programme. The final segment consisted of a cooling programme at 40°C. The expression level of each gene was quantified, expressed as C_t, the cycle number at which the LightCycler system detected the upstroke of the exponential phase of PCR product accumulation, and normalized by the level of expression of β-actin in each individual sample. The mRNA expression levels of various genes studied in the experimental groups and control groups were compared using the $2^{-[\Delta\Delta Ct]}$ method (Livak and Schmittgen 2001)**.**

Table 2 Sequence of specific primers

Primer	Forward	Reverse	Amplicon size
TNF-α	caacaaggaggagaagttcc	ctctgcttggtggtttgctac	134bp
IL-1β	ggaacccgtgtcttcctaaag	ctgacttggcagaggacaaag	123bp
$TNF\text{-}R_1$	ggcccacttctaatgtgtgaa	aggctacaagagggagacagc	163bp
$IL\text{-}1R_1$	taaacctctgcctcttgacga	tgcttcccctggtatgtgtag	146bp
M-CSF	agagctcctgcctaccaagac	tcctaaaggaaagggtcctga	195bp
CSF-1R	ggagatcttctcgcttggtct	ggaaggtgggtcttctggtag	173bp
MCP-1	tctcttcctccaccactatgca	ggctgagacagcacgtggat	91bp
CCR_2	cgcagagttgacaagttgtg	gccatggatgaactgaggta	233bp
β-actin	tcatgaagtgtgacgttgacatccgt	cctagaagcatttgcggtgcaggatg	285bp

2.5.2.4 Detection of PCR product

PCR products were run on agarose gel using electrophoresis. 1.5% agarose gel was prepared by heating agarose in the TAE buffer. 5% of ethidum bromide was added into the gel and the gel was cooled, poured onto a gel tray and allowed to solidify. 10µl of each real time PCR product was loaded in each lane of the gel and electrophoresed at 110V for 45min in TAE buffer with 10µl of 100bp DNA ladder. The PCR products in gel were visualized with an ultraviolet trans-illuminator and photographed. The 100bp DNA ladder was used to determine the size of the amplified DNA.

2.6. Western Blotting

2.6.1. Materials

Protease inhibitor cocktail kit (Pierce, USA, Cat. No. 78410)

Tissue protein extraction reagent (Pierce, USA, Cat. No. 78503)

Mammalian protein extraction reagent (Pierce, USA, Cat. No. 78503)

Protein assay kit (Bio-Rad, USA, Cat. No. 5000002)

Bovine serum albumin (BSA) (Bio-Rad, USA, Cat. No. #500-0007)

10% resolving gel:

H_2O	7.9ml
30% acrylamide mix	6.7ml
1.5 M Tris (pH 8.8)	5.0ml
10% sodium dodecyl sulphate (SDS)	0.2ml
10% ammonium persulfate	0.2ml
TEMED	0.008ml

5% stacking gel:

H_2O	5.5ml
30% acrylamide mix	1.3ml
1.0 M Tris (pH 6.8)	1.0ml
10% SDS	0.08ml
10% ammonium persulfate	0.08ml
TEMED	0.008ml

1x SDS gel-loading buffer:

50mM Tris.Cl (pH 6.8)

100mM dithiothreitol

2% SDS

0.1% bromophenol blue

10% glycerol

Tris-glycine electrophoresis buffer:

25mM Tris

250mM glycine

0.1% SDS

Transfer buffer:

25mM Tris

250mM glycine

20% Methanol

1X Tris-buffered saline (TBS):

Tris base 2.42 g

NaCl 0.8 g

H_2O up to 1 liter; adjusted to pH 7.6 with 2N HCl

1X Tris-buffered saline tween (TBST):

1X TBS 1 liter

0.1% Tween 20

The primary antibodies used are listed in Table 3.

Table 3 All antibodies used in experiments

Antibody	Host	Company	Cat. NO.	Concentration
TNF-α	rabbit	Chemicon, USA	AB1837P	1:1000
IL-1β	rabbit	Chemicon, USA	AB1832P	1:5000
$TNF\text{-}R_1$	rabbit	Santa Cruz, USA	sc-7895	1:500
$IL\text{-}1R_1$	rabbit	Santa Cruz, USA	sc-689	1:500
M-CSF	rabbit	Santa Cruz, USA	sc-13103	1:200
CSF-1R	rabbit	Santa Cruz, USA	sc-692	1:500
MCP-1	goat	Santa Cruz, USA	sc-1785	1:100
CC_1	mouse	Oncogene, USA	OP80	1:20
CCR_2	goat	Santa Cruz, USA	sc-31563	1:200
GFAP	mouse	Chemicon, USA	MAB360	1:1000
phospho-c-Jun	rabbit	Cell Signaling Technology, USA	9164s	1:500
c-Jun	rabbit	Cell Signaling Technology, USA	9162	1:500
phospho-JNK	rabbit	Cell Signaling Technology, USA	9251s	1:500
JNK	rabbit	Cell Signaling Technology, USA	9252	1:500
phospho-p38	rabbit	Cell Signaling Technology, USA	9211s	1:500
p38	rabbit	Cell Signaling Technology, USA	9212	1:500
phospho-ERK1/2	rabbit	Cell Signaling Technology, USA	9101s	1:500
ERK1/2	rabbit	Cell Signaling Technology, USA	9102	1:500
phospho-NF-kappaB	rabbit	Santa Cruz, USA	sc-109	1:200
NF-kappaB	rabbit	Cell Signaling Technology, USA	3031S	1:500
phosph-IkappaB	rabbit	Cell Signaling Technology, USA	9241S	1:500
IkappaB	rabbit	Cell Signaling Technology, USA	9242	1:500
Myelin basic protein (MBP)	goat	Santa Cruz, USA	sc-13912	1:1000
Neurofilament (NF-200)	mouse	Sigma-Aldrich, USA	N0142	1:1000
β-actin	Mouse	Sigma-Aldrich, USA	A1978	1:10000

Goat anti-rabbit IgG conjugated with horseradish peroxidase (Cell Signaling Technology, USA, Cat. No. 7074)

Goat anti-mouse IgG conjugated with horseradish peroxidase (Pierce, USA, Cat. No. 31430,)

Stripping buffer (Pierce, USA, Cat. No. 0021059)

2.6.2. Procedure

The PWM was dissected under the Leica stereo microscope (MZ 6; Leica Pte Ltd, Singapore). Proteins were extracted from the PWM or microglial cells or astrocytes using protein extraction kit according to the manufacturer's protocol. Protein concentrations were determined by the Bradford method (Bradford 1976) using BSA (Sigma-Aldrich, MO, USA) as a standard. Briefly, the PWM was resuspended in 600µl of protein extraction buffer and homogenized for 1 min, then centrifuged for 15 min at 14,000 x g at 4℃. For cells, the cultures were washed with cold PBS twice and resuspended in 600µl of protein extraction buffer. Cells were then scraped from the culture flask. The supernatant was collected by centrifugation at 14,000 x g at 4ºC for 15 min and stored at -20ºC for further use.

The concentration of protein extracts was determined using a protein assay kit. Four different concentrations (0.06, 0.12, 0.24, and 0.48mg/ml) of BSA were prepared as protein standards. 10µl of each standard or sample and 200µl of protein assay dye reagent were added together to each well of a 96-well plate, and mixed thoroughly. The mixtures were incubated at room temperature for 10 min, and the absorbance at 595nm was measured using a microplate reader (GENios,

Tecan, Switzerland). The concentration of protein extract of the samples was determined according to the standard curve of BSA.

Aliquots of protein extracts (20 μg each) were heated to 100ºC for 3 min in 1x SDS gel-loading buffer to denature the proteins before they were separated by 10% sodium dodecyl sulphate-polyacrylamide gel electrophoresis (SDS-PAGE). Next, the proteins were transferred from the gel to the 0.2μm polyvinylidene fluoride (PVDF) membranes using a semi-dry electrophoretic transfer cell (Bio-Rad, USA). Membranes were washed with TBST buffer and then blocked with 5% non-fat milk in TBST for 1h at room temperature. Subsequently, the membranes were incubated with appropriate primary antibodies overnight at 4ºC in an orbital shaker. The primary antibodies used are as follows (Table 3): rabbit anti- phospho-p38, p38, phospho-ERK1/2, ERK1/2, phospho-JNK, JNK, TNF-α, IL-1β, TNF-R_1, IL-$1R_1$, phospho-p^{65} NF-kappaB, phospho-IkappaB-α, IkappaB-a, p^{65} NF-kappaB, M-CSF, CSF-1R and goat anti-rat CCR_2, MBP and mouse anti-β-actin. The following day, blots were incubated with secondary IgG antibody conjugated with horseradish peroxidase for 1h at room temperature. Equal amount of protein loading was confirmed by reprobing with total kinases or β-actin antibodies. Immunopositive bands were visualized by enhanced chemiluminescence, and quantified by scanning densitometer and Quantity One software, version 4.4.1 (Bio-Rad, USA).

2.7. Immunofluorescence labeling

2.7.1. Materials

All primary antibodies used in immunofluorescence labeling are listed in Table 3.

CY_3-conjugated goat anti-rabbit IgG (1:100; Sigma, Cat. No. AP307 F) lectin (1:100)

Fluorescein isothiocyanate (FITC) conjugated goat anti-mouse (1:100 Chemicon International; Cat. No. AP130F)

CY_3-conjugated sheep anti-rabbit IgG (1:100, Sigma; Cat. No.c2306)

FITC-conjugated goat-anti-rabbit secondary antibody (Chemicon, USA, AP307F)

FITC-conjugated donkey-anti-goat secondary antibody (Chemicon, USA, AP106F)

4', 6-diamidino-2-phenylindole dihydrochloride (DAPI) (Sigma, USA, Cat. No. D1306)

Fluorescent Mounting Medium (DakoCytomation, Denmark, Cat. No. S302380)

PBS (10X) (Invitrogen, USA, Cat. No. 14200166)

0.1M PBS containing 0.1% Triton-X 100 (PBS-TX)

4% paraformaldehyde (PF):

Paraformaldehyde (Sigma)	4g
0.1M phosphate buffer (pH 7.4)	100ml

2.7.2. Procedure for double immunoflourescence

2.7.2.1 Double immunoflourescence *in vivo*

Double immunofluorescence staining in the PWM from hypoxic rats along with their corresponding controls was carried out to confirm the cellular location of TNF-α, IL-1β, MCP-1, CCR_2, M-CSF, TNF-R_1, IL-1R_1 and CSF-1R expression. Coronal frozen sections of the brain at the level of optic chiasma of 40μm thickness were cut and rinsed in PBS. Endogenous peroxidase activity was blocked with 0.3% hydrogen peroxide in methanol for 30 min followed by rinsing with PBS. The sections were divided into five groups. The sections in the group Ⅰ were incubated with antibodies directed against TNF-α, IL-1β, MCP-1, CCR_2, M-CSF (Table 3) overnight in a humidified chamber. This and all incubations to follow were at room temperature. On the following day, the sections were washed, and incubated with secondary antibody: CY_3-conjugated goat anti-rabbit IgG (1:100; Sigma, Cat. No. AP307 F) for 1h. After this, the sections were washed and incubated with lectin (*Lycopersicon esculentum*; 1:100) for 1h. The sections in the group Ⅱ were incubated overnight with a cocktail mix of TNF-R_1, IL-1R_1 and monoclonal antibody against adenomatus polyposis coli (CC_1) (Table 3). CC_1 antibody specifically stains the cell bodies of oligodendrocytes (Jantaratnotai *et al*. 2003). Subsequent antibody detection was carried out with secondary antibodies: FITC-conjugated goat anti-mouse (1:100 Chemicon International; Cat. No. AP130F) for 1h. The sections were then washed and incubated with CY_3-conjugated sheep anti-rabbit IgG (1:100, Sigma; Cat. No.c2306) for 1h. The

sections in the group Ⅲ were incubated overnight with a cocktail mix of CSF-1R, TNF-α, IL-1β and GFAP (Table 3). Subsequent antibody detection was carried out with secondary antibodies: FITC-conjugated goat anti-mouse (1:100 Chemicon International; Cat. No. AP130F) or with CY_3-conjugated sheep anti-rabbit IgG (1:100, Sigma; Cat. No. 2306) for 1h. The sections in the group Ⅳ were incubated overnight with a cocktail mix of TNF-R_1, IL-$1R_1$ and NF-200 (Table 3) antibodies. NF-200 antibody specifically stains the axons. Subsequent antibody detection was carried out with secondary antibodies: FITC-conjugated goat anti-mouse (1:100 Chemicon International; Cat. No. AP130F) or with CY_3-conjugated sheep anti-rabbit IgG (1:100, Sigma; Cat. No.c 2306) for 1h. The sections in the group Ⅴ were incubated overnight with a cocktail mix of MBP and NF-200 (Table 3) antibodies. Subsequent antibody detection was carried out with secondary antibodies: FITC-conjugated donkey anti-goat (1:100 Santa Cruz Biotechnology; Cat. No.sc-2024) or with CY_3-conjugated sheep anti-mouse IgG (1:100, Sigma; Cat. No.c2181) for 1h. Following rinsing in PBS, the sections were mounted with a fluorescent mounting medium (DAKO Cytomation, Denmark). Cellular colocalization was examined in a confocal microscope (LSM FV1000; Olympus Company Pte Ltd, Tokyo, Japan).

2.7.2.2 Double immunoflourescence *in vitro*

For cultured microglial cells, the cells were treated with 3% oxygen for either 45 min (for c-Jun and phospho-c-Jun detection) or 4 h (for TNF-α, IL-1β, M-CSF or MCP detection). After the hypoxic treatment, the cells were fixed in 4%

paraformaldehyde for 30 min, blocked in 1% BSA for 30 min, and incubated with primary antibodies overnight at 4℃. Immunofluorescence labeling was carried out using primary antibodies directed against TNF-α, IL-1β, M-CSF or MCP, anti-phospho-c-Jun (Table 3). The cells were then incubated with CY_3-conjugated goat-anti-rabbit secondary antibody (1:100, Sigma; Cat. No. AP307 F) for 1h. After this, the cells used for the detection of TNF-α, IL-1β, M-CSF and MCP expression were washed and incubated with lectin (1:100) for 1h.

The cultured astrocytes were treated with M-CSF (25ng/ml) for 12h. After this, the cells were fixed in 4% paraformaldehyde for 30 min, blocked in 1% BSA for 30 min, and incubated with primary antibodies overnight at 4℃. Immunofluorescence labeling was carried out using primary antibodies directed against CSF-1R, TNF-α, IL-1β and GFAP (Table 3). The cells were then incubated with CY_3-conjugated goat-anti-rabbit secondary antibody (1:100, Sigma; Cat. No. AP307 F) or with FITC-conjugated goat anti-mouse (1:100 Chemicon International; Cat. No. AP130F) for 1h.

Finally, all the microglia or astrocytes were counterstained with DAPI and examined under a confocal microscope (LSM FV1000; Olympus Company Pte Ltd, Tokyo, Japan).

Quantitative analysis of the number of phospho-c-Jun nuclear positive cells was carried out through counting 8 randomly selected microscopic fields at X40 objective by a blinded observer. Each area contained about 40 cells in the control and microglial cultures treated with hypoxia. The cells with only blue nuclei were

counted as phospho-c-Jun negative, while those with blue nuclei overlapped with red were counted as phospho-c-Jun positive. The percentage of cells with positive expression for phosphor-c-Jun was calculated and averaged. Each experiment was done in triplicate.

2.8. Electron microscopy

The hypoxic rats and their corresponding controls were perfused with a mixed aldehyde fixative composed of 2% paraformaldehyde and 3% glutaraldehyde in 0.1M phosphate buffer, pH 7.2. After perfusion, the brain was removed and coronal slices (approximately 1mm thickness) were cut. Blocks of PWM were trimmed from these slices. Vibratome sections of 80-100 μm thickness were prepared from these blocks and rinsed overnight in 0.1M phosphate buffer. They were then postfixed for 2h in 1% osmium tetraoxide, dehydrated and embedded in Araldite mixture. Ultrathin sections were cut and viewed in a Philips CM 120 electron microscope.

2.9. Detection of oligodendrocyte apoptosis by fluorescence terminal deoxynucleotidyl transferase (Tdt)-mediated dUTP nick end labelling (TUNEL) assay

TUNEL assays were performed with an *in situ* cell death detection kit (Roche Diagnostics), according to the manufacturer's instructions. Briefly, frozen sections were incubated at room temperature with CC_1 antibody (Oncogene, mouse monoclonal IgG 1:20; Cat. No.OP80) overnight. Subsequent antibody detection was carried out with secondary antibody: CY_3-conjugated sheep anti-mouse IgG

(1:100, Sigma; Cat. No. C2181) for 1h at 37°C in the dark. Then, the sections were washed and added 50ul TUNEL reaction mixture on sample. They were incubated in a humidified atmosphere for 60 min at 37℃ in the dark. Subsequently, the sections were washed and counterstained with DAPI. Finally, they were mounted with a fluorescent mounting medium and examined under a confocal microscope. The number of total and TUNEL positive oligodendrocytes in the PWM was calculated through counting 8 randomly selected microscopic fields in sections obtained from each rat (n=3) at X60 objective by a blinded observer. The percentage of TUNEL positive oligodendrocytes against the total number of oligodendrocytes was calculated and averaged.

2.10. Cell counting and proliferation of AMC by lectin and 5-bromo-2'-deoxyuridine (BrdU) labeling

Lectin and BrdU labeling was used for cell enumeration and proliferation of AMC, respectively, in the PWM. BrdU (Sigma, MO, USA; Cat. No.B5002) was dissolved in 0.9% sodium chloride (10mg/ml) and injected intraperitoneally (100mg/kg) into neonatal rats 2h before sacrifice. The rats were anesthetized with 0.6% sodium pentobarbital, and then perfused transcardially with 4% paraformaldehyde in PBS (pH 7.4). The brain was removed and post-fixed in 4% paraformaldehyde for 2h at 4℃, stored in 15% sucrose in PBS overnight. Coronal frozen sections of the brain at 30μm thickness at the level of optic chiasma were cut. A total of 8 sections at 30μm thickness each separated by a distance of 180 μm were collected from each rat. Endogenous peroxidase activity was blocked

with 0.3% hydrogen peroxide in methanol for 30 min followed by rinsing with PBS. Subsequently, the sections were incubated in 2N HCl for 30 minutes at 37℃ to denature the DNA and then rinsed with PBS. They were incubated with mouse monoclonal antibody directed against BrdU (Sigma, MO, USA; Cat. No. B2531) overnight in a humidified chamber. On the following day, the sections were washed and incubated with secondary antibody: CY_3-conjugated sheep anti-mouse IgG (1:100; Sigma, MO, USA; Cat. No. c-2181) for 1h. After this, the sections were washed and incubated with lectin (1:100) for 1h. Following rinsing in PBS, they were mounted with a fluorescent mounting medium (DAKO Cytomation, Denmark). Cell number and proliferation were determined in a confocal microscope (LSM FV1000; Olympus Company Pte Ltd, Tokyo, Japan). Lectin as well as BrdU labeled microglial cells in the PWM were identified and enumerated in the corresponding areas in different rats (n=3). A total of 8 randomly selected microscopic fields (each measuring an area of 4.5 mm^2) at X40 objective from each section was scrutinized. Cells with a lectin (green) labeled fluorescent cell body overlapping with BrdU (red) labeled nucleus were counted as proliferating microglial cells, while those emitting only green fluorescence were nonproliferating microglial cells. The total number and percentage of proliferating microglial cells were calculated and averaged.

2.11. Intracerebral stereotactic injection of MCP-1

Wistar rats at 7 days of age were divided into sham-operated, vehicle (saline) injection and MCP-1 injection groups (n=8 for each respective group). Following

anesthetized with 6% sodium pentobarbital (60mg/kg), a scalp incision was made along the sagittal suture to access the skull, and a sharp beveled 10μl syringe needle was used to perforate the thin and soft skull. Four microlitres of MCP-1 protein (Chemicon; Cat.No. GF 041) dissolved in saline (100 μg/ml) or saline alone was stereotaxically injected into the PWM at the following coordinates: 1 mm posterior and 1 mm lateral to the bregma at a depth of 2 mm from the dural surface using a 10μl Hamiton syringe (Lehnardt *et al.* 2002). The tip of the needle was later confirmed in sections to reach the PWM of the above-mentioned rats. A hole was made on the skull of the sham-operated rats (*n*=8), but microinjections were not conducted. Rats were killed at 8 hours after injection.

2.12. Cell counting of AMC following MCP-1 injection labeled with lectin or OX-42.

The rats receiving MCP-1 intracerebral injection were anesthetized with 0.6% sodium pentobarbital, and then perfused transcardially with 4% paraformaldehyde in PBS (pH 7.4). The brain was removed and post-fixed in 4% paraformaldehyde for 2h at 4℃, stored in 15% sucrose in PBS overnight. Coronal frozen sections of the brain at 30μm thickness at the level of optic chiasma were cut. Lectin or OX-42 labeled AMC along and around the needle track in the PWM were identified and counted. Four sections (30μm thick) each separated by a 90μm interval derived from MCP-1 injected and sham-operated rats were examined for labeled cells. Endogenous peroxidase activity was blocked with 0.3% hydrogen peroxide in methanol for 30 min followed by rinsing with PBS. The tissue

sections labeled with lectin were then incubated with lectin (1:100) for 1h at room temperature. Following rinsing in PBS, they were mounted with a fluorescent mounting medium (DAKO Cytomation, Denmark).

However, lectin labeled both microglia and blood vessels. Therefore, OX-42, another microglial marker which does not recognize blood vessels, was used to stain microglial cells. The tissue sections labeled with OX-42 were then incubated with mouse monoclonal antibody directed against OX-42 (1:100; Harlan-Sera-Laboratory, Loughborough, UK; Cat. No.O-MAS 370b) overnight in a humidified chamber. On the following day, the sections were washed and incubated with secondary antibody: FITC-conjugated rabbit anti-mouse IgG (1:100; Chemicon International; Cat. No.F9137) for 1h. After this, they were washed and mounted with a fluorescent mounting medium (DAKO Cytomation, Denmark).

Cell counting was carried out under a confocal microscope (LSM FV1000; Olympus Company Pte Ltd, Tokyo, Japan). Lectin or OX-42 positive microglial cells around the needle track in the PWM and in the corresponding area on the contralateral side was enumerated in 4 randomly selected microscopic fields (each measuring 4.5 mm^2) from 8 rats, respectively, at X 40 objective.

2.13. ELISA

2.13.1. Materials

MCP-1 ELISA kit (Pierce, USA, Cat. No. ERMCP1)

ELISA plate reader (Molecular Devices, USA)

2.13.2. Analysis of MCP-1 by ELISA

For the PWM, tissue proteins were extracted using protein extraction kit according to the manufacturer's protocol. Protein concentrations were determined by the Bradford method (Bradford 1976) using BSA (Sigma-Aldrich, MO, USA) as a standard. For microglial cultures, cells were subjected to hypoxia exposure for 1, 2, 4 and 6h or hypoxia plus BAY 11-7082 (10mM; Calbiochem, San Diego, CA, USA) for 4 h, and the culture medium from each experiment was collected. MCP-1 concentration in the PWM or released from microglial cells in the culture medium was measured using the rat MCP-1 ELISA kit (Pierce, Rockford, IL, USA; Cat. No. ERMCP1) according to the manufacturer's protocol. Briefly, samples including standards of known MCP-1 content were incubated in 96-well plates coated with MCP-1 antiserum for 2 h. The samples were treated in subsequent steps with enzyme working reagent for 30 min and tetramethylbenzidine One-Step substrate reagent for 30 min in the dark and the reaction plates were read within 30 min in an ELISA plate reader (Molecular Devices, Eugene, OR, USA) at 450 nm.

2.14. Chemotaxis

2.14.1. Materials

48-well Boyden. microchamber (Neuro Probe, USA, Cat. No. AP48)

Fibronectin (BD bioscience, USA, Cat No: 354008)

2.14.2. Procedure

In vitro migration of microglia in response to microglia conditioned medium was assessed using polyvinylcarbonate-free membranes with 10 μm pore size in a modified 48-well microchemotaxis Boyden chamber (Neuroprobe, Cabin John, MD, USA) as described previously (Cross and Woodroofe 1999b;Zhou *et al.* 2007a). The membrane was coated with 20 μg/mL of fibronectin (BD Bioscience, Bedford, MA, USA; Cat. No. 354008) for 24 h. Microglial cells were plated at 2.5×10^5 per well on a 24 multi-well culture dish for 24h and incubated with 3% oxygen for 4 h. To examine the chemotactic migration of microglia, 28 μL of DMEM or conditioned medium collected from the control and hypoxia treated microglial cultures was added to the lower chambers. In addition, rabbit anti-MCP-1 antiserum (10 μg/mL; Cytolab, Rehovot, Israel; Cat. No. 500-P76) or another unrelated antiserum raised in rabbit (10 μg/mL; anti-iNOS; Chemicon; Cat. No. AB5382) as the control was added in the hypoxia-treated microglia conditioned medium in the lower chambers to test the neutralization effects of anti-MCP-1.

Microglial cells (1×10^6/mL) in 50 μL of serum free migration medium, DMEM and 0.5% BSA were incubated in the upper chambers for 6 h at 37°C in a humidified atmosphere of 5% CO_2 and 95% air. At the end of experiment, the upper surfaces of membranes were scraped free of cells and debris, fixed in 4% paraformaldehyde and stained using crystal violet. Cells that had migrated through

pores and adhered to the lower surfaces of the membranes were counted under the light microscope and photographed.

2.15 Statistical Analysis

The data of experiments were presented as mean ±standard deviation (SD). The SD was calculated using the formula given below:

$$SD=\sqrt{\frac{\sum x^2-\left(\sum x\right)^2/n}{n-1}}$$

Where, x = individual observation, and n = number of observations

Statistical significance was evaluated by the Student's *t*-test. Results were considered as significant at $p<0.05$.

Chapter 3

Results

3.1 Real time RT-PCR analysis of TNF-α, IL-1β, TNF-R_1 and IL-1R_1, M-CSF, CSF-1R, MCP-1 and CCR_2 mRNA expression in the PWM

The location of PWM is shown in Fig.1. TNF-α mRNA expression was significantly increased in the PWM at 3 and 24 h , 3 and 7d after the hypoxic exposure in comparison with the corresponding controls ($p < 0.05$) (Fig 2A). Increase in IL-1β mRNA expression paralleled that of TNF-α mRNA after the hypoxic exposure at 3 and 24 h, 3 and 7d as compared with the corresponding controls ($p < 0.05$) (Fig 2B). There was no significant change in mRNA expressions of TNF-α and IL-1β at 14d after hypoxia when compared with the corresponding control rats (Fig 2A, B). TNF-R_1 mRNA expression remained relatively unchanged at 3 and 24h (Fig 2C), but was markedly increased at 3d and was sustained till 14d in hypoxic rats when compared with the controls ($p < 0.05$) (Fig 2C). Increased IL-1R_1 mRNA expression was first observed at 24h peaking at 3d and was maintained at a high level till 14d after the hypoxic exposure in comparison with the controls ($p < 0.05$) (Fig 2D). There was no significant change in IL-1R_1 mRNA expression at 3h after the hypoxic exposure when compared with the corresponding control rats (Fig 2D). M-CSF mRNA expression was significantly increased in the PWM at 3 and 24 h, 3 and 7d after the hypoxic exposure in comparison with the corresponding controls ($p < 0.05$) (Fig 3A). There was no significant change in mRNA expression of M-CSF at 14d after hypoxia when compared with the corresponding control rats (Fig 3A). CSF-1R mRNA expression remained relatively unchanged at 3h (Fig 3B), but was

markedly increased at 24h and was sustained till 14d in hypoxic rats when compared with the controls ($p < 0.05$) (Fig 3B). MCP-1 and CCR_2 mRNA expression levels were significantly increased in the PWM at 3, 24 h, 3 and 7d after the hypoxic exposure in comparison with the corresponding controls (Fig 3C, D)($p < 0.05$). There was no significant difference between the mRNA expression of MCP-1 and CCR_2 at 14d when compared with the corresponding control rats (Fig 3A).

3.2 Western blotting or ELISA analysis of TNF-α, IL-1β, TNF-R_1 and IL-1R_1, M-CSF, CSF-1R, MCP-1 and CCR_2 protein expression in the PWM

The immunoreactive bands of TNF-α and IL-1β protein levels that appeared at approximately 30kDa and 17 kDa, respectively (Fig 4A), increased significantly ($p < 0.05$) in optical density at 3 , 24 h, 3 ,7 and 14 d after hypoxic exposure as compared with the controls (Fig 4B and Fig 4C). The immunoreactive band of TNF-R_1 protein levels appeared at approximately 55kDa (Fig 4A). The optical density was increased significantly ($p < 0.05$) at 7 and 14 d after hypoxic exposure as compared with the controls (Fig 4D). However, there was no expression of TNF-R_1 protein at 3, 24h and 3d in the both hypoxic and control rats. The immunoreactive band of IL-1R_1 protein levels appeared at approximately 80kDa (Fig 4A). It was augmented significantly ($p < 0.05$) at 24h, 3, 7 and 14 d after hypoxic exposure when compared with the controls (Fig 4E). There was no significant change in protein expression of IL-1R_1 at 3h after the hypoxic exposure

when compared with the corresponding control rats.

The immunoreactive band of M-CSF protein levels that appeared at approximately 18.5kDa (Fig 5A), increased significantly ($p < 0.05$) in optical density at 3 , 24 h, 3, 7 and 14d after hypoxic exposure as compared with the controls (Fig 5A, B). The immunoreactive band of CSF-1R protein level, appeared at approximately 170kDa (Fig 5A), was augmented significantly ($p < 0.05$) at 24h, 3, 7 and 14 d after hypoxic exposure when compared with the controls (Fig 5A, C). There was no significant difference between the protein expression of CSF-1R at 3h after the hypoxic exposure when compared with the corresponding control rats. ELISA analysis showed that MCP-1 protein release was significantly increased at 3, 24h, 3 and 7d after the hypoxic exposure as compared with the corresponding controls (Fig 5F) ($p < 0.05$). There was no significant change in the protein release of MCP-1 at 14d after the hypoxic exposure when compared with the corresponding control rats. The immunoreactive bands of CCR_2 protein levels that appeared at approximately 47kDa (Fig 5D), increased significantly ($p < 0.05$) in optical density at 3 , 24 h, 3 and 7 d after hypoxic exposure as compared with the controls (Fig 5D, E).

3.3 Cellular localization of TNF-α, IL-1β, TNF-R_1 and IL-1R_1, M-CSF, CSF-1R, MCP-1 and CCR_2 protein expression in the PWM by double labeling

In the PWM of the control rats sacrificed at 24h, TNF-α as well as IL-1β expression was specifically detected in sporadic cells, confirmed to be the AMC

by double labelling with lectin staining (Fig 6 A-C, G-I). At 24 h following hypoxic exposure, immunoreactivity for TNF-α and IL-1β was detected and enhanced in large numbers of AMC (Fig 6 D-F, J-L) when compared with the controls (Fig 6 A-C, G-I). However, there was no noticeable change in TNF-α and IL-1β expression in the astrocytes at 24h after the hypoxic exposure (Fig 7 D-F; Fig 8 D-F) when compared with the corresponding control rats (Fig 7 A-C; Fig 7 A-C). In the PWM of the control rats sacrificed at 7 and 14d, TNF-α and IL-1β immuno expression was detected in occasional cells, confirmed to be the astrocytes by double labeling with GFAP (Fig 7 A-C, G-I, M-O; Fig 8 A-C, G-I, M-O). At 7 and 14d following hypoxic exposure, very intense TNF-α and IL-1β immunoreactivity was detected in large numbers of astrocytes which appeared hypertrophic (Fig 7 J-L, P-R; Fig 8 J-L, P-R) when compared with the controls (Fig 7 G-I, M-O; Fig 8 G-I, M-O).

Expression of TNF-R_1 and IL-$1R_1$ was localized in the soma of occasional oligodendrocytes as confirmed by double immunofluorescence showing colocalization of CC_1 (Fig 9 A-L). At 7d following hypoxic exposure, immunoreactivity for TNF-R_1 and IL-$1R_1$ was markedly enhanced in the soma of oligodendrocytes (Fig 9 D-F, J-L) as compared with the control (Fig 9 A-C, G-I). In the control rats at 14 days, moderate TNF-R_1 and IL-$1R_1$ immunofluorescence was localized in some small cells as well as the axons as confirmed by double immunofluorescence showing colocalization of NF-200 (Fig 10 A-C, G-I). Following hypoxic exposure, TNF-R_1 and IL-$1R_1$ immunoreactivity was markedly

enhanced being more conspicuous along the closely packed axons (Fig 10 D-F, J-L).

In the PWM of the control rats, moderate M-CSF expression was specifically detected in sporadic cells, confirmed to be the AMC by double labelling with lectin staining (Fig 11 A-C, G-I). At 3 and 7d following hypoxic exposure, M-CSF immunoreactivity was enhanced in AMC (Fig 11 D-F, J-L) when compared with the controls (Fig 11 A-C, G-I). CSF-1R expression was barely detected in the astrocytes in the control rats (Fig 12 A-C, G-I) as confirmed by its co-localization with GFAP. At 7 and 14d following hypoxic exposure, CSF-1R immunoreactivity was markedly enhanced in the astrocytes (Fig 12 D-F, J-L).

In the control rats, MCP-1 and CCR_2 expression was specifically detected in the AMC as confirmed by double labeling with lectin (Fig 13 A-L, Fig 14 A-L, Fig 15 A-L). At 3, 24 h, 3 and 7d following hypoxic exposure, intense MCP-1 immunoreactivity was induced in large numbers of AMC (Fig 13 D-F, J-L; Fig 14 D-F, J-L) when compared with the controls (Fig 13 A-C, G-I; Fig 14 A-C, G-I). At 3 h and 3d following hypoxic exposure, immunoreactivity for CCR_2 was detected and enhanced in large numbers of AMC (Fig 15 D-F, J-L) when compared with the controls (Fig 15 A-C, G-I).

3.4 MBP and NF-200 protein expression in the PWM

MBP and NF-200 protein expression was significantly decreased in the

PWM at 14 days after the hypoxic exposure in comparison with the corresponding controls (Fig 16 A-H). The immunoreactive bands of MBP protein levels (Fig 16 A), decreased significantly ($p < 0.05$) in optical density at 14 d after hypoxic exposure as compared with the controls (Fig 16 A, B). However, MBP protein expression was undetected at 3 and 24h, 3 and 7 days in both the hypoxic and control rats. Confocal images showed that the MBP positive processes and NF-200 positive axons were extensively disrupted following the hypoxic exposure (Fig 16 F, G) as compared with the control (Fig 16 C, D).

3.5 Apoptosis of oligodendrocytes in the PWM

Immunoreactive CC_1 labeled oligodendrocytes characterized by an oval cell body were identified in the PWM in the control rats (Fig 17A-C). There was less evidence of cells marked by TUNEL labeling (Figure 17 B). Following hypoxia exposure, however, CC_1 immunoreactive cells showing TUNEL labeled nucleus were increased significantly (Fig 17 D-F). The percentage of TUNEL positive oligodendrocytes at 7d following hypoxic exposure was significantly higher than that in the corresponding controls (Fig 17 G). Another salient feature in the hypoxic rats was that the number of CC_1 positive immunoreactive oligodendrocytes/mm^2 was decreased significantly (Fig 17 D-F, H).

3.6 Ultrastructural observations

Apoptotic and necrotic cells were common features in the PWM of hypoxic rats at 24h, 3 and 7d (Fig 18 A-D). Necrotic cells were characterized by swollen

and vacuolated cytoplasm, disrupted organelles, and disintegrated membranes in the PWM at 24h (Fig. 18 A) and 7d (Fig. 18 C) after the hypoxic exposure. Apoptotic cells which occurred in the PWM at 24h (Fig. 18 B) and 7d (Fig. 18 C) after the hypoxic exposure exhibited nuclear shrinkage and chromatin condensation. Both degenerating cell types appeared to be phagocytosed by the AMC (Fig 18 E-F). Both apoptotic and necrotic cells were rarely encountered in the PWM of the control rats. The most striking structural alteration after the hypoxic exposure was swelling of a variable number of axons which appeared club shaped in sections throughout the period of study (Fig 19 A, C). Many of the dilated axons were vesiculated (Fig 19 A, C). Hypoxia also affected the myelinated axons which appeared distorted (Fig 19 B, D). In some sectional profiles, myelin-like figures appeared to be internalized in the axoplasm (Fig 19 B, D).

3.7 Increase in cell numbers of AMC in the PWM in hypoxic neonatal rats

The number of AMC was significantly increased in the PWM at 3, 24h, 3 and 7d after the hypoxic exposure in comparison with the corresponding controls (Fig 20 A-L; Fig 20 M; Fig 21 A-L; Fig 21 M)($p < 0.01$). Very few AMC were double labeled with lectin and BrdU at 3, 24h and 3d after the hypoxic exposure and the matching controls (Fig 20 A-L; Fig 21 A-F) ($p < 0.01$). There was no significant difference in the proliferation rate of microglia at these time points between the hypoxic rats and the corresponding controls (Fig 20 N; Fig 21 N). The rate was determined by the ratio between double labeled cells against microglia labeled by

lectin only. More lectin labeled AMC were BrdU immunoreactive at 7d after the hypoxic exposure in comparison with the control (Fig 21 G-L). The proliferation rate of AMC in the hypoxic rats was significantly increased as compared with the controls (Fig 21 N) ($p < 0.01$).

3.8 MCP-1 induced microglial migration in vivo

Lectin or OX-42 labeling showed a large accumulation of microglial cells around the needle track in the PWM of 7d old rats receiving MCP-1 injection (Fig 22 G-H; Fig 23 G-H) when compared with those given saline injection or sham-operated rats (Fig 22 A-B, D-E, J; Fig 23 A-B, D-E, J). More microglial cells were observed in the PWM ipsilateral to MCP-1 injection when compared to the corresponding areas on the contralateral side (Fig 22 G-J; Fig 23 G-J). In rats given saline injection, the number of microglial cells along the needle track was not significantly different from the corresponding areas contralaterally (Fig 22 D-F, J; Fig 23 D-F, J).

3.9 In vitro mRNA and protein expression of TNF-α, IL-1β, M-CSF and MCP-1 in activated microglia under hypoxic conditions

An upregulation of TNF-α mRNA expression was observed at different time points after hypoxia peaking at 2h ($p < 0.05$) when compared with the matching controls (Fig 24 A). The IL-1β mRNA expression was likewise increased after the hypoxic exposure peaking at 1 h as compared with the controls ($p < 0.05$) (Fig 24 B). M-CSF mRNA (Fig 24 C) expression was significantly upregulated peaking at

4h ($p < 0.05$) after the hypoxic exposure when compared with the controls. MCP-1 mRNA expression was significantly increased at different time points after hypoxia peaking at 4h ($p < 0.05$) when compared with the matching controls (Fig 24 D).

Upregulation of TNF-α protein peaking at 4h ($p < 0.05$) after the hypoxic exposure was observed when compared with the controls (Fig 25 A, B). The IL-1β protein quantity also increased significantly after the hypoxic exposure peaking at 4h as compared with the controls ($p < 0.05$) (Fig 25 A, C). Double immunofluorescence labeling showed that the lectin labeling in microglial cells was completely co-localized with TNF-α and IL-1β expression (Fig 26 A-L). At 4h after hypoxia, the expression of TNF-α and IL-1β in microglial cells was increased significantly (Fig 26 D-F, J-L) in comparision with the control cells (Fig 26 A-C, G-I).

M-CSF protein (Fig 25 A, D) expression was significantly upregulated peaking at 4h ($p < 0.05$) after the hypoxic exposure when compared with the controls. Double immunofluorescence labeling showed that the lectin labeling in microglial cells was completely co-localized with M-CSF expression (Fig 27 A-F). At 4h after hypoxia, M-CSF immunofluorescence in microglial cells was markedly increased (Fig 27 D-F) in comparison with the control cells (Fig 27 A-C).

MCP-1 protein release as revealed by ELISA at 1, 2, 4 and 6h after the hypoxic exposure peaking at 4h ($p < 0.05$) was augmented when compared with

the controls (Fig 25 E). Double immunofluorescence labeling showed that lectin labeling in microglial cells was completely co-localized with MCP-1 expression (Fig 27 G-L). At 4h after hypoxia, MCP-1 immunoexpression in AMC was markedly increased (Fig 27 G-I) in comparision with those in the control rats (Fig 32 J-L).

3.10 Hypoxia induced the TNF-α and IL-β production via activation of MAP kinase pathway in activated microglia

MAP kinase signaling transduction pathway plays a significant role in inducing the expression of inflammatory genes in many immune cell types. We, therefore, examined whether hypoxia induced the activation of MAP kinases in primary microglial cultures. Western blot analysis showed that the hypoxia treatment induced rapid and time-dependent phosphorylation of JNK (Fig 28 A, H) and p38 (Fig 28 B, I) in microglial cells. The phosphorylated JNK and p38 levels increased at 30 min and gradually declined to basal levels at 4h. In addition, hypoxia treatment induced phosphorylation of ERK1/2 in microglial cells (Fig 28 C, J). The phosphorylated ERK level was increased to peak at 30min of incubation. Unlike JNK and p38, however, ERK1/2 level was only moderately decreased at 1, 2 and 4h after hypoxia. Since JNK mediates N-terminal phosphorylation of c-Jun, effect of hypoxia on the c-Jun phosphorylation was examined. Phospho-c-Jun immunoreactivity was detected in a few microglial cells in the control. It was markedly induced in a majority of microglial cells in cultures treated with 3% oxygen (Fig 29 D-F) when compared with the controls (Fig 29 A-C). The

percentage of phospho-c-JUN positive microglial cells treated with 3% oxygen was significantly higher than the controls (Fig 29 G) ($p < 0.01$). Majority of the microglial cells exhibited total c-Jun immunoreactivity, and the treatment of hypoxia did not affect the total c-Jun immunoreactivity in microglial cells.

It was hypothesized that hypoxia induced TNF-α and IL-1β production in activated microglial cells by altering the MAP kinase pathways. In order to address this, TNF-α and IL-1β productions were measured by Western blotting in hypoxia-induced microglial cells exposed to pharmacological agents, SP600125 and SB203580, which are selective inhibitors of JNK and p38, respectively. Incubation of microglial cells with SP600125 or SB203580, 30min prior to hypoxia treatment for 4h decreased the hypoxia-induced TNF-α and IL-1β expression (Fig 28 D, K; F, M; E, L; G, N).

3.11 Hypoxia induced MCP-1 production via activation of NF-kappaB signaling pathway in microglia

Western blot analysis showed that hypoxia induced rapid and time-dependent increase in NF-kappaB (Fig 30 B, F) (*$p< 0.05$) and phosphorylation of NF-kappaB (Fig 30 A, E) (*$p< 0.05$). The NF-kappaB and phosphorylated NF-kappaB levels increased at 15 min peaking at 1h. In addition, hypoxia treatment induced rapid degradation of phosphorylated IkappaB whose level declined gradually at 15, 30 min, 1 and 2h after hypoxic exposure (Fig 30 C, G)(*$p< 0.05$). There was no significant difference in the expression of IkappaB at

different time points after hypoxic exposure when compared with the controls (Fig 30 D, H) (**p> 0.05).

It was hypothesized from the above results that hypoxia induced MCP-1 production in activated microglial cells was via the NF-kappaB signaling pathways. To ascertain this, MCP-1 production was measured by ELISA in hypoxia-induced microglial cells culture medium exposed to the pharmacological agent, BAY, a selective inhibitor of NF-kappaB. Incubation of microglial cells with BAY, 30min prior to hypoxia treatment for 4h, decreased the hypoxia-induced MCP-1 release (Fig 30 I) (*$p < 0.05$).

3.12 TNF-α, IL-1β and CSF-1R mRNA and protein expression in activated astrocytes after M-CSF treatment

An upregulated TNF-α mRNA expression was observed at 3, 6 and 12h after M-CSF treatment peaking at 3h ($p < 0.05$) when compared with the matching controls (Fig 31 A). IL-1β mRNA expression was concomitantly increased peaking at 3 h as compared with the controls ($p < 0.05$) (Fig 31 B). There was no significant change in the expression levels of TNF-α and IL-1β mRNA at 24h when compared with the corresponding controls (Fig 31 A, B). CSF-1R mRNA expression was significantly increased at different time points following treatment with M-CSF peaking at 12h ($p < 0.05$) when compared with the matching controls (Fig 31 C). Upregulation of TNF-α protein level peaking at 3h ($p < 0.05$) after the hypoxic exposure was observed when compared with the controls (Fig 31 D, E).

IL-1β protein level also increased significantly after the hypoxic exposure peaking at 3h as compared with the controls ($p < 0.05$) (Fig 31 D, F). CSF-1R protein levels were increased significantly ($p < 0.05$) at 3, 6, 12 and 24h with M-CSF treatment when compared with the control (Fig 31 D, G). Double immunofluorescence labeling showed that GFAP labeling in the astrocytes was completely co-localized with TNF-α, IL-1β and CSF-1R expression (Fig 32 A-R). At 12h, TNF-α, IL-1β and CSF-1R immunofluorescence in the astrocytes was greatly intensified (Fig 32 D-F, J-L, P-R) in comparison with the control cells (Fig 32 A-C, G-I, M-O).

3.13 Increased TNF-α and IL-β production in activated astrocytes after M-CSF treatment was via activation of MAP kinase pathway

Whether MAP kinases were activated in primary astrocytes cultures after M-CSF treatment was further examined. Western blot analysis showed that the treatment with M-CSF induced rapid and time-dependent phosphorylation of JNK (Fig 33 A, H) in the astrocytes. The phosphorylated JNK levels increased at 15 min and gradually declined to basal levels at 2h. However, the time-dependent phosphorylation of p38 was not observed in the astrocytes after M-CSF treatment (Fig 33 B, I). In addition, treatment with M-CSF induced phosphorylation of ERK1/2 in the astrocytes (Fig 33 C, J). The phosphorylated ERK level peaked at 15min after M-CSF treatment, but unlike JNK, ERK1/2 level was only moderately decreased at 1 and 2h.

It was hypothesized that TNF-α and IL-1β production induced after M-CSF treatment in activated astrocytes was mediated by the MAP kinase pathways. To ascertain this, TNF-α and IL-1β production was measured by Western blotting in M-CSF-treated astrocytes exposed to pharmacological agents, SP600125 and SB203580, which are selective inhibitors of JNK and p38, respectively. Incubation of astrocytes with SP600125, 30 min prior to treatment with M-CSF for 3h decreased the M-CSF treatment-induced TNF-α and IL-1β expression (Fig 33 D, K; Fig 33 E, L). However, incubation of astrocytes with SB203580, 30 min prior to treatment with M-CSF for 3h did not alter the M-CSF treatment-induced TNF-α and IL-1β expression (Fig 33 F, M; Fig 33 G, N). This indicates that TNF-α and IL-β production induced in activated astrocytes after M-CSF treatment was via activation of JNK-MAP kinase pathway.

3.14 Migration of microglia to medium derived from microglial culture subjected to hypoxia

The chemotactic effects of the conditioned-medium derived from the control (untreated) microglial culture, microglia culture treated with hypoxia with or without anti-MCP-1 antiserum on the migration of microglial cells were next investigated. Only a few crystal violet-stained microglia transmigrated through the membrane of insert in a transwell chamber in the DMEM medium (Fig.34A, B). The conditioned-medium derived from hypoxia-treated microglial cultures attracted significantly more migratory microglial cells than the control medium (Fig.34A, B). The number of hypoxia-induced transmigrated microglia, however,

was markedly reduced in hypoxia + anti-MCP-1 antiserum medium (Fig.34A, B). When the hypoxia-treated medium was treated with an unrelated antiserum from the same species of anti-MCP-1 as the control, the migration of microglia was not affected (Fig.34A, B) (*$p < 0.01$).

Chapter 4

Discussion

PWMD refers to damage of the immature deep cerebral white matter peripheral to the lateral ventricles, occuring in the perinatal period (Folkerth *et al.* 2004). Inflammatory response induced by various stimuli has been recognized as a common feature in the pathogenesis of PWMD (Chew *et al.* 2006). Production of inflammatory mediators such as cytokines, chemokines and free radicals has been thought to be associated with PWMD (Folkerth 2006; Chew *et al.* 2006). Activated microglia and astrocytes release inflammatory mediators under pathological conditions. Studies have shown that besides microglial cells in the brain, astrocytes have the ability to produce inflammatory mediators (such as TNF-α) and free radicals (Sawada *et al.* 1995). A large number of cytokines and chemokines produced by activated microglial cells or astrocytes execute noxious effects on developing oligodendrocytes progenitors and axons through their respective receptors.

4.1 Microglia are activated and induce a robust and persistent inflammatory response in the PWM in hypoxic neonatal rats

It has been well documented that hypoxia is an important stimulus that initiates an inflammatory response with enormous production of inflammatory chemokines and cytokines (Carloni *et al.* 2006; Guo and Bhat 2006; Saed *et al.* 2005). Microglia activation with overproduction of inflammatory cytokines, free radicals, NO and excess glutamate release is a hallmark feature in the development of hypoxic brain injury. It is well established that microglial cells are activated and involved in hypoxia-induced damage in the developing brain (Kaur

et al., 2008; Li et al., 2008b; Li et al., 2009). Activated microglia can change their cellular morphology, proliferate, potentiate phagocytosis, actively migrate to the site of injury, and produce various factors including growth factors, NO, cytokines, and chemokines and thereby cause an inflammatory response (Farber and Kettenmann, 2006; Dheen et al., 2007; Hanisch and Kettenmann, 2007). Concomitantly, activated microglia produce other molecules such as syndecan-2 and exhibit enhanced expression of ion channels such as Kv1.2 and Kv1.1 (Li *et al.* 2008a; Kaur *et al.* 2009; Wu *et al.* 2009). All these would further promote the release of inflammatory cytokines, chemokines and ROS by microglia and greatly amplify the brain injury in the hypoxic neonatal rats (Li *et al.* 2008a; Kaur *et al.* 2009; Wu *et al.* 2009).

In addition to inflammatory cytokines and chemokines, recent studies have also demonstrated that the expression of N-methyl-D-aspartic acid (NMDA) receptors is upregulated on the microglia in hypoxic conditions (Kaur *et al* 2006). Immunostimulated microglia are reported to aggravate the NMDA receptor-induced excitotoxicity by expression of iNOS (Kaur *et al* 2006). Microglial cells also express α-amino-3-hydroxy-5-methyl-4-isoxazole propionic acid -kainate (AMPA-KA) receptors (Noda *et al.* 2000; Sivakumar V *et al* 2009), the activation of which increases the generation of TNF-α which induces oligodendrocyte death (Selmaj *et al.* 1988; Louis *et al.* 1993), destruction of myelin sheath and the dysfunction of axons (Merrill *et al.* 1996).

The present study has shown an up-regulation of TNF-α, IL-1β, MCP-1 and

M-CSF mRNA expression in the PWM of neonatal rats following a hypoxic exposure up to 7d suggesting that an inflammatory response occurs in the PWM of neonatal rats after hypoxic insult. ELISA analysis showed that MCP-1 protein release was significantly increased up to 7d after the hypoxic exposure. Western blotting results have further demonstrated that protein expression of TNF-α, IL-1β and M-CSF in the PWM was increased throughout the period of study i.e. up to 14d in hypoxic rats. However, there was no significant difference between the mRNA expressions of TNF-α, IL-1β and M-CSF at 14d in hypoxic rats when compared with the corresponding control rats. A possible explanation is that TNF-α, IL-1β and M-CSF protein synthesis occurs later than their mRNA expression. Double immunofluorescence staining has shown that expression of TNF-α, IL-1β, MCP-1 and M-CSF was detected in AMC as verified by their co-localization with lectin, a cellular marker for microglial cells. AMC expressed TNF-α, IL-1β, MCP-1 and M-CSF up to 7 days in hypoxic rats. This suggests that in the evolution of inflammation in the developing brain, the AMC would be the main cellular source for proinflammatory chemokine and cytokine production up to 7 days after hypoxic insult. Concomitantly, the present study has also found an up-regulated TNF-α and IL-1β expression in the astrocytes in the same brain area at 7 and 14d following a hypoxic exposure. It has been reported that under inflammatory conditions microglia may be responsible for the early phase of inflammatory response and astrocytes may contribute to inflammatory response at later stages (Sawada *et al.* 1995). Taken together, this suggests that in the

progression of inflammation in the white matter in the developing brain, while the AMC play major role at an early stage or acute phase in production of TNF-α, IL-1β, MCP-1 and M-CSF, the astrocytes would be the main cellular source for proinflammatory cytokine production at a late stage i.e 7-14d after hypoxic insult.

4.2 *In vitro* Hypoxia induce microglia release TNF-α, IL-1β, MCP-1 and M-CSF

Hypoxia is a known activator of microglial cells. The present *in vitro* study has found that the mRNA and protein expression of inflammatory chemokines and cytokines such as TNF-α, IL-1β, MCP-1 and M-CSF in cultured microglia was increased significantly after hypoxia exposure for 4h. This suggests that hypoxia can elicit isolated microglia to produce inflammatory cytokines and chemokines directly.

4.2.1 MCP-1 is released by activated AMC via NF-kappaB signaling pathway under hypoxic conditions

It has been reported recently that NF-kappaB proteins function as dimeric transcription factors that control genes regulating a broad range of biological processes including inflammation, stress responses, innate and adaptive immunity (Li and Verma 2002;Pomerantz and Baltimore 2002). Under physiological conditions, NF-kappaB proteins are bound and inhibited by IkappaB proteins (Karin *et al.* 2002). Under pathological conditions, IKK complexes (IKKβ, IKKα and NEMO) are activated, which phosphorylate IkappaB proteins. Phosphorylation of IkappaB leads to its rapid ubiquitination and proteasomal

degradation, freeing NF-kappaB (Ghosh and Karin 2002). Active NF-kappaB proteins are subsequently phosphorylated, then translocated to the nucleus where they induce target gene expression (Pahl 1999). The present results have demonstrated that the NF-kappaB and phosphorylated NF-kappaB levels were markedly increased at 1h but gradually declined to basal levels at 2h in hypoxic microglial cells. The phosphorylated IkappaB was gradually degraded at each time point after hypoxic exposure in the microglial cells. Incubation of microglial cells with BAY 11-7082, a selective inhibitor of NF-kappaB (Ohkita *et al.* 2002), 30 minutes prior to hypoxia treatment for 4h decreased the hypoxia-induced MCP-1 release. On the basis of this, we speculate that hypoxia induced release of MCP-1 from microglial cells in the PWM occurs through NF-kappaB signaling pathway.

4.2.2 TNF-α and IL-1β are produced by activated AMC via MAP kinase pathway under hypoxic condition

Recently, MAP kinase pathway has been identified as being responsible for inducing inflammatory gene expression (Bhat *et al.* 1998; Da *et al.* 1997; Won *et al.* 2001). Members of MAP kinase family include three subgroups: c-Jun N-terminal kinase/stress-activated protein kinase (JNK/SAPK), p38 MAP kinase and extracellular signal regulated kinase (ERK) (Hommes *et al.* 2003b). The JNK and p38 are cell stress and inflammation activated pathways that are associated with the regulation of cell apoptosis and inflammatory cytokine production (Kyriakis *et al.* 1994a; Lee *et al.* 1994). The ERK signalling pathway is involved in cell growth, proliferation and survival (Chang and Karin 2001). The JNK, p38

and ERK kinases are activated by phosphorylation of both tyrosine and threonine residues which are phosphorylated by specific upstream MAP kinase (Park *et al.* 2002). Usually these phosphorylated MAP kinases result in the phosphorylation and subsequent activation of transcription factors, producing corresponding gene transcription (Hommes *et al.* 2003). The present results have demonstrated that the phosphorylated JNK and p38 levels were markedly increased at 30 min and gradually declined to basal levels at 4h in hypoxic microglial cells. The phosphorylated ERK level was increased to peak at 30min of hypoxic treatment. However, unlike JNK and p38, ERK1/2 level was found to be decreased only moderately after hypoxic exposure at 1, 2 and 4h. The c-Jun phosphorylation was markedly induced in a majority of microglial cell nuclei in cultures treated with 3% oxygen for 45 min as compared with control microglial cells. Incubation of microglial cells with SP600125 or SB203580 which are selective inhibitors of JNK and p38, respectively, 30min prior to hypoxia treatment for 4h decreased the hypoxia-induced TNF-α and IL-1β release. On the basis of this, we suggest that hypoxia induce production of inflammatory cytokines such as TNF-α and IL-1β from activated microglial cells via MAP kinase signaling pathway.

4.3 AMC induce PWMD through generation of TNF-α, IL-1β, MCP-1 and M-CSF

TNF-α, IL-1β, MCP-1 and M-CSF produced by activated microglia in the hypoxic neonatal rats execute their different effects on target cells through their respective receptors, which leads to cell death in the hypoxic PWM.

4.3.1 MCP-1 mediates migration of AMC in the PWM in hypoxic neonatal rats

The present results have shown that the cell number of AMC was significantly increased up to 7 days in the PWM. On the other hand, there was no significant difference in the proliferation rate of microglia at early time points after hypoxic exposure when compared with the corresponding control rats. However, at 7 days following hypoxic exposure, the proliferation rate of AMC in the PWM was significantly increased. The results suggest that the rise in AMC soon after hypoxic exposure was attributed primarily to the migration of AMC from the neigboring areas of the brain or from invasion of their precursor cells, namely, circulating monocytes into the postnatal hypoxic brain. The increase in number of AMC at 7d after hypoxic exposure may partly be due to self proliferation as revealed by their labeling with BrdU.

MCP-1 is a chemokine which modulates migration of activated microglial cells, neuroblasts and leukocytes to the inflammatory sites in CNS (Rankine *et al.* 2006; Yan *et al.* 2007; Lu *et al.* 1998). Accumulating evidence suggests that activated microglia can produce chemokines which facilitate chemotaxis of leukocytes and microglial cells themselves and exacerbate the CNS inflammation in some diseases (Ambrosini and Aloisi 2004; Hanisch 2002). The present study has shown an upregulation of mRNA and protein expression of CCR_2 and its specific localization in the AMC in the PWM. A large number of microglial cells were observed around the needle track in the PWM of the MCP-1 injected rats

when compared with sham operated or those receiving saline injection. The results suggest that MCP-1 either produced by activated microglial cells or administered intracerebrally can induce the chemotactic migration of microglial cells from other brain regions or blood to the PWM in the hypoxic neonatal rats. It has been reported that through binding with its G protein-coupled receptor CCR_2**,** MCP-1 induces changes in actin polymerization and subsequent reorganization of the actin cytoskeleton, formation of focal adhesions and pseudopod extension which contributes to the microglial migration when activated (Cross and Woodroofe 1999).

In addition, the present *in vitro* chemotaxis assay has confirmed that MCP-1 released by activated microglia under hypoxic condition induced the migration of microglia. In the light of this, it is concluded that under hypoxic condition, activated microglia actively generate MCP-1 which would then induce the migration of microglial cells themselves either via autocrine or paracrine fashion since the cells exhibit MCP-1 receptor, namely, CCR_2.

It is conceivable that the migration and aggregation of microglial cells would aggravate the inflammatory response occurring in the PWM of hypoxic neonatal rats resulting in PWMD. According to the *in vitro* results, NF-kappaB is implicated in the release of MCP-1 from activated microglial cells under hypoxic conditions. Therefore, the present results have further extended that NF-kappaB is involved in the hypoxic PWMD.

4.3.2 M-CSF promotes the release of TNF-α and IL-1β from astrocytes via activation of MAP kinase pathway in the PWM in hypoxic neonatal rats

M-CSF, a multifunction cytokine, is expressed by activated microglia, cultured neurons and endothelia. It regulates cellular proliferation, migration, activation and proinflammatory response through its transmembrane receptor, CSF-1R (Cecchini *et al.* 1994; Dai *et al.* 2002). The present study has shown an up-regulated expression of CSF-1R mRNA in the PWM of neonatal rats following a hypoxic exposure up to 14d. Western blotting results have further demonstrated that protein expression of CSF-1R in the PWM was increased throughout the period of study i.e. up to 14d in hypoxic rats. Double immunofluorescence labeling has shown that CSF-1R expression was localized in the astrocytes at 7 and 14d. Simultaneously, as mentioned earlier, astrocytes are the main source of inflammatory cytokines such as TNF-α and IL-1β after 7d following a hypoxic exposure. It is therefore, suggested that M-CSF produced by AMC in the early phase after hypoxia may promote the release of proinflammatory cytokines from astrocytes bearing CSF-1R.

Additionally, the present *in vitro* results have shown that expression of TNF-α, IL-1β and CSF-1R in cultured astrocytes was enhanced following M-CSF treatment. In the light of this, it is concluded that activated microglia generate M-CSF that would then induce astrocytes in their production of proinflammatory cytokines via the CSF-1R under hypoxic conditions.

The CSF-1R consists of an extracellular ligand-binding domain, a transmembrane domain, and an intracellular tyrosine domain (Pixley and Stanley 2004). M-CSF binds to CSF-1R and activates the receptor by autophosphorylation in transmembrane domain, thereby initiating a series of membrane-proximal tyrosine phosphorylation cascades, resulting in rapid stimulation of gene transcription, protein translation and cytoskeletal remodeling (Pixley and Stanley 2004;Yeung and Stanley 2003). The CSF-1R signaling pathways are complex and poorly understood at present. Recently, it has been reported that M-CSF, by binding to its high-affinity receptor CSF-1R, induces the proliferation of monocyte/macrophages via activated ERK signaling pathway (Rovida *et al.* 2008). The present results have demonstrated that the phosphorylated JNK and ERK1/2 levels were markedly increased at 15 min and gradually declined to basal levels at 2h in the primary cultured astrocytes treated with M-CSF protein. However, unlike JNK and ERK1/2, phosphorylated p38 level remained unchanged in the astrocytes after M-CSF treatment at 15, 30min, 1 and 2h. Incubation of astrocytes with SP600125, a selective inhibitor of JNK, 30 min prior to M-CSF protein treatment for 3h decreased the M-CSF-induced TNF-α and IL-1β expression. However, incubation of astrocytes with SB203580, a selective inhibitors of p38, 30 min prior to M-CSF protein treatment for 3h did not affect the M-CSF-induced TNF-α and IL-1β expression. On the basis of this, we speculate that M-CSF induces expression of proinflammatory cytokines in astrocytes via JNK kinase signaling pathway. Taken together, the present results suggest that one of the

causative factors of a strong and persistent inflammatory response in the PWM of neonatal rats after hypoxic insult may be attributed to M-CSF produced by AMC. AMC released M-CSF would then induce the neighboring astrocytes to express proinflammatory cytokines such as TNF-α and IL-1β via JNK kinase signaling pathway. The prolonged release of TNF-α and IL-1β by AMC and astrocytes in temporal sequence over a protracted period may be an explanation for the sustained neuroinflammation in hypoxic PWM lesion.

4.3.3 TNF-α and IL-1β result in oligodendrocytes loss, myelination deficits and axonal injury via binding to their respective receptors

TNF-α acts through its TNF-R_1 or TNF-R_2. TNF-R_1 has an intracellular death domain and its activation elicits caspase signal pathways that leads to cell apoptosis (Nakazawa *et al.* 2006), whereas TNF-R_2 activates the Akt signaling pathway to promote cell growth and proliferation (Fontaine *et al.* 2002). In the CNS under physiological conditions, TNF-α is expressed to induce growth and proliferation of some cells via binding to TNF-R_2 (Arnett *et al.* 2001). Under pathological conditions, excessive expression of TNF-α may induce apoptosis of some cells via binding to TNF-R_1. Oligodendrocytes and astrocytes primarily express TNF-R_1 (Dopp *et al.* 1997; Bohatschek *et al.* 2004). Our results have shown that the expression of TNF-R_1 in the oligodendrocytes increased significantly after hypoxic exposure. This was coupled with increased cell death by apoptosis and necrosis in the PWM. The apoptotic cells were confirmed to be the oligodendrocytes by double immunofluorescence labeling. Concomitantly, it

was also found that the number of oligodendrocytes was reduced. Therefore, we speculate that TNF-α produced by AMC in hypoxic conditions had induced the oligodendrocyte apoptosis via TNF-R_1 on the oligodendrocytes in hypoxic rats. Although IL-1β can bind equally to type Ⅰ and type Ⅱ IL-1R, signal transduction across the plasma membrane has been reported to be accomplished via the type Ⅰ receptor (Curtis *et al.* 1989). At present there is no evidence that a signal can be transmitted through the type Ⅱ receptor (Grehan *et al.* 1997a). Unlike TNF-α, IL-1β was reported as being non toxic to cells of oligodendrocyte lineage as oligodendrocyte apoptosis was not induced through this receptor (Vela *et al.* 2002). However, some studies have demonstrated that IL-1β can block oligodendrocyte proliferation at the late progenitor/pro-oligodendrocyte stage (Vela *et al.* 2002c). Our results demonstrated that the expression of IL-$1R_1$ on the CC_1 immunoreactive positive oligodendrocytes at 7d after hypoxic exposure was increased significantly. It is therefore, postulated that IL-1β produced by AMC under hypoxic conditions may delay the white matter development and recovery via inhibition of oligodendrocyte progenitor proliferation. The present study has further found an upregulated expression of TNF-R_1 and IL-$1R_1$ on the axons in the PWM in hypoxic rats. This was coupled with the disruption of MBP positive processes of oligodendrocytes and NF-200 positive axons of neurons in the PWM. Ultrastructural observations have further found that many of the swollen axons were vesiculated and the myelin sheaths appeared distorted at 7 and 14 days after the hypoxic exposure. The present ultrastructural study has also shown that

apoptotic and necrotic cells were a common feature in the PWM of hypoxic rats and these cells appeared to be phagocytosed by the AMC. However, apoptotic and necrotic cells were rarely encountered in the PWM of the control rats. Therefore, based on above-mentioned results, it is postulated that overproduction of TNF-α and IL-1β may damage axons and delay their myelination by oligodendrocytes via binding to their respective receptors.

Taken together, our studies suggest that hypoxia may initiate inflammation by direct activation of microglia that would damage oligodendrocytes and axons directly or indirectly. Therefore, we speculate that one of the mechanisms through which hypoxia damages the PWM may be the activation of microglial cells and production of inflammatory cytokines and chemokines such as TNF-α, IL-1β, MCP-1 and M-CSF via MAP kinase or NF-kappaB signaling pathway. AMC released M-CSF would then induce the neighboring astrocytes to express proinflammatory cytokines such as TNF-α and IL-1β via JNK kinase signaling pathway. The prolonged release of TNF-α and IL-1β by AMC and astrocytes in temporal sequence over a protracted period may cause the PWM lesion. Hence, microglial cells may play a pivotal role in the pathogenesis of PWMD in hypoxic conditions in the neonatal brain. Moreover, our finding that NF-kappaB and MAP kinase signaling pathways are involved in the process of the hypoxic PWMD has provided a potential site of pharmacological intervention for the treatment of such damage.

Chapter 5

Conclusion

It is evident from the overall data that activated AMC induce a strong and persistent inflammatory response with enormous production of inflammatory mediators namely, TNF-α, IL-1β, M-CSF and MCP-1 in the PWM of neonatal rats after a hypoxic insult. MCP-1 is a chemokine that mediates migration of microglia to the site of injury in CNS. Our study reveals that the cell number of AMC was significantly increased up to 7 days, which was due to migration of these cells. The AMC were readily activated as evidenced by their immediate increase in production of the inflammatory chemokine MCP-1 along with its receptor CCR_2 via NF-kappaB signaling pathway. It is concluded that under hypoxic condition, activated microglia actively generate MCP-1 which would then induce the migration of microglial cells in an autocrine or paracrine fashion since the cells exhibit MCP-1 receptor, namely, CCR_2. Undoubtedly, it is suggested that the migration of AMC would augment the inflammatory response occurring in the PWM of the hypoxic neonatal rats and this may exacerbate the PWMD.

In the present study, it has been found that the AMC in the PWM in the neonatal brain were the primary cellular source of M-CSF, TNF-α and IL-1β at early phase i.e. 24h-7d following hypoxic exposure. Concomitantly, the ambient astrocytes upregulated CSF-1R, TNF-α and IL-1β expression at a late stage i.e 7-14d after hypoxic insult. Additionally, the present *in vitro* study has shown that expression of CSF-1R, TNF-α and IL-1β in cultured astrocytes was enhanced following M-CSF treatment via the JNK kinase signaling pathway. So the possible interaction between AMC and astrocytes via the above-mentioned M-CSF and its

receptor would lead to release of proinflammatory cytokines such as TNF-α and IL-1β from the latter cell type via the JNK kinase signaling pathway. It is suggested that the process would persist and augment the inflammatory response in the PWM of the hypoxic neonatal rats. Furthermore, the *in vitro* study has shown that MAP kinase signaling pathway was involved in the expression of TNF-α and IL-1β in microglia subjected to hypoxia. Therefore, we speculate that under hypoxic conditions, the AMC in the PWM in the neonatal brain produce inflammatory cytokines such as TNF-α and IL-1β via MAPK signaling pathway. Taken the above-mentioned findings together, it is suggested that in the progression of inflammation in the white matter of the developing brain, while the AMC play a major role at an early stage or acute phase in production of TNF-α and IL-1β, the astrocytes activated by AMC via M-CSF would be the main cellular source for proinflammatory cytokine production at a late stage i.e 7-14d after hypoxic insult.

Expression of TNF-R_1 and IL-1R_1 was localized in the soma of oligodendrocytes and on the axons in the PWM. TNF-α and IL-1β interact with their respective receptors expressed on the oligodendrocytes and axons leading to damage of oligodendrocyte processes and myelination disturbance of the axons. This was also accompanied by the common occurrence of apoptosis and reduction in the number of oligodendrocytes. Therefore, the possible interaction between AMC and oligodendrocytes as well as axons via the above-mentioned proinflammatory cytokines and their respective receptors would lead to damage of

the latter. It is suggested that the decrease in the number of oligodendrocytes and disruption of axons would result in myelination deficits, a hallmark of PWMD.

In conclusion, the overall data demonstrated the cellular and molecular events leading to PWMD in hypoxic neonatal rats, as summarized in **Fig. 35**. A better understanding of the above process will undoubtedly help provide a platform for developing potential therapeutic strategies for mitigation of the hypoxia induced damage in neonatal brain in which AMC is implicated.

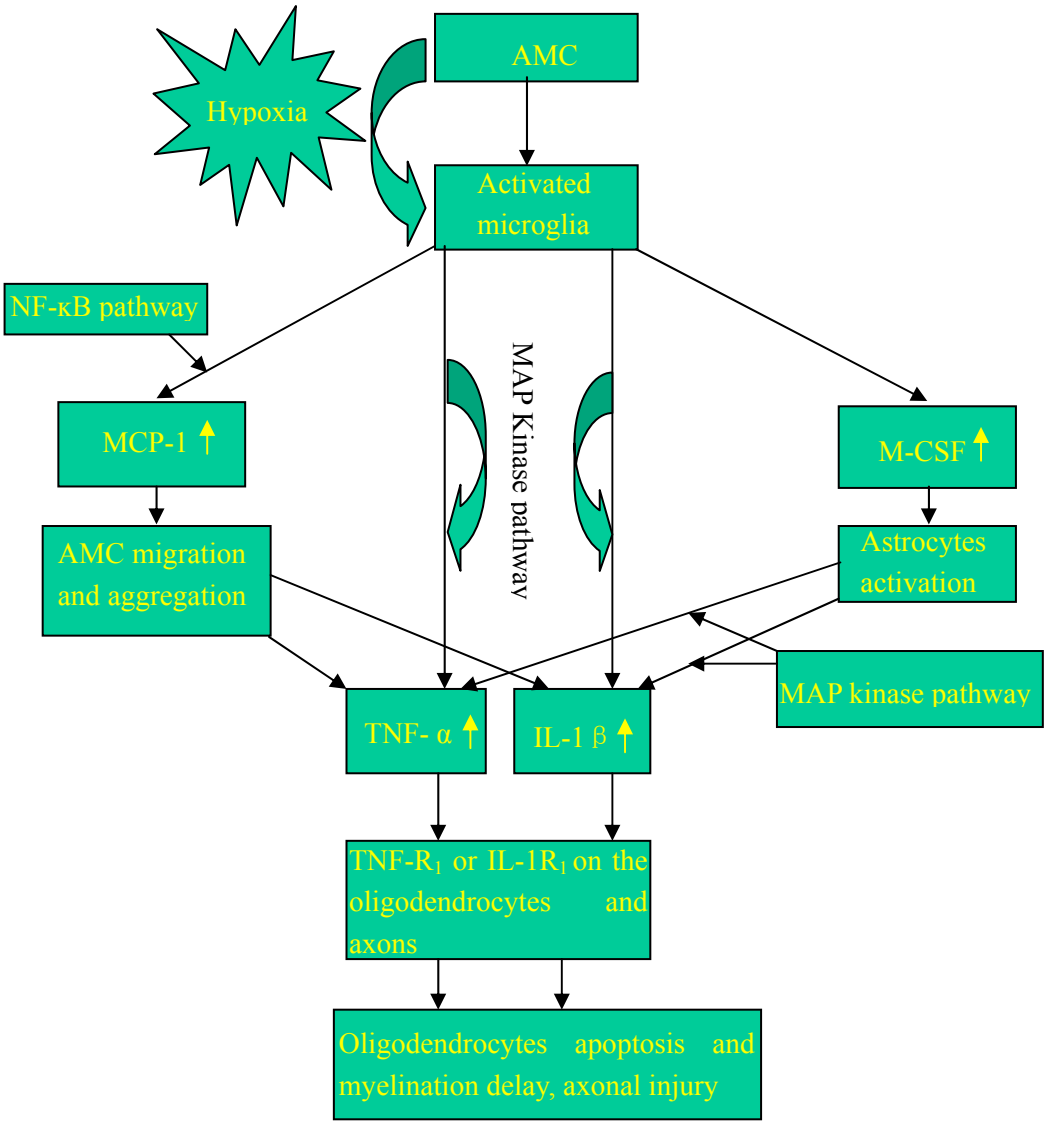

Fig 35. An illustration demonstrates the cellular and molecular events associated with PWMD in the hypoxic developing brain. Hypoxia activates amoeboid microglial cells (AMC) or ramified microglia (RM) and, hence, induces severe and persistent inflammatory response with overproduction of proinflammatory cytokines which causes axon injury, oligodendrocyte apoptosis, and myelination delay.

Scope for the Future Study

Inflammatory mediators produced by activated AMC and astrocytes are known to result in oligodendrocyte damage and disruption of axons. This study has shown that these mediators are released from AMC or astrocytes through MAP kinase or NF-kappaB signaling pathway under hypoxic conditions. Therefore, we will investigate the effect of some anti-inflammatory therapy to mitigate the hypoxia-induced PWMD in neonatal brain in our future studies. Moreover, the complex cross-talk between oligodendrocytes and axons in the course of myelination is disturbed in hypoxia. Thus, future research needs to concentrate on identification of mechanisms related to myelination disturbances.

References

Reference List

Ambrosini E. and Aloisi F. (2004) Chemokines and glial cells: a complex network in the central nervous system130. *Neurochem. Res.* **29,** 1017-1038.

Arai Y., Deguchi K. and Takashima S. (1998) Vascular endothelial growth factor in brains with periventricular leukomalacia. *Pediatr. Neurol.* **19,** 45-49.

Arnett H. A., Mason J., Marino M., Suzuki K., Matsushima G. K. and Ting J. P. (2001) TNF alpha promotes proliferation of oligodendrocyte progenitors and remyelination. *Nat. Neurosci.* **4,** 1116-1122.

Babcock A. A., Kuziel W. A., Rivest S. and Owens T. (2003) Chemokine expression by glial cells directs leukocytes to sites of axonal injury in the CNS 1. *J. Neurosci.* **23,** 7922-7930.

Babior B. M. (2000) Phagocytes and oxidative stress. *Am. J. Med.* **109,** 33-44.

Back S. A., Luo N. L., Borenstein N. S., Levine J. M., Volpe J. J. and Kinney H. C. (2001) Late oligodendrocyte progenitors coincide with the developmental window of vulnerability for human perinatal white matter injury. *J. Neurosci.* **21,** 1302-1312.

Ballabh P., Braun A. and Nedergaard M. (2004) Anatomic analysis of blood vessels in germinal matrix, cerebral cortex, and white matter in developing infants. *Pediatr. Res.* **56,** 117-124.

Baud O., Ville Y., Zupan V., Boithias C., Lacaze-Masmonteil T., Gabilan J. C., Frydman R. and Dehan M. (1998) Are neonatal brain lesions due to intrauterine infection related to mode of delivery? *Br. J. Obstet. Gynaecol.* **105,** 121-124.

Baumann N. and Pham-Dinh D. (2001) Biology of oligodendrocyte and myelin in the mammalian central nervous system. *Physiol Rev.* **81,** 871-927.

Bhat N. R., Zhang P., Lee J. C. and Hogan E. L. (1998) Extracellular signal-regulated kinase and p38 subgroups of mitogen-activated protein kinases regulate inducible nitric oxide synthase and tumor necrosis factor-alpha gene expression in endotoxin-stimulated primary glial cultures. *J. Neurosci.* **18,** 1633-1641.

Biran V., Joly L. M., Heron A., Vernet A., Vega C., Mariani J., Renolleau S. and Charriaut-Marlangue C. (2006) Glial activation in white matter following ischemia in the neonatal P7 rat brain. *Exp. Neurol.* **199,** 103-112.

Block M. L. and Hong J. S. (2007) Chronic microglial activation and progressive dopaminergic neurotoxicity. *Biochem. Soc. Trans.* **35,** 1127-1132.

Bohatschek M., Kloss C. U., Hristova M., Pfeffer K. and Raivich G. (2004) Microglial major histocompatibility complex glycoprotein-1 in the axotomized facial motor nucleus: regulation and role of tumor necrosis factor receptors 1 and 2. *J. Comp Neurol.* **470,** 382-399.

Bradford M. M. (1976) A rapid and sensitive method for the quantitation of microgram quantities of protein utilizing the principle of protein-dye binding. *Anal. Biochem.* **72,** 248-254.

Brockhaus J., Moller T. and Kettenmann H. (1996) Phagocytozing ameboid microglial cells studied in a mouse corpus callosum slice preparation. *Glia* **16,** 81-90.

Byrnes K. R. and Faden A. I. (2007) Role of Cell Cycle Proteins in CNS Injury. *Neurochem. Res.* **32,** 1799-1807.

Cai Z., Pang Y., Xiao F. and Rhodes P. G. (2001) Chronic ischemia preferentially causes white matter injury in the neonatal rat brain. *Brain Res.* **898,** 126-135.

Cai Z, Sigrest T, Hersey K, Rhodes PG. (1995) Intrauterine hypoxia-ischemia increases N-methyl-D-aspartate-induced cGMP formation and glutamate accumulation in cultured rat cerebellar granule cells. *Pediatr Res.* **38,** 107-112.

Calvo C. F., Yoshimura T., Gelman M. and Mallat M. (1996) Production of monocyte chemotactic protein-1 by rat brain macrophages. *Eur. J. Neurosci.* **8,** 1725-1734.

Carloni S., Mazzoni E., Cimino M., De Simoni M. G., Perego C., Scopa C. and Balduini W. (2006) Simvastatin reduces caspase-3 activation and inflammatory markers induced by hypoxia-ischemia in the newborn rat. *Neurobiol. Dis.* **21,** 119-126.

Casaccia-Bonnefil P. (2000) Cell death in the oligodendrocyte lineage: a molecular perspective of life/death decisions in development and disease. *Glia* **29,** 124-135.

Cecchini M. G., Dominguez M. G., Mocci S., Wetterwald A., Felix R., Fleisch H., Chisholm O., Hofstetter W., Pollard J. W. and Stanley E. R. (1994) Role of colony stimulating factor-1 in the establishment and regulation of tissue macrophages during postnatal development of the mouse. *Development* **120,** 1357-1372.

Chan F. K., Chun H. J., Zheng L., Siegel R. M., Bui K. L. and Lenardo M. J. (2000) A domain in TNF receptors that mediates ligand-independent receptor assembly and signaling. *Science* **288,** 2351-2354.

Chang L. and Karin M. (2001) Mammalian MAP kinase signalling cascades. *Nature* **410,** 37-40.

Che X., Ye W., Panga L., Wu D. C. and Yang G. Y. (2001) Monocyte chemoattractant protein-1 expressed in neurons and astrocytes during focal ischemia in mice1. *Brain Res.* **902,** 171-177.

Chen Z. J. (2005) Ubiquitin signalling in the NF-kappaB pathway. *Nat. Cell Biol.* **7,** 758-765.

Chew LJ, Takanohashi A, Bell M. (2006) Microglia and inflammation: impact on developmental brain injuries. *Ment Retard Dev Disabil Res Rev.***12,** 105-112.

Conant K., Garzino-Demo A., Nath A., McArthur J. C., Halliday W., Power C., Gallo R. C. and Major E. O. (1998) Induction of monocyte chemoattractant protein-1 in HIV-1 Tat-stimulated astrocytes and elevation in AIDS dementia. *Proc. Natl. Acad. Sci. U. S. A* **95,** 3117-3121.

Croll S. D., Goodman J. H. and Scharfman H. E. (2004) Vascular endothelial growth factor (VEGF) in seizures: a double-edged sword. *Adv. Exp. Med. Biol.* **548,** 57-68.

Cross A. K. and Woodroofe M. N. (1999) Chemokines induce migration and changes in actin polymerization in adult rat brain microglia and a human fetal microglial cell line in vitro1. *J. Neurosci. Res.* **55,** 17-23.

Curtis B. M., Gallis B., Overell R. W., McMahan C. J., DeRoos P., Ireland R., Eisenman J., Dower S. K. and Sims J. E. (1989) T-cell interleukin 1 receptor cDNA expressed in Chinese hamster ovary cells regulates functional responses to interleukin 1. *Proc. Natl. Acad. Sci. U. S. A* **86,** 3045-3049.

Cuthill D. J., Fowler J. H., McCulloch J. and Dewar D. (2006) Different patterns of axonal damage after intracerebral injection of malonate or AMPA. *Exp. Neurol.* **200,** 509-520.

Da S. J., Pierrat B., Mary J. L. and Lesslauer W. (1997) Blockade of p38 mitogen-activated protein kinase pathway inhibits inducible nitric-oxide synthase expression in mouse astrocytes. *J. Biol. Chem.* **272,** 28373-28380.

Dai X. M., Ryan G. R., Hapel A. J., Dominguez M. G., Russell R. G., Kapp S.,

Sylvestre V. and Stanley E. R. (2002) Targeted disruption of the mouse colony-stimulating factor 1 receptor gene results in osteopetrosis, mononuclear phagocyte deficiency, increased primitive progenitor cell frequencies, and reproductive defects. *Blood* **99,** 111-120.

Dalmau I, Vela JM, González B, Castellano B. (1998) Expression of purine metabolism-related enzymes by microglial cells in the developing rat brain. *J Comp Neurol* **398**, 333-346.

Dalmau I, Vela JM, González B, Finsen B, Castellano B. (2003) Dynamics of microglia in the developing rat brain. *J Comp Neurol* **458**,144-157.

Dammann O., Hagberg H. and Leviton A. (2001) Is periventricular leukomalacia an axonopathy as well as an oligopathy? *Pediatr. Res.* **49,** 453-457.

Danbolt N. C. (1994) The high affinity uptake system for excitatory amino acids in the brain. *Prog. Neurobiol.* **44,** 377-396.

Denes A., Vidyasagar R., Feng J., Narvainen J., McColl B. W., Kauppinen R. A. and Allan S. M. (2007) Proliferating resident microglia after focal cerebral ischaemia in mice. *J. Cereb. Blood Flow Metab*. **27,** 1941-1953.

De Vries LS, Regev R, Dubowitz LM, Whitelaw A, Aber VR. (1988) Perinatal risk factors for the development of extensive cystic leukomalacia. *Am J Dis Child.* **142**, 732-735

Deng W, Wang H, Rosenberg PA, Volpe JJ, Jensen FE. (2004) Role of metabotropic glutamate receptors in oligodendrocyte excitotoxicity and oxidative stress. *Proc Natl Acad Sci U S A.* **101,** 7751-7756

Dheen S. T., Jun Y., Yan Z., Tay S. S. and Ling E. A. (2005) Retinoic acid inhibits expression of TNF-alpha and iNOS in activated rat microglia. *Glia* **50,** 21-31.

Dheen ST, Kaur C, Ling EA. (2007) Microglial activation and its implications in the brain diseases. *Curr Med Chem* **14,** 1189-1197.

Di G. S., Movsesyan V., Ahmed F., Cernak I., Schinelli S., Stoica B. and Faden A. I. (2005) Cell cycle inhibition provides neuroprotection and reduces glial proliferation and scar formation after traumatic brain injury. *Proc. Natl. Acad. Sci. U. S. A* **102,** 8333-8338.

Dobrogowska D. H., Lossinsky A. S. and Vorbrodt A. W. (1998) Ultrastructural study of the clearance of intracerebrally infused native and modified albumin-gold complexes. *Histol. Histopathol.* **13,** 647-656.

Domercq M, Sánchez-Gómez MV, Sherwin C, Etxebarria E, Fern R, Matute C. (2007) System xc- and glutamate transporter inhibition mediates microglial toxicity to oligodendrocytes. *J Immunol.* **178,** 6549-6556.

Dougherty R. F., Ben-Shachar M., Bammer R., Brewer A. A. and Wandell B. A. (2005) Functional organization of human occipital-callosal fiber tracts. *Proc. Natl. Acad. Sci. U. S. A* **102,** 7350-7355.

Dringen R., Gebhardt R. and Hamprecht B. (1993) Glycogen in astrocytes: possible function as lactate supply for neighboring cells. *Brain Res.* **623,** 208-214.

Ehrlich L. C., Hu S., Sheng W. S., Sutton R. L., Rockswold G. L., Peterson P. K. and Chao C. C. (1998) Cytokine regulation of human microglial cell IL-8 production157. *J. Immunol.* **160,** 1944-1948.

El-Khoury N., Braun A., Hu F., Pandey M., Nedergaard M., Lagamma E. F. and Ballabh P. (2006) Astrocyte end-feet in germinal matrix, cerebral cortex, and white matter in developing infants. *Pediatr. Res.* **59,** 673-679.

Eugenin EA, Dyer G, Calderon TM, Berman JW. (2005) HIV-1 tat protein induces a migratory phenotype in human fetal microglia by a CCL2 (MCP-1)-dependent mechanism: possible role in NeuroAIDS. *Glia.* **49,** 501-510

Farber K, Kettenmann H. (2006) Functional role of calcium signals for microglial function. *Glia.* **54,** 656-665.

Fenoglio C., Galimberti D., Lovati C., Guidi I., Gatti A., Fogliarino S., Tiriticco M., Mariani C., Forloni G., Pettenati C., Baron P., Conti G., Bresolin N. and Scarpini E. (2004) MCP-1 in Alzheimer's disease patients: A-2518G polymorphism and serum levels. *Neurobiol. Aging* **25,** 1169-1173.

Fern R., Davis P., Waxman S. G. and Ransom B. R. (1998) Axon conduction and survival in CNS white matter during energy deprivation: a developmental study. *J. Neurophysiol.* **79,** 95-105.

Filley C. M. (2005) Neurobehavioral aspects of cerebral white matter disorders. *Psychiatr. Clin. North Am.* **28,** 685-688.

Folkerth R. D. (2006) Periventricular leukomalacia: overview and recent findings. *Pediatr. Dev. Pathol.* **9,** 3-13.

Folkerth R. D., Haynes R. L., Borenstein N. S., Belliveau R. A., Trachtenberg F., Rosenberg P. A., Volpe J. J. and Kinney H. C. (2004) Developmental lag in superoxide dismutases relative to other antioxidant enzymes in premyelinated human telencephalic white matter. *J. Neuropathol. Exp. Neurol.* **63,** 990-999.

Folkerth RD, Keefe RJ, Haynes RL, Trachtenberg FL, Volpe JJ, Kinney HC. (2004) Interferon-gamma expression in periventricular leukomalacia in the human brain. Brain Pathol. **14**, 265-74

Fontaine V., Mohand-Said S., Hanoteau N., Fuchs C., Pfizenmaier K. and Eisel U. (2002) Neurodegenerative and neuroprotective effects of tumor Necrosis factor

(TNF) in retinal ischemia: opposite roles of TNF receptor 1 and TNF receptor 2. *J. Neurosci.* **22,** RC216.

Fowler J. H., Edgar J. M., Pringle A., McLaughlin M., McCulloch J., Griffiths I. R., Garbern J. Y., Nave K. A. and Dewar D. (2006) Alpha-amino-3-hydroxy-5-methylisoxazole-4-propionic acid-mediated excitotoxic axonal damage is attenuated in the absence of myelin proteolipid protein. *J. Neurosci. Res.* **84,** 68-77.

Galasso JM, Liu Y, Szaflarski J, Warren JS, Silverstein FS. (2000) Monocyte chemoattractant protein-1 is a mediator of acute excitotoxic injury in neonatal rat brain. *Neuroscience.* **101,** 737-44.

Gebicke-Haerter PJ, Spleiss O, Ren LQ, Li H, Dichmann S, Norgauer J, Boddeke HW. (2001) Microglial chemokines and chemokine receptors. *Prog Brain Res.***132,** 525-532.

Ghosh S. and Karin M. (2002) Missing pieces in the NF-kappaB puzzle. *Cell* **109 Suppl,** S81-S96.

Glabinski A. R., Bielecki B. and Ransohoff R. M. (2003) Chemokine upregulation follows cytokine expression in chronic relapsing experimental autoimmune encephalomyelitis. *Scand. J. Immunol.* **58,** 81-88.

Grehan S., Uhlar C. M., Sim R. B., Herbert J. and Whitehead A. S. (1997) Expression of a biologically active recombinant mouse IL-1 receptor antagonist and its use in vivo to modulate aspects of the acute phase response. *J. Immunol.* **159,** 369-378.

Gunn M. D., Nelken N. A., Liao X. and Williams L. T. (1997) Monocyte chemoattractant protein-1 is sufficient for the chemotaxis of monocytes and lymphocytes in transgenic mice but requires an additional stimulus for

inflammatory activation. *J. Immunol.* **158,** 376-383.

Guo G. and Bhat N. R. (2006) Hypoxia/reoxygenation differentially modulates NF-kappaB activation and iNOS expression in astrocytes and microglia. *Antioxid. Redox. Signal.* **8,** 911-918.

Hanisch U. K. (2002) Microglia as a source and target of cytokines. *Glia.* **40,** 140-155.

Hanisch UK, Kettenmann H. (2007) Microglia: active sensor and versatile effector cells in the normal and pathologic brain. *Nat Neurosci.* **10,** 1387-1394.

Hao A. J., Dheen S. T. and Ling E. A. (2002) Expression of macrophage colony-stimulating factor and its receptor in microglia activation is linked to teratogen-induced neuronal damage. *Neuroscience* **112,** 889-900.

Hayashi M., Luo Y., Laning J., Strieter R. M. and Dorf M. E. (1995) Production and function of monocyte chemoattractant protein-1 and other beta-chemokines in murine glial cells1. *J. Neuroimmunol.* **60,** 143-150.

Haynes RL, Baud O, Li J, Kinney HC, Volpe JJ, Folkerth DR. (2005) Oxidative and nitrative injury in periventricular leukomalacia: a review. *Brain Pathol.* **15,** 225-233.

Haynes RL, Folkerth RD, Keefe RJ, Sung I, Swzeda LI, Rosenberg PA, Volpe JJ, Kinney HC. (2003) Nitrosative and oxidative injury to premyelinating oligodendrocytes in periventricular leukomalacia. *J Neuropathol Exp Neurol.* **62,** 441-450

He J., Chen Y., Farzan M., Choe H., Ohagen A., Gartner S., Busciglio J., Yang X., Hofmann W., Newman W., Mackay C. R., Sodroski J. and Gabuzda D. (1997) CCR3 and CCR5 are co-receptors for HIV-1 infection of microglia181. *Nature* **385,** 645-649.

Henze C., Hartmann A., Lescot T., Hirsch E. C. and Michel P. P. (2005) Proliferation of microglial cells induced by 1-methyl-4-phenylpyridinium in mesencephalic cultures results from an astrocyte-dependent mechanism: role of granulocyte macrophage colony-stimulating factor13. *J. Neurochem.* **95,** 1069-1077.

Hirayama A., Okoshi Y., Hachiya Y., Ozawa Y., Ito M., Kida Y., Imai Y., Kohsaka S. and Takashima S. (2001) Early immunohistochemical detection of axonal damage and glial activation in extremely immature brains with periventricular leukomalacia. *Clin. Neuropathol.* **20,** 87-91.

Hommes D. W., Peppelenbosch M. P. and van Deventer S. J. (2003) Mitogen activated protein (MAP) kinase signal transduction pathways and novel anti-inflammatory targets. *Gut* **52,** 144-151.

Hughes P. M., Allegrini P. R., Rudin M., Perry V. H., Mir A. K. and Wiessner C. (2002) Monocyte chemoattractant protein-1 deficiency is protective in a murine stroke model1. *J. Cereb. Blood Flow Metab* **22,** 308-317.

Ichijo H., Nishida E., Irie K., Ten D. P., Saitoh M., Moriguchi T., Takagi M., Matsumoto K., Miyazono K. and Gotoh Y. (1997) Induction of apoptosis by ASK1, a mammalian MAPKKK that activates SAPK/JNK and p38 signaling pathways. *Science* **275,** 90-94.

Ivacko J, Szaflarski J, Malinak C, Flory C, Warren JS, Silverstein FS. (1997) Hypoxic-ischemic injury induces monocyte chemoattractant protein-1 expression in neonatal rat brain. *J Cereb Blood Flow Metab.* **17,** 759-770.

Jacobson L, Flodmark O, Martin L. (2006) Visual field defects in prematurely born patients with white matter damage of immaturity: a multiple-case study. *Acta Ophthalmol Scand.* 84, 357-362.

Jantaratnotai N, Ryu JK, Kim SU, McLarnon JG. (2003) Amyloid beta peptide-induced corpus callosum damage and glial activation in vivo. *Neuroreport*. **14**, 1429-1433

Jones S. J., Ledgerwood E. C., Prins J. B., Galbraith J., Johnson D. R., Pober J. S. and Bradley J. R. (1999) TNF recruits TRADD to the plasma membrane but not the trans-Golgi network, the principal subcellular location of TNF-R1. *J. Immunol.* **162,** 1042-1048.

Kadhim H., Tabarki B., De P. C., Rona A. M. and Sebire G. (2002) Interleukin-2 in the pathogenesis of perinatal white matter damage. *Neurology* **58,** 1125-1128.

Kadhim H., Tabarki B., Verellen G., De P. C., Rona A. M. and Sebire G. (2001) Inflammatory cytokines in the pathogenesis of periventricular leukomalacia. *Neurology* **56,** 1278-1284.

Káradóttir R, Cavelier P, Bergersen LH, Attwell. (2005) NMDA receptors are expressed in oligodendrocytes and activated in ischaemia. *Nature* **438,** 1162-1166.

Karin M., Cao Y., Greten F. R. and Li Z. W. (2002) NF-kappaB in cancer: from innocent bystander to major culprit. *Nat. Rev. Cancer* **2,** 301-310.

Kaur C., Dheen S. T. and Ling E. A. (2007) From blood to brain: amoeboid microglial cell, a nascent macrophage and its functions in developing brain. *Acta Pharmacol. Sin.* **28,** 1087-1096.

Kaur C., Hao A. J., Wu C. H. and Ling E. A. (2001) Origin of microglia. *Microsc. Res. Tech.* **54,** 2-9.

Kaur C. and Ling E. A. (2009) Periventricular white matter damage in the hypoxic neonatal brain: Role of microglial cells. *Prog. Neurobiol.* **87,** 264-280.

Kaur C, Ling EA, Wong WC. (1985) Transformation of amoeboid microglial cells into microglia in the corpus callosum of the postnatal rat brain. An electron microscopical study. *Arch Histol Jpn.* **48,** 17-25.

C. Kaur, V Sivakumar, E.A Ling. Melatonin protects periventricular white matter from damage due to hypoxia. *Journal of Pineal Research.* (accepted).

Kaur C., Sivakumar V., Ang L. S. and Sundaresan A. (2006a) Hypoxic damage to the periventricular white matter in neonatal brain: role of vascular endothelial growth factor, nitric oxide and excitotoxicity. *J. Neurochem.* **98,** 1200-1216.

Kaur C, Sivakumar V, Lu J, Ling EA. (2007) Increased vascular permeability and nitric oxide production in response to hypoxia in the pineal gland. *J Pineal Res.* **42**, 338-349.

Kaur C, Sivakumar V, Lu J, Tang FR, Ling EA. (2008) Melatonin attenuates hypoxia-induced ultrastructural changes and increased vascular permeability in the developing hippocampus. *Brain Pathol.* **18,** 533-547.

Kaur C, Sivakumar V, Yip GW, Ling EA. (2009) Expression of syndecan-2 in the amoeboid microglial cells and its involvement in inflammation in the hypoxic developing brain.*Glia.* **57,** 336-349.

Kaur C., Too H. F. and Ling E. A. (2004) Phagocytosis of Escherichia coli by amoeboid microglial cells in the developing brain. *Acta Neuropathol.* **107,** 204-208.

Kaur C, You Y. (2000) Ultrastructure and function of the amoeboid microglial cells in the periventricular white matter in postnatal rat brain following a hypoxic exposure. *Neurosci Lett.* **290**, 17-20.

Kinney H. C. and Back S. A. (1998) Human oligodendroglial development: relationship to periventricular leukomalacia. *Semin. Pediatr. Neurol.* **5,** 180-189.

Kliot M., Smith G. M., Siegal J. D. and Silver J. (1990) Astrocyte-polymer implants promote regeneration of dorsal root fibers into the adult mammalian spinal cord. *Exp. Neurol.* **109,** 57-69.

Koprowski H, Zheng YM, Heber-Katz E, Fraser N, Rorke L, Fu ZF, Hanlon C, Dietzschold B. (1993) In vivo expression of inducible nitric oxide synthase in experimentally induced neurologic diseases. *Proc Natl Acad Sci U S A.* **90,** 3024-3027

Kyriakis J. M., Banerjee P., Nikolakaki E., Dai T., Rubie E. A., Ahmad M. F., Avruch J. and Woodgett J. R. (1994) The stress-activated protein kinase subfamily of c-Jun kinases. *Nature* **369,** 156-160.

Ladeby R., Wirenfeldt M., Garcia-Ovejero D., Fenger C., ssing-Olesen L., Dalmau I. and Finsen B. (2005) Microglial cell population dynamics in the injured adult central nervous system. *Brain Res. Brain Res. Rev.* **48,** 196-206.

Lavi E., Strizki J. M., Ulrich A. M., Zhang W., Fu L., Wang Q., O'Connor M., Hoxie J. A. and Gonzalez-Scarano F. (1997) CXCR-4 (Fusin), a co-receptor for the type 1 human immunodeficiency virus (HIV-1), is expressed in the human brain in a variety of cell types, including microglia and neurons179. *Am. J. Pathol.* **151,** 1035-1042.

Ledgerwood E. C., Pober J. S. and Bradley J. R. (1999) Recent advances in the molecular basis of TNF signal transduction. *Lab Invest* **79,** 1041-1050.

Lee J. C., Laydon J. T., McDonnell P. C., Gallagher T. F., Kumar S., Green D., McNulty D., Blumenthal M. J., Heys J. R., Landvatter S. W. and . (1994) A protein kinase involved in the regulation of inflammatory cytokine biosynthesis. *Nature* **372,** 739-746.

Lee S. C., Liu W., Roth P., Dickson D. W., Berman J. W. and Brosnan C. F. (1993)

Macrophage colony-stimulating factor in human fetal astrocytes and microglia. Differential regulation by cytokines and lipopolysaccharide, and modulation of class II MHC on microglia. *J. Immunol.* **150,** 594-604.

Lehnardt S., Lachance C., Patrizi S., Lefebvre S., Follett P. L., Jensen F. E., Rosenberg P. A., Volpe J. J. and Vartanian T. (2002) The toll-like receptor TLR4 is necessary for lipopolysaccharide-induced oligodendrocyte injury in the CNS. *J. Neurosci.* **22,** 2478-2486.

Li JJ, Lu J, Kaur C, Sivakumar V, Wu CY, Ling EA. (2008b) Effects of hypoxia on expression of transforming growth factor-beta1 and its receptors I and II in the amoeboid microglial cells and murine BV-2 cells. *Neuroscience.* **156,** 662-672.

Li JJ, Lu J, Kaur C, Sivakumar V, Wu CY, Ling EA. (2009) Expression of angiotensin II and its receptors in the normal and hypoxic amoeboid microglial cells and murine BV-2 cells. *Neuroscience.* **158,** 1488-1499.

Li F, Lu J, Wu CY, Kaur C, Sivakumar V, Sun J, Li S, Ling EA. (2008a) Expression of Kv1.2 in microglia and its putative roles in modulating production of proinflammatory cytokines and reactive oxygen species. *J Neurochem.* **106,** 2093-2105.

Li J, Baud O, Vartanian T, Volpe JJ, Rosenberg PA. (2005) Peroxynitrite generated by inducible nitric oxide synthase and NADPH oxidase mediates microglial toxicity to oligodendrocytes. *Proc Natl Acad Sci U S A.* **102,** 9936-9941.

Li Q. and Verma I. M. (2002) NF-kappaB regulation in the immune system. *Nat. Rev. Immunol.* **2,** 725-734.

Li YB, Kaur C, Ling EA. (1997) Labeling of amoeboid microglial cells and intraventricular macrophages in fetal rats following a maternal injection of a

fluorescent dye. *Neurosci Res*. **28,** 119-125.

Ling EA. (1980) Cytochemical localization of peroxidase in amoeboid cells in the corpus callosum in postnatal rats. *Arch Histol Jpn.* **43,** 305-310.

Ling EA. (1977) Light and electron microscopic demonstration of some lysosomal enzymes in the amoeboid microglia in neonatal rat brain. *J Anat.* **123,** 637-648.

Ling EA, Kaur C, Wong WC. (1991) Expression of major histocompatibility complex and leukocyte common antigens in amoeboid microglia in postnatal rats. *J Anat* **177,** 117-126.

Ling EA, Ng YK, Wu CH, Kaur C. (2001) Microglia: its development and role as a neuropathology sensor. *Prog Brain Res* **132,** 61-79.

Ling E. A. and Wong W. C. (1993) The origin and nature of ramified and amoeboid microglia: a historical review and current concepts. *Glia* **7,** 9-18.

Lipovsky M. M., Gekker G., Hu S., Ehrlich L. C., Hoepelman A. I. and Peterson P. K. (1998) Cryptococcal glucuronoxylomannan induces interleukin (IL)-8 production by human microglia but inhibits neutrophil migration toward IL-8 158. *J. Infect. Dis.* **177,** 260-263.

Livak K. J. and Schmittgen T. D. (2001) Analysis of relative gene expression data using real-time quantitative PCR and the 2(-Delta Delta C (T)) Method163. *Methods* **25,** 402-408.

Lokensgard J. R., Gekker G., Ehrlich L. C., Hu S., Chao C. C. and Peterson P. K. (1997) Proinflammatory cytokines inhibit HIV-1(SF162) expression in acutely infected human brain cell cultures3. *J. Immunol.* **158,** 2449-2455.

Louis JC, Magal E, Takayama S, Varon S. (1993) CNTF protection of oligodendrocytes against natural and tumor necrosis factor-induced death. *Science.* **259,** 689-692.

Lu B., Rutledge B. J., Gu L., Fiorillo J., Lukacs N. W., Kunkel S. L., North R., Gerard C. and Rollins B. J. (1998) Abnormalities in monocyte recruitment and cytokine expression in monocyte chemoattractant protein 1-deficient mice. *J. Exp. Med.* **187,** 601-608.

Ludwin S. K. (1997) The pathobiology of the oligodendrocyte. *J. Neuropathol. Exp. Neurol.* **56,** 111-124.

McCarran W. J. and Goldberg M. P. (2007) White matter axon vulnerability to AMPA/kainate receptor-mediated ischemic injury is developmentally regulated. *J. Neurosci.* **27,** 4220-4229.

McCarthy K. D. and de V. J. (1980) Preparation of separate astroglial and oligodendroglial cell cultures from rat cerebral tissue. *J. Cell Biol.* **85,** 890-902.

McManus C. M., Brosnan C. F. and Berman J. W. (1998) Cytokine induction of MIP-1 alpha and MIP-1 beta in human fetal microglia161. *J. Immunol.* **160,** 1449-1455.

Ment L. R., Stewart W. B., Fronc R., Seashore C., Mahooti S., Scaramuzzino D. and Madri J. A. (1997) Vascular endothelial growth factor mediates reactive angiogenesis in the postnatal developing brain. *Brain Res. Dev. Brain Res.* **100,** 52-61.

Merrill JE, Benveniste EN. (1996) Cytokines in inflammatory brain lesions: helpful and harmful.*Trends Neurosci.* **19,** 331-338.

Merrill JE, Ignarro LJ, Sherman MP, Melinek J, Lane TE. (1993) Microglial cell cytotoxicity of oligodendrocytes is mediated through nitric oxide. *J Immunol.* **151,** 2132-2141.

Micu I, Jiang Q, Coderre E, Ridsdale A, Zhang L, Woulfe J, Yin X, Trapp BD, McRory JE, Rehak R, Zamponi GW, Wang W, Stys PK. (2006) NMDA receptors mediate calcium accumulation in myelin during chemical ischaemia. *Nature.* **439,** 988-992.

Min J. K., Lee Y. M., Kim J. H., Kim Y. M., Kim S. W., Lee S. Y., Gho Y. S., Oh G. T. and Kwon Y. G. (2005) Hepatocyte growth factor suppresses vascular endothelial growth factor-induced expression of endothelial ICAM-1 and VCAM-1 by inhibiting the nuclear factor-kappaB pathway. *Circ. Res.* **96,** 300-307.

Minami M. and Satoh M. (2003) Chemokines and their receptors in the brain: pathophysiological roles in ischemic brain injury1. *Life Sci.* **74,** 321-327.

Mitrovic B., Parkinson J. and Merrill J. E. (1996) An in Vitro Model of Oligodendrocyte Destruction by Nitric Oxide and Its Relevance to Multiple Sclerosis. *Methods* **10,** 501-513.

Mitrovic B., St Pierre B. A., kenzie-Graham A. J. and Merrill J. E. (1994) The role of nitric oxide in glial pathology. *Ann. N. Y. Acad. Sci.* **738,** 436-446.

Mu D., Jiang X., Sheldon R. A., Fox C. K., Hamrick S. E., Vexler Z. S. and Ferriero D. M. (2003) Regulation of hypoxia-inducible factor 1alpha and induction of vascular endothelial growth factor in a rat neonatal stroke model. *Neurobiol. Dis.* **14,** 524-534.

Muessel M. J., Klein R. M., Wilson A. M. and Berman N. E. (2002) Ablation of the chemokine monocyte chemoattractant protein-1 delays retrograde neuronal

degeneration, attenuates microglial activation, and alters expression of cell death molecules1. *Brain Res. Mol. Brain Res.* **103,** 12-27.

Mulhern R. K., Palmer S. L., Reddick W. E., Glass J. O., Kun L. E., Taylor J., Langston J. and Gajjar A. (2001) Risks of young age for selected neurocognitive deficits in medulloblastoma are associated with white matter loss. *J. Clin. Oncol.* **19,** 472-479.

Nakazawa T., Nakazawa C., Matsubara A., Noda K., Hisatomi T., She H., Michaud N., Hafezi-Moghadam A., Miller J. W. and Benowitz L. I. (2006) Tumor necrosis factor-alpha mediates oligodendrocyte death and delayed retinal ganglion cell loss in a mouse model of glaucoma. *J. Neurosci.* **26,** 12633-12641.

Nedergaard M., Ransom B. and Goldman S. A. (2003) New roles for astrocytes: redefining the functional architecture of the brain. *Trends Neurosci.* **26,** 523-530.

Nishiyori A., Minami M., Ohtani Y., Takami S., Yamamoto J., Kawaguchi N., Kume T., Akaike A. and Satoh M. (1998) Localization of fractalkine and CX3CR1 mRNAs in rat brain: does fractalkine play a role in signaling from neuron to microglia? 180. *FEBS Lett.* **429,** 167-172.

Noda M, Nakanishi H, Nabekura J, Akaike N. (2000) AMPA-kainate subtypes of glutamate receptor in rat cerebral microglia. *J Neurosci.* **20,** 251-258.

Nohava K., Malipiero U., Frei K. and Fontana A. (1992) Neurons and neuroblastoma as a source of macrophage colony-stimulating factor. *Eur. J. Immunol.* **22,** 2539-2545.

Ohkita M., Takaoka M., Shiota Y., Nojiri R., Sugii M. and Matsumura Y. (2002) A nuclear factor-kappaB inhibitor BAY 11-7082 suppresses endothelin-1 production in cultured vascular endothelial cells. *Jpn. J. Pharmacol.* **89,** 81-84.

Ohno M. and Aotani H. (2000) [Periventricular leukomalacia]. *Ryoikibetsu.*

Shokogun. Shirizu. 742-745.

Oka A., Belliveau M. J., Rosenberg P. A. and Volpe J. J. (1993) Vulnerability of oligodendroglia to glutamate: pharmacology, mechanisms, and prevention. *J. Neurosci.* **13,** 1441-1453.

Okoshi Y, Itoh M, Takashima S. (2001) Characteristic neuropathology and plasticity in periventricular leukomalacia. *Pediatr Neurol.* 25, 221-226.

Pahl H. L. (1999) Activators and target genes of Rel/NF-kappaB transcription factors. *Oncogene* **18,** 6853-6866.

Pang Y., Cai Z. and Rhodes P. G. (2000) Effects of lipopolysaccharide on oligodendrocyte progenitor cells are mediated by astrocytes and microglia. *J. Neurosci. Res.* **62,** 510-520.

Panickar K. S. and Norenberg M. D. (2005) Astrocytes in cerebral ischemic injury: morphological and general considerations. *Glia* **50,** 287-298.

Park S. Y., Lee H., Hur J., Kim S. Y., Kim H., Park J. H., Cha S., Kang S. S., Cho G. J., Choi W. S. and Suk K. (2002) Hypoxia induces nitric oxide production in mouse microglia via p38 mitogen-activated protein kinase pathway. *Brain Res. Mol. Brain Res.* **107,** 9-16.

Perlman J. M., Broyles R. S. and Rogers C. G. (1997) Neonatal neurologic characteristics of preterm twin infants <1,250 gm birth weight. *Pediatr. Neurol.* **17,** 322-326.

Peterson P. K., Hu S., Salak-Johnson J., Molitor T. W. and Chao C. C. (1997) Differential production of and migratory response to beta chemokines by human microglia and astrocytes. *J. Infect. Dis.* **175,** 478-481.

Pixley F. J. and Stanley E. R. (2004) CSF-1 regulation of the wandering

macrophage: complexity in action. *Trends Cell Biol.* **14,** 628-638.

Pomerantz J. L. and Baltimore D. (2002) Two pathways to NF-kappaB. *Mol. Cell* **10,** 693-695.

Pouly S., Antel J. P., Ladiwala U., Nalbantoglu J. and Becher B. (2000) Mechanisms of tissue injury in multiple sclerosis: opportunities for neuroprotective therapy. *J. Neural Transm. Suppl* 193-203.

Proescholdt MA, Heiss JD, Walbridge S, Mühlhauser J, Capogrossi MC, Oldfield EH, Merrill MJ. (1999) Vascular endothelial growth factor (VEGF) modulates vascular permeability and inflammation in rat brain. *J Neuropathol Exp Neurol.* **58,** 613-627.

Rankine E. L., Hughes P. M., Botham M. S., Perry V. H. and Felton L. M. (2006) Brain cytokine synthesis induced by an intraparenchymal injection of LPS is reduced in MCP-1-deficient mice prior to leucocyte recruitment. *Eur. J. Neurosci.* **24,** 77-86.

Remington L. T., Babcock A. A., Zehntner S. P. and Owens T. (2007) Microglial recruitment, activation, and proliferation in response to primary demyelination. *Am. J. Pathol.* **170,** 1713-1724.

Resch B., Vollaard E., Maurer U., Haas J., Rosegger H. and Muller W. (2000) Risk factors and determinants of neurodevelopmental outcome in cystic periventricular leucomalacia. *Eur. J. Pediatr.* **159,** 663-670.

Rezaie P. and Dean A. (2002) Periventricular leukomalacia, inflammation and white matter lesions within the developing nervous system. *Neuropathology.* **22,** 106-132.

Rothe M., Wong S. C., Henzel W. J. and Goeddel D. V. (1994) A novel family of putative signal transducers associated with the cytoplasmic domain of the 75 kDa

tumor necrosis factor receptor. *Cell* **78,** 681-692.

Rovida E., Spinelli E., Sdelci S., Barbetti V., Morandi A., Giuntoli S. and Dello S. P. (2008) ERK5/BMK1 is indispensable for optimal colony-stimulating factor 1 (CSF-1)-induced proliferation in macrophages in a Src-dependent fashion. *J. Immunol.* **180,** 4166-4172.

Saed G. M., Munkarah A. R., bu-Soud H. M. and Diamond M. P. (2005) Hypoxia upregulates cyclooxygenase-2 and prostaglandin E(2) levels in human peritoneal fibroblasts. *Fertil. Steril.* **83 Suppl 1,** 1216-1219.

Saliba E. and Marret S. (2001) Cerebral white matter damage in the preterm infant: pathophysiology and risk factors. *Semin. Neonatol.* **6,** 121-133.

Saura J., Tusell J. M. and Serratosa J. (2003) High-yield isolation of murine microglia by mild trypsinization. *Glia* **44,** 183-189.

Sawada M., Suzumura A. and Marunouchi T. (1995) Cytokine network in the central nervous system and its roles in growth and differentiation of glial and neuronal cells. *Int. J. Dev. Neurosci.* **13,** 253-264.

Sawada M., Suzumura A., Yamamoto H. and Marunouchi T. (1990) Activation and proliferation of the isolated microglia by colony stimulating factor-1 and possible involvement of protein kinase C. *Brain Res.* **509,** 119-124.

Schobitz B., de Kloet E. R., Sutanto W. and Holsboer F. (1993) Cellular localization of interleukin 6 mRNA and interleukin 6 receptor mRNA in rat brain. *Eur. J. Neurosci.* **5,** 1426-1435.

Selmaj KW, Raine CS. (1988) Tumor necrosis factor mediates myelin and oligodendrocyte damage in vitro.*Ann Neurol.* **23,** 339-346.

Sheldon R. A., Chuai J. and Ferriero D. M. (1996) A rat model for

hypoxic-ischemic brain damage in very premature infants. *Biol. Neonate* **69,** 327-341.

Shimohama S., Tanino H., Kawakami N., Okamura N., Kodama H., Yamaguchi T., Hayakawa T., Nunomura A., Chiba S., Perry G., Smith M. A. and Fujimoto S. (2000) Activation of NADPH oxidase in Alzheimer's disease brains. *Biochem. Biophys. Res. Commun.* **273,** 5-9.

Simpson J. E., Newcombe J., Cuzner M. L. and Woodroofe M. N. (1998) Expression of monocyte chemoattractant protein-1 and other beta-chemokines by resident glia and inflammatory cells in multiple sclerosis lesions. *J. Neuroimmunol.* **84,** 238-249.

Sivakumar V, Ling EA, Lu J, Kaur C. (2009) Role of glutamate and its receptors and insulin-like growth factors in hypoxia induced periventricular white matter injury. *Glia.* Sep 30. [Epub ahead of print]

Sivakumar V, Lu J, Ling EA, Kaur C. (2008) Vascular endothelial growth factor and nitric oxide production in response to hypoxia in the choroid plexus in neonatal brain. *Brain Pathol.* **18**, 71-85.

Skoff R. P., Bessert D. A., Barks J. D., Song D., Cerghet M. and Silverstein F. S. (2001) Hypoxic-ischemic injury results in acute disruption of myelin gene expression and death of oligodendroglial precursors in neonatal mice. *Int. J. Dev. Neurosci.* **19,** 197-208.

Sorensen T. L., Tani M., Jensen J., Pierce V., Lucchinetti C., Folcik V. A., Qin S., Rottman J., Sellebjerg F., Strieter R. M., Frederiksen J. L. and Ransohoff R. M. (1999) Expression of specific chemokines and chemokine receptors in the central nervous system of multiple sclerosis patients. *J. Clin. Invest* **103,** 807-815.

Sridhar K, Kumar P, Katariya S, Narang A. (2001) Postasphyxial encephalopathy in preterm neonates.*Indian J Pediatr.* 68, 1121-1125.

Stanley E. R., Berg K. L., Einstein D. B., Lee P. S., Pixley F. J., Wang Y. and Yeung Y. G. (1997) Biology and action of colony--stimulating factor-1. *Mol. Reprod. Dev.* **46,** 4-10.

Sturrock RR. (1980) Myelination of the mouse corpus callosum. *Neuropathol Appl Neurobiol.* 6, 415-420.

Stys P. K. (2005) General mechanisms of axonal damage and its prevention. *J. Neurol. Sci.* **233,** 3-13.

Sugai K., Ito M., Tateishi I., Funabiki T. and Nishikawa M. (2006) Neonatal periventricular leukomalacia due to severe, poorly controlled asthma in the mother. *Allergol. Int.* **55,** 207-212.

Sun AY, Chen YM. (1998) Oxidative stress and neurodegenerative disorders. *J Biomed Sci.* **5,** 401-414.

Talos DM, Follett PL, Folkerth RD, Fishman RE, Trachtenberg FL, Volpe JJ, Jensen FE. (2006) Developmental regulation of AMPA receptor subunit expression in forebrain and relationship to regional susceptibility to hypoxic/ischemic injury. II. Human cerebral white matter and cortex. J Comp Neurol. 497, 61-77.

Taub D. D., Proost P., Murphy W. J., Anver M., Longo D. L., van D. J. and Oppenheim J. J. (1995) Monocyte chemotactic protein-1 (MCP-1), -2, and -3 are chemotactic for human T lymphocytes. *J. Clin. Invest* **95,** 1370-1376.

Tezel G. (2008) TNF-alpha signaling in glaucomatous neurodegeneration. *Prog Brain Res.* **173,** 409-421.

Thomas J. L., Spassky N., Perez Villegas E. M., Olivier C., Cobos I., Goujet-Zalc C., Martinez S. and Zalc B. (2000) Spatiotemporal development of oligodendrocytes in the embryonic brain. *J. Neurosci. Res.* **59,** 471-476.

Torres C., Aranguez I. and Rubio N. (1995) Expression of interferon-gamma receptors on murine oligodendrocytes and its regulation by cytokines and mitogens. *Immunology* **86,** 250-255.

Tsuji M., Saul J. P., du P. A., Eichenwald E., Sobh J., Crocker R. and Volpe J. J. (2000) Cerebral intravascular oxygenation correlates with mean arterial pressure in critically ill premature infants. *Pediatrics* **106,** 625-632.

Urrea C., Castellanos D. A., Sagen J., Tsoulfas P., Bramlett H. M. and Dietrich W. D. (2007) Widespread cellular proliferation and focal neurogenesis after traumatic brain injury in the rat. *Restor. Neurol. Neurosci.* **25,** 65-76.

Vannucci R. C. and Vannucci S. J. (2005) Perinatal hypoxic-ischemic brain damage: evolution of an animal model. *Dev. Neurosci.* **27,** 81-86.

Vela J. M., Molina-Holgado E., revalo-Martin A., Almazan G. and Guaza C. (2002) Interleukin-1 regulates proliferation and differentiation of oligodendrocyte progenitor cells. *Mol. Cell Neurosci.* **20,** 489-502.

Vigneswaran R. (2000) Infection and preterm birth: evidence of a common causal relationship with bronchopulmonary dysplasia and cerebral palsy. *J. Paediatr. Child Health* **36,** 293-296.

Vilhardt F. (2005) Microglia: phagocyte and glia cell. *Int. J. Biochem. Cell Biol.* **37,** 17-21.

Volpe J. J. (2001) Neurobiology of periventricular leukomalacia in the premature infant. *Pediatr. Res.* **50,** 553-562.

Volpe J. J. (2003) Cerebral white matter injury of the premature infant-more common than you think. *Pediatrics* **112,** 176-180.

Won J. S., Lee J. K. and Suh H. W. (2001) Forskolin inhibits expression of

inducible nitric oxide synthase mRNA via inhibiting the mitogen activated protein kinase in C6 cells. *Brain Res. Mol. Brain Res.* **89,** 1-10.

Wu Y. W. and Colford J. M., Jr. (2000) Chorioamnionitis as a risk factor for cerebral palsy: A meta-analysis. *JAMA* **284,** 1417-1424.

Wu CY, Kaur C, Sivakumar V, Lu J, Ling EA. (2009) Kv1.1 expression in microglia regulates production and release of proinflammatory cytokines, endothelins and nitric oxide. *Neuroscience.* **158,** 1500-1508.

Xu J, Ling EA. (1994) Upregulation and induction of major histocompatibility complex class I and II antigens on microglial cells in early postnatal rat brain following intraperitoneal injections of recombinant interferon-gamma. *Neuroscience.* **60,** 959-967

Xu J, Ling EA. (1994) Upregulation and induction of surface antigens with special reference to MHC class II expression in microglia in postnatal rat brain following intravenous or intraperitoneal injections of lipopolysaccharide. *J Anat.* **184,** 285-296

Yamasaki Y, Itoyama Y, Kogure K. (1996) Involvement of cytokine production in pathogenesis of transient cerebral ischemic damage. *Keio J Med.* **45**, 225-229.

Yan Y. P., Sailor K. A., Lang B. T., Park S. W., Vemuganti R. and Dempsey R. J. (2007) Monocyte chemoattractant protein-1 plays a critical role in neuroblast migration after focal cerebral ischemia. *J. Cereb. Blood Flow Metab.* **27,** 1213-1224.

Yeung Y. G. and Stanley E. R. (2003) Proteomic approaches to the analysis of early events in colony-stimulating factor-1 signal transduction. *Mol. Cell Proteomics.* **2,** 1143-1155.

You Y. and Kaur C. (2000) Expression of induced nitric oxide synthase in

amoeboid microglia in postnatal rats following an exposure to hypoxia. *Neurosci. Lett.* **279,** 101-104.

Zajicek J. P., Wing M., Scolding N. J. and Compston D. A. (1992) Interactions between oligodendrocytes and microglia. A major role for complement and tumour necrosis factor in oligodendrocyte adherence and killing. *Brain* **115 (Pt 6),** 1611-1631.

Zawadzka M. and Kaminska B. (2003) Immunosuppressant FK506 affects multiple signaling pathways and modulates gene expression in astrocytes. *Mol. Cell Neurosci.* **22,** 202-209.

Zhang K. and Sejnowski T. J. (2000) A universal scaling law between gray matter and white matter of cerebral cortex. *Proc. Natl. Acad. Sci. U. S. A* **97,** 5621-5626.

Zhou Y., Ling E. A. and Dheen S. T. (2007) Dexamethasone suppresses monocyte chemoattractant protein-1 production via mitogen activated protein kinase phosphatase-1 dependent inhibition of Jun N-terminal kinase and p38 mitogen-activated protein kinase in activated rat microglia. *J. Neurochem.* **102,** 667-678.

Zhu Z, Zhang Q, Yu Z, Zhang L, Tian D, Zhu S, Bu B, Xie M, Wang W. (2007) Inhibiting cell cycle progression reduces reactive astrogliosis initiated by scratch injury in vitro and by cerebral ischemia in vivo. *Glia.* **55,** 546-558

Figures and figure legends

Fig. 1 A coronal section of the brain in a 7 day old rat. The circled area represents the PWM.

Fig. 2 Real time RT-PCR analysis of TNF-α, IL-1β, TNF-R_1, IL-$1R_1$ mRNA expression in the PWM of postnatal rats at 3, 24 h, 3, 7 and 14 d after the hypoxic exposure and their corresponding controls. Panel A (TNF-α), B (IL-1β), C (TNF-R_1) and D (IL-$1R_1$) show the graphical representation of the fold changes quantified by normalization to the β-actin as an internal control. Each bar represents the mean ± SD. There is significant difference in mRNA levels after the hypoxic exposure when compared with the corresponding controls. *$p < 0.05$.

Fig. 3 Real time RT-PCR analysis of M-CSF, CSF-1R, MCP-1 and CCR_2 mRNA expression in the PWM of postnatal rats at 3, 24 h, 3, 7 and 14 d after the hypoxic exposure and their corresponding controls. Panel A (M-CSF), B (CSF-1R), C (MCP-1) and D (CCR_2) show the graphical representation of the fold changes quantified by normalization to the β-actin as an internal control. Each bar represents the mean ± SD. There is significant difference in mRNA levels after the hypoxic exposure when compared with the corresponding controls. *$p < 0.05$.

Fig. 4 Western blotting of TNF-α, IL-1β, TNF-R_1 and IL-$1R_1$ protein expression in the PWM tissue supernatants of rats at 3 , 24 h, 3 , 7 and 14 d after the hypoxic exposure and their corresponding controls (Cn). The upper panels (A) show TNF-α (30 kDa) , IL-1β (17 kDa) , TNF-R_1 (55 kDa), IL-$1R_1$ (80 kDa) and β -actin (42kDa) immunoreactive bands, respectively. The lower panels (B, TNF-α), (C IL-1β), (D, TNF-R_1) and (E, IL-$1R_1$) are bar graphs showing significant changes in the optical density following hypoxic exposure when compared with their corresponding controls (mean ± SD). β -actin as internal control. * $p < 0.05$.

Fig. 5 M-CSF, CSF-1R, CCR_2 and MCP-1 protein expression in the PWM at 3, 24h, 3, 7 and 14 days after hypoxic exposure and corresponding control rats. A shows M-CSF (18.5KDa), CSF-1R (170KDa) and β-actin (42KDa) immunoreactive bands, respectively. B, C shows bar graphs depicting significant changes in the optical density of M-CSF and CSF-1R, respectively, following hypoxic exposure when compared with their corresponding controls. Bar graph D shows CCR_2 (47KDa) and β-actin (42KDa) immunoreactive bands, respectively. Bar graph in E shows significant changes in the optical density of CCR_2 following hypoxic exposure when compared with their corresponding controls. F shows that hypoxia triggered release of MCP-1 is significantly increased at 3, 24h, 3, 7 and 14d. Significant difference in mRNA and protein levels in the PWM after the hypoxic exposure is evident when compared with controls. (* $p< 0.05$).

Fig. 6 Confocal images showing the distribution of lectin labelled (A, D, G, J; green), TNF-α (B, E; red) and IL-1β (H, K; red) immunoreactive amoeboid microglial cells (AMC; arrows) in the PWM at 24h after the hypoxic exposure and the corresponding control rat. The colocalized expression of lectin and TNF-α as well as lectin and IL-1β in AMC can be seen in C and F, I and L. The expression of TNF-α (E) and IL-1β (K) in AMC (arrows) is markedly enhanced after the hypoxic exposure. Scale bars: A- L, 50μm.

Fig. 7 Confocal images showing the distribution of GFAP labeled (A, D, G, J, M, P; green), and TNF-α (B, E, H, K, N, Q; red) immunoreactive astrocytes (arrows) in the PWM at 24h, 7 and 14d after the hypoxic exposure and the corresponding control rats. The colocalized expression of GFAP and TNF-α in astrocytes can be seen in C, F, I, L, O and R. Note TNF-α expression in astrocytes (arrows) is markedly enhanced at 7 and 14d after the hypoxic exposure. Scale bars: A-R, 10μm.

Fig. 8 Confocal images showing the distribution of GFAP labeled (A, D, G, J; M, P, green), and IL-1β (B, E, H, K, N, Q; red) immunoreactive astrocytes (arrows) in the PWM at 24h, 7 and 14d after the hypoxic exposure and the corresponding control rats. The colocalized expression of GFAP and IL-1β in astrocytes can be seen in C, F, I, L, O and R. Note IL-1β expression in astrocytes (arrows) is markedly enhanced at 7 and 14d after the hypoxic exposure. Scale bars: A-R, 10μm.

Fig. 9 Confocal images showing the distribution of CC_1 (A, D, G, J; green) , TNF-R_1 (B, E; red) and IL-$1R_1$ (H, K; red) in oligodendrocytes (arrows) and their processes in the PWM at 7d after the hypoxic exposure and the corresponding control. The colocalized expression of CC_1 with TNF-R_1 and IL-$1R_1$ is depicted in C and F, I and L. Note the expression of TNF-R_1 and IL-$1R_1$ is upregulated after the hypoxic exposure. The percentage of TNF-R_1 and IL-$1R_1$ immunoreactive positive oligodendrocytes is significantly increased as shown in bar graph M (* $p < 0.01$). Scale bars: A-L, 20μm.

Fig. 10 Confocal images showing the distribution of NF-200 (A, D, G, J; green) , TNF-R_1 (B, E; red) and IL-$1R_1$ (H, K; red) in axons (arrows) in the PWM at 14d after the hypoxic exposure and the corresponding control. Colocalized expression of NF-200 with TNF-R_1 and IL-$1R_1$ is depicted in C and F, I and L. Note the expression of TNF-R_1 and IL-$1R_1$ is upregulated after the hypoxic exposure. Scale bars: A-L, 20μm.

Fig. 11 Confocal images showing the distribution of lectin labeled (A, D, G, J; green), and M-CSF (B, E, H, K; red) immunoreactive amoeboid microglial cells (AMC; arrows) in the PWM at 3 and 7d after the hypoxic exposure and in the corresponding control rat. The colocalized expression of lectin and M-CSF in AMC can be seen in C, F, I and L. Note M-CSF expression in AMC (arrows) is markedly enhanced after the hypoxic exposure. Scale bars: A- L, 50μm.

Fig. 12 Confocal images showing the distribution of GFAP labeled (A, D, G, J; green), and CSF-1R (B, E, H, K; red) immunoreactive astrocytes (arrows) in the PWM at 7 and 14d after the hypoxic exposure and the corresponding control rats. The colocalized expression of GFAP and CSF-1R in astrocytes can be seen in C, F, I and L. Note CSF-1R expression in astrocytes (arrows) is markedly enhanced after the hypoxic exposure. Scale bars: A- L, 10μm.

Fig. 13 Confocal images showing the distribution of lectin labeled (A, D, G, J; green), and MCP-1 (B, E, H, K; red) immunoreactive AMC (arrows) in the PWM at 3 and 24h after the hypoxic exposure and the corresponding control rats. Lectin labeling clearly overlaps MCP-1 immunofluorescence in C, F, I and L. Note MCP-1 expression in AMC (arrows) is markedly enhanced after the hypoxic exposure. Scale bars: A- L, 50μm.

Fig. 14 Confocal images showing the distribution of lectin labeled (A, D, G, J; green), and MCP-1 (B, E, H, K; red) immunoreactive AMC (arrows) in the PWM at 3 and 7d after the hypoxic exposure and the corresponding control rats. Colocalized expression of lectin and MCP-1 in AMC is evident in C, F, I and L. The expression of MCP-1 in AMC (arrows) is markedly enhanced after the hypoxic exposure. Scale bars: A- L, 50μm.

Fig. 15 Confocal images showing the distribution of lectin labeled (A, D, G, J; green), and CCR_2 (B, E, H, K; red) immunoreactive AMC (arrows) in the PWM at 3h and 3d after the hypoxic exposure and the corresponding control rats. Colocalized expression of lectin and CCR_2 in AMC is evident in C, F, I and L. The expression of CCR_2 in AMC (arrows) is markedly enhanced after the hypoxic exposure. Scale bars: A- L, 20μm.

Fig. 16 MBP and NF-200 protein expression in the PWM at 14 days after the hypoxic exposure and the corresponding control rats. A shows MBP and β-actin (42KDa) immunoreactive bands, respectively. Bar graph in B shows significant decrease in the optical density of MBP following hypoxic exposure when compared with the corresponding controls (* $p < 0.01$). Confocal images show the expression of MBP (C, green), NF-200 (D, red), and co-localized expression of MBP and NF-200 (E) in the PWM at 14 days of control rats. F-H show the expression of MBP (F, green), NF-200 (G, red), and co-localized expression of MBP and NF-200 (H) at 14 days after the hypoxic exposure. Note the MBP positive processes and NF-200 positive axons are disrupted following the hypoxic exposure (F, G) as compared with the control (C, D). Scale bars: C-H, 50μm.

Fig. 17 Confocal images showing CC_1 immunolabeled oligodendrocytes (arrows)(A, D; red) and apoptotic cells (arrows)(B, E; green) as detected by TUNEL in the PWM of a control and a hypoxic rat at 7d after the hypoxic exposure. The colocalized expression of CC_1 and TUNEL labeling can be seen in C and F. Bar graphs in G and H show the significant increase in percentage of apoptotic nuclei (G) and decrease in the number of CC1 positive oligodendrocytes/mm^2 (H) in the PWM after the hypoxic exposure (* $p < 0.01$). Scale bars: A-F, 20μm.

Fig. 18 Electron micrographs showing necrotic cells in the PWM at 24h (A) and 7d (C) after the hypoxic exposure. B and D show apoptotic cells. E and F show AMC with internalized necrotic (E) and apoptotic (F) cells (arrows) in the PWM at 7d after the hypoxic exposure.

Fig. 19 Electron micrographs of non-myelinated (A, B, C) and myelinated (B, D) axons (AX) in the PWM at 7 and 14 days after the hypoxic exposure. Note the swelling and vacuolation of non-myelinated axons (A, C) and distortion of myelin sheaths (arrows, B, D). Scale bars A, C =0.5μm, B=0.2μm, D=1μm.

Fig. 20 Confocal images showing the distribution of lectin labeled (A, D, G, J; green), and BrdU (B, E, H, K; red) immunoreactive amoeboid microglial cells (AMC) in the PWM at 3 and 24h after the hypoxic exposure and the corresponding control rats. Colocalized expression of lectin and BrdU is seen in merged images in C, F, I and L. Note the number of AMC is markedly increased in hypoxic rats; however, fewer BrdU positive AMC are observed. Bar graph in M shows a significant increase in the cell number of AMC in the PWM at 3 and 24h after the hypoxic exposure when compared with their corresponding controls (* $p < 0.01$). Bar graph in N shows the percentage of BrdU positive AMC against the total AMC population at 3 and 24h after the hypoxic exposure when compared with their corresponding controls. Scale bars: A- L, 50μm.

Fig. 21 Confocal images showing the distribution of lectin labeled (A, D, G, J; green), and BrdU (B, E, H, K; red) immunoreactive AMC in the PWM at 3 and 7d after the hypoxic exposure and the corresponding control rats. Merged images in C, F, I and L show the colocalized expression of lectin and BrdU in these cells. The number of AMC is drastically increased. BrdU positive AMC is noticeably increased at 7d after the hypoxic exposure when compared with the corresponding control. Bar graph in M shows a significant increase in the cell number of AMC in the PWM at 3 and 7d after the hypoxic exposure when compared with their corresponding controls (* $p < 0.01$). Bar graph in N shows the percentage of BrdU positive AMC against the total AMC population at 3 and 7d after the hypoxic exposure when compared with their corresponding controls (* $p < 0.01$). Scale bars: A- L, 50μm.

Fig. 22 MCP-1 induces microglial cell migration *in vivo*. Few lectin positive microglial cells are distributed in the PWM (arrowhead) of the sham-operated (A) and saline injected rats (D). Many lectin positive microglial cells migrate to MCP-1 (500 ng/mL) injection site (G). Images in B–C, E-F, H-I are enlarged view of areas outlined in A, D and G. Arrowheads indicate lectin positive microglial cells in the ipsilateral or contralateral PWM. Arrows represent needle track in the PWM. Boxed area represents the injection site and its peripheral areas; circled area represents the corresponding area in the contralateral side. Bar graph in J shows a significant increase in the cell number of AMC in the PWM ipsilateral to MCP-1 injection when compared to the corresponding areas on the contralateral side and those given saline injection or sham-operated rats (* $p < 0.01$). Scale bar: B-C, E-F, H-I 50 μm; A, D, G 500μm.

Fig. 23 MCP-1 induces microglial cell migration *in vivo*. Few OX-42 positive microglial cells are distributed in the PWM (arrowhead) of the sham-operated (A) and saline injected rats (D). Many OX-42 positive microglial cells migrate to MCP-1 (500 ng/mL) injection site (G). Images in B–C, E-F, H-I are enlarged view of areas outlined in A, D and G. Arrowheads indicate OX-42 positive microglial cells in the ipsilateral or contralateral PWM. Arrows represent needle track in the PWM. Boxed area represents the injection site and its peripheral areas; circled area represents the corresponding area in the contralateral side. Bar graph in J shows a significant increase in the cell number of AMC in the PWM ipsilateral to MCP-1 injection when compared to the corresponding areas on the contralateral side and those given saline injection or sham-operated rats (* $p < 0.01$). Scale bar: B-C, E-F, H-I 50 μm; A, D, G 500μm.

Fig. 24 mRNA expression of TNF-α, IL-1β, M-CSF and MCP-1 in cultured control microglia and at 1, 2, 4 and 6 h after hypoxic exposure. A (TNF-α mRNA), B (IL-1β mRNA), C (M-CSF mRNA) and D (IL-1β mRNA) show the graphical representation of the fold changes quantified by normalization to the β-actin as an internal control. Significant differences in mRNA and protein levels in microglial cells after the hypoxic exposure are evident when compared with controls, * $p < 0.05$.

Fig. 25 Protein expression of TNF-α, IL-1β, M-CSF and MCP-1 in cultured control microglia and at 1, 2, 4 and 6 h after hypoxic exposure. The panels A show TNF-α (30 kDa), IL-1β (17 kDa) and M-CSF (18.5 kDa) immunoreactive protein bands. B, C and D are bar graphs showing changes in the optical density of TNF-α, IL-1β and M-CSF, respectively, following hypoxic exposure. Bar graph E is ELISA analysis showing hypoxia triggered release of MCP-1 is significantly increased in the medium at 1, 2, 4 and 6h after hypoxic exposure. Significant differences in protein levels in microglial cells after the hypoxic exposure are evident when compared with controls, * $p < 0.05$.

Fig. 26 Confocal images of cultured control microglia showing the expression of lectin (A, G; green), TNF-α (B, red), IL-1β (H, red) and co-localized expression of lectin and TNF-α (C) as well as lectin and IL-1β (I). D-F show the expression of lectin (D, green), TNF-α (E, red) and co-localized expression of lectin and TNF-α (F) after treatment with 3% oxygen for 4h. Note the elevated expression of TNF-α following treatment with 3% oxygen for 4h (E) as compared with the control cells (B). J-L show the expression of lectin (J, green), IL-1β (K, red) and co-localized expression of lectin and IL-1β (L) after treatment with 3% oxygen for 4h. The expression of IL-1β is greatly increased in the microglial cells after hypoxic exposure for 4h. The bar graph M shows a significant increase in the percentage of TNF-α and IL-1β immunoreactive microglia after the hypoxic exposure when compared with the control cells (* $p < 0.01$). Scale bars: A-L, 50μm.

Fig. 27 Confocal images of cultured control microglia showing the expression of lectin (A, G; green), M-CSF (B, red), MCP-1 (H, red) and co-localized expression of lectin and M-CSF (C) as well as lectin and MCP-1 (I). D-F show the expression of lectin (D, green), M-CSF (E, red) and co-localized expression of lectin and M-CSF (F) after treatment with 3% oxygen for 4h. Note the elevated expression of M-CSF following treatment with 3% oxygen for 4h (E) as compared with the control cells (B). J-L show the expression of lectin (J, green), MCP-1 (K, red) and co-localized expression of lectin and MCP-1 (L) after treatment with 3% oxygen for 4h. The expression of MCP-1 is greatly increased in the microglial cells after hypoxic exposure for 4h. Scale bars: A-L, 50μm.

Fig. 28 Western blot analysis showing hypoxia induced TNF-α and IL-1β production via activation of MAPK pathway in microglia. The panels A, B, C show JNK, p38, ERK phosphorylation and total JNK, p38, ERK immunoreactive bands. The panels D, E and F, G show immunoreactive bands which indicate that SP600125 (a JNK inhibitor) and SB203580 (a p38 inhibitor) suppress the expression TNF-α and IL-1β, respectively, in the microglial cells after hypoxic exposure for 4h. H-J are bar graphs showing significant changes in the optical density of JNK, p38 and ERK phosphorylation, respectively, following hypoxic exposure. K-N are bar graphs showing significant suppression in expression of TNF-α and IL-1β by SP600125 and SB203580, respectively, * $p < 0.05$.

Fig. 29 Confocal images of cultured microglia showing the expression of the N-terminal phosphorylated c-JUN (phos-c-JUN) (B, red), counter-staining with DAPI (A, blue), and co-localized expression of DAPI and phos-c-JUN (C). D-F show the expression of phos-c-JUN (E, red), counter-staining with DAPI (D, blue), and co-localized expression of DAPI and phos-c-JUN (F) after treatment of cells with 3% oxygen for 45 min. The expression of phos-c-JUN in the nucleus is greatly increased after hypoxia for 45 min. G represents the percentage of phospho-c-JUN positive control microglial cells and cells treated with 3% oxygen (*$p < 0.01$). Scale bars: A-F, 50μm.

Fig. 30 Western blot analysis showing hypoxia induced MCP-1 production via activation of NF-kappaB signaling pathway in microglia. Panels A, B, C, D show phos-NF-kappaB, NF-kappaB, phos-IkappaB and IkappaB immunoreactive bands. E-G are bar graphs showing significant changes in the optical density of phos-NF-kappaB, NF-kappaB and phos-IkappaB, respectively, following hypoxic exposure. H is a bar graph showing no significant change in the optical density of IkappaB following hypoxic exposure. In bar graph I, ELISA analysis shows that BAY 11-7082 (a NF-kappaB inhibitor) suppresses the release of MCP-1 in the microglial cells after hypoxic exposure for 4h. (*$p< 0.05$)(ns: $p> 0.05$).

Fig. 31 mRNA and protein expression of TNF-α, IL-1β and CSF-1R in cultured control astrocytes and at 3 , 6 , 12 and 24 h after treatment with M-CSF in A-G. A (TNF-α mRNA), B (IL-1β mRNA) and C (CSF-1R mRNA) show the graphical representation of the fold changes quantified by normalization to the β-actin as an internal control. Panel D shows TNF-α (30 kDa), IL-1β (17 kDa) and CSF-1R (170kDa) immunoreactive protein bands. E, F and G are bar graphs showing changes in the optical density of TNF-α, IL-1β and CSF-1R, respectively, following M-CSF treatment. Significant differences in mRNA and protein levels in astrocytes with M-CSF treatment are evident when compared with controls, * $p < 0.05$.

Fig. 32 Confocal images of cultured control astrocytes showing the expression of GFAP (A, G, M; green), TNF-α (B, red), IL-1β (H, red), CSF-1R (N, red) and co-localized expression of GFAP and TNF-α (C), GFAP and IL-1β (I) as well as GFAP and CSF-1R (O). D-F show the expression of GFAP (D, green), TNF-α (E, red) and co-localized expression of GFAP and TNF-α (F) after treatment with M-CSF for 12h. J-L show the expression of GFAP (J, green), IL-1β (K, red) and co-localized expression of GFAP and IL-1β (L) after treatment with M-CSF for 12h. P-R show the expression of GFAP (P, green), CSF-1R (Q, red) and co-localized expression of GFAP and CSF-1R (R) after treatment with M-CSF for 12h. The expression of TNF-α (E), IL-1β (K) and CSF-1R (Q) is greatly increased in the astrocytes after treatment with M-CSF for 12h as compared with the control cells (B, H, N).Scale bars: A-R, 50μm.

Fig. 33 Western blot analysis showing M-CSF induced TNF-α and IL-1β production via activation of MAPK pathway in astrocytes. Panels A, B and C show JNK, p38, ERK phosphorylation and total JNK, p38, ERK immunoreactive bands. Panels D and E show immunoreactive bands which indicate that SP600125 (a JNK inhibitor) suppress the expression TNF-α and IL-1β, respectively, in the astrocytes after M-CSF treatment for 3h. Panels F and G show immunoreactive bands which indicate that SB203580 (a p38 inhibitor) can not suppress the expression TNF-α and IL-1β, respectively, in the astrocytes after M-CSF treatment for 3h. H and J are bar graphs showing significant changes in the optical density of JNK and ERK phosphorylation, respectively, following treatment with M-CSF. I is a bar graph showing no significant changes in the optical density of p38 phosphorylation following treatment with M-CSF. K-L are bar graphs showing significant suppression in expression of TNF-α and IL-1β by SP600125, respectively. M-N are bar graphs showing no significant suppression in expression of TNF-α and IL-1β by SB203580, respectively, * $p < 0.05$, ns: $p > 0.05$

Fig. 34 *In vitro* chemotaxis assay shows the effects of DMEM, control, hypoxia 4h and hypoxia 4h + anti-MCP-1 antiserum, hypoxia 4h + unrelated antiserum treated microglial cultures on the migration of microglia. (A) Chamotaxis assay results show a few crystal violet-stained microglia transmigrate through the membrane of insert in a transwell chamber in the DMEM medium. Optimized conditioned medium derived from hypoxia treated microglial cultures attracts more microglial cells than the control medium. The number of hypoxia-induced transmigrated microglia is markedly reduced in hypoxia 4h + anti-MCP-1 antiserum treated medium. The medium of hypoxia treated culture with rabbit anti-MCP-1 antiserum attracts less microglia than that from hypoxia 4h + unrelated antiserum (rabbit anti-iNOS). (B) Quantitative analysis shows that hypoxia-induced migration is suppressed significantly by anti-MCP-1 antiserum. Data represent the mean percentage of migrated cells per microscopic field relative to spontaneous migration toward the DMEM medium (0.5% BSA). Mean ± SD (n = 4 independent experiments), (*p< 0.05).

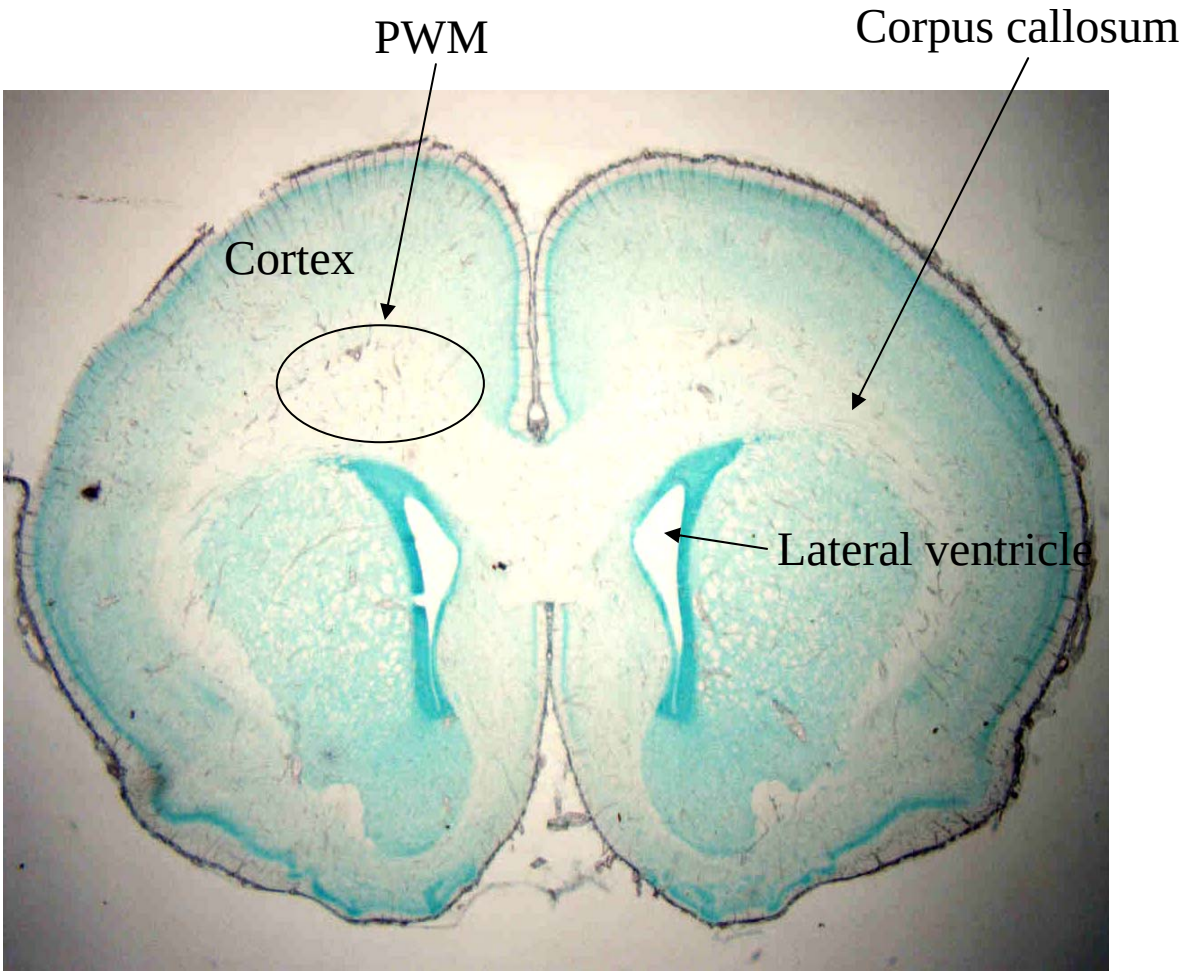

Fig. 1

A

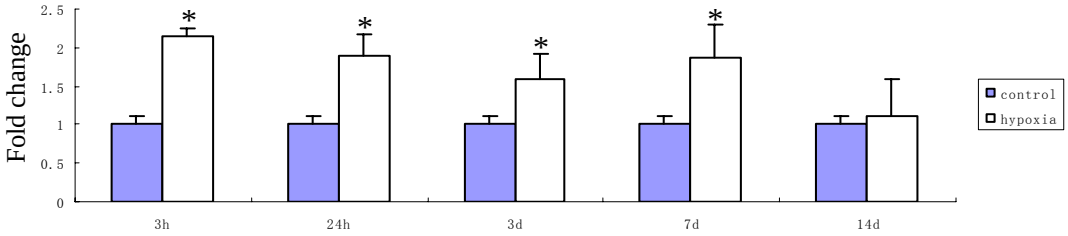

TNF- α

B

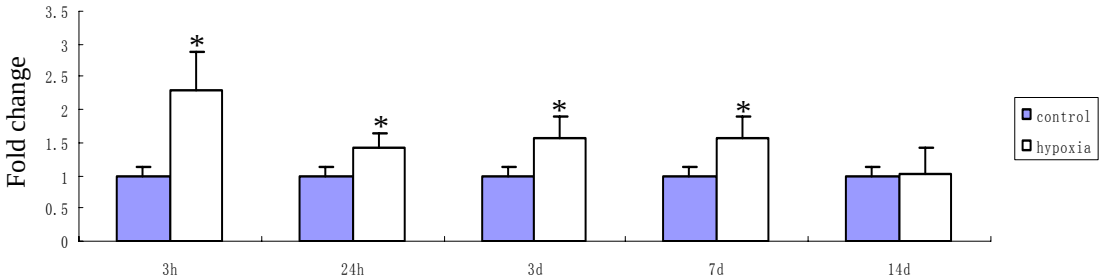

IL-1 β

C

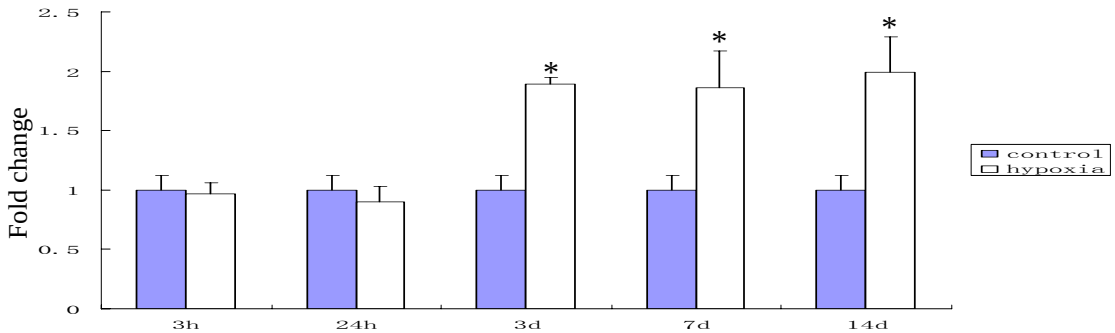

TNF-R_1

D

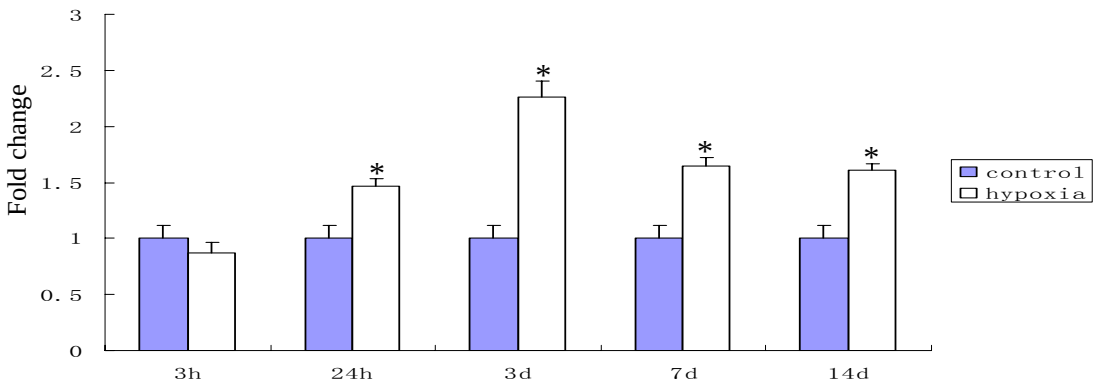

IL-1R_1

Fig.2

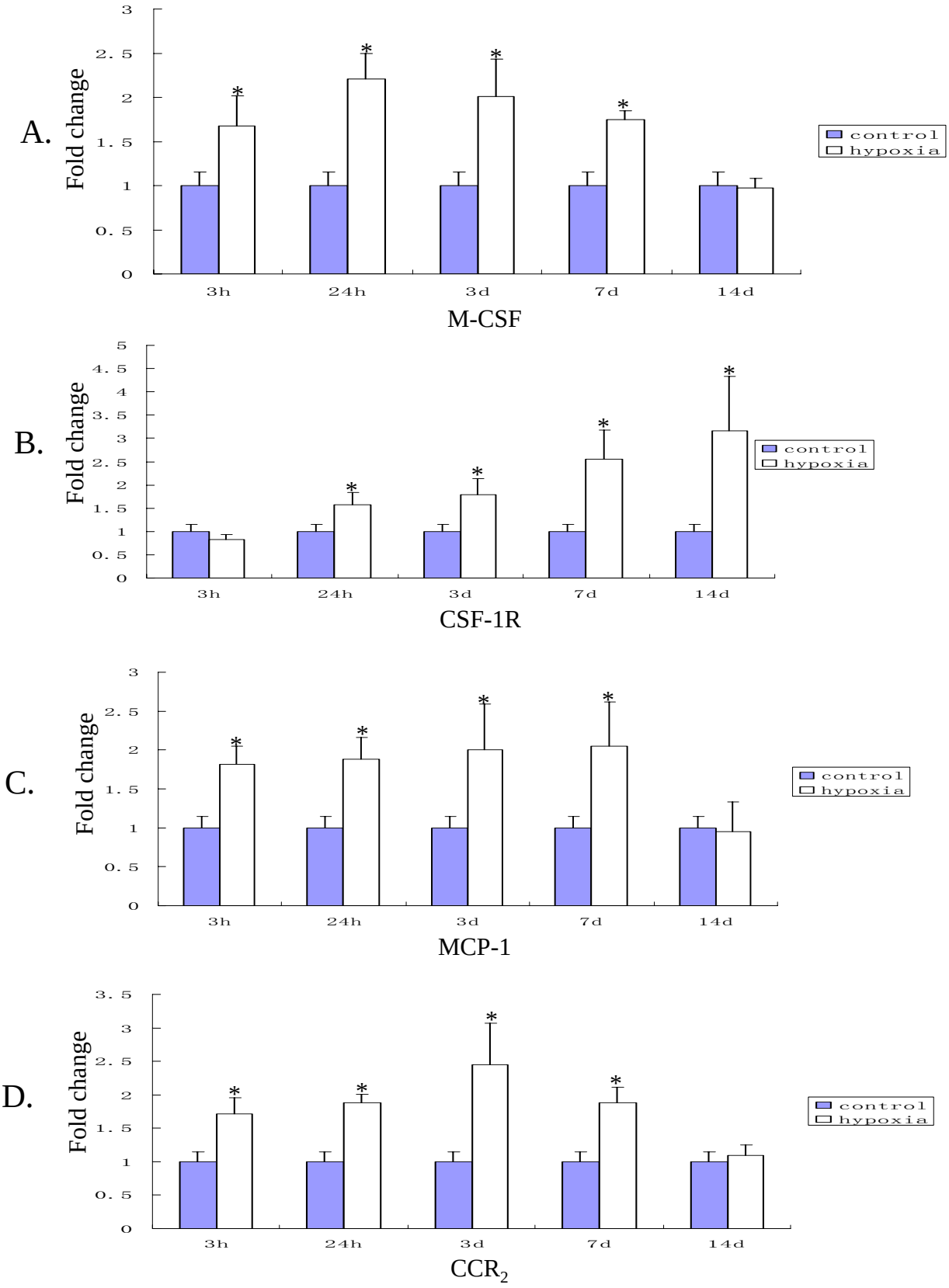
A.
Fold change
3
2.5
2
1.5
1
0.5
0
3h
24h
3d
7d
14d
control
hypoxia
M-CSF
B.
Fold change
5
4.5
4
3.5
3
2.5
2
1.5
1
0.5
0
3h
24h
3d
7d
14d
control
hypoxia
CSF-1R
C.
Fold change
3
2.5
2
1.5
1
0.5
0
3h
24h
3d
7d
14d
control
hypoxia
MCP-1
D.
Fold change
3.5
3
2.5
2
1.5
1
0.5
0
3h
24h
3d
7d
14d
control
hypoxia
CCR2

Fig. 3

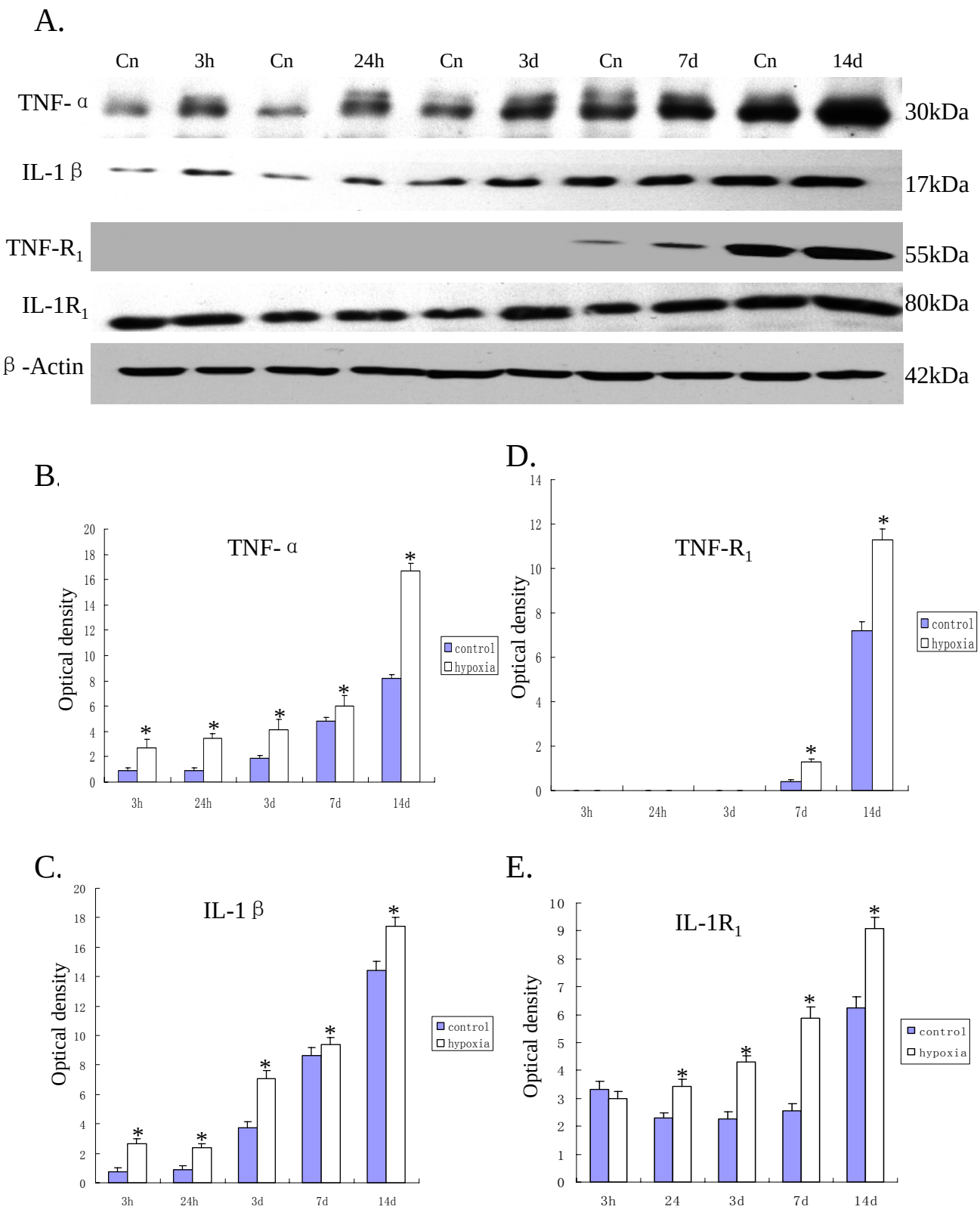
A.
Cn
3h
Cn
24h
Cn
3d
Cn
7d
Cn
14d
TNF- α
30kDa
IL-1 β
17kDa
TNF-R1
55kDa
IL-1R1
80kDa
β -Actin
42kDa
B.
TNF- α
Optical density
control
hypoxia
3h
24h
3d
7d
14d
D.
TNF-R1
Optical density
control
hypoxia
C.
IL-1 β
Optical density
control
hypoxia
E.
IL-1R1
Optical density
control
hypoxia

Fig.4

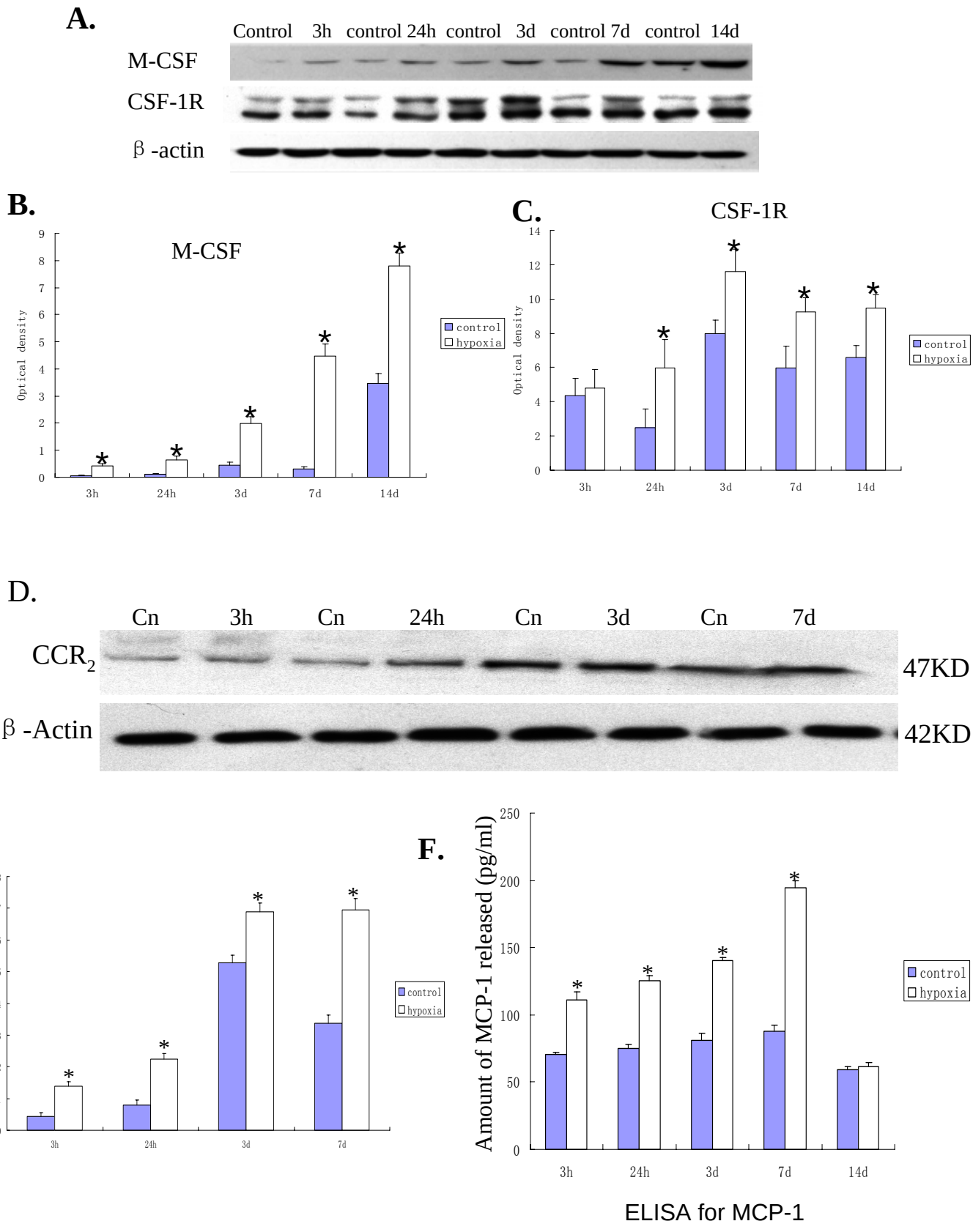
A.
Control
3h
control 24h
control
3d
control 7d
control
14d
M-CSF
CSF-1R
β -actin
B.
M-CSF
Optical density
control
hypoxia
3h
24h
3d
7d
14d
C.
CSF-1R
Optical density
control
hypoxia
3h
24h
3d
7d
14d
D.
Cn
3h
Cn
24h
Cn
3d
Cn
7d
CCR2
47KD
β -Actin
42KD
E.
Optical density
control
hypoxia
3h
24h
3d
7d
F.
Amount of MCP-1 released (pg/ml)
control
hypoxia
3h
24h
3d
7d
14d
ELISA for MCP-1

Fig.5

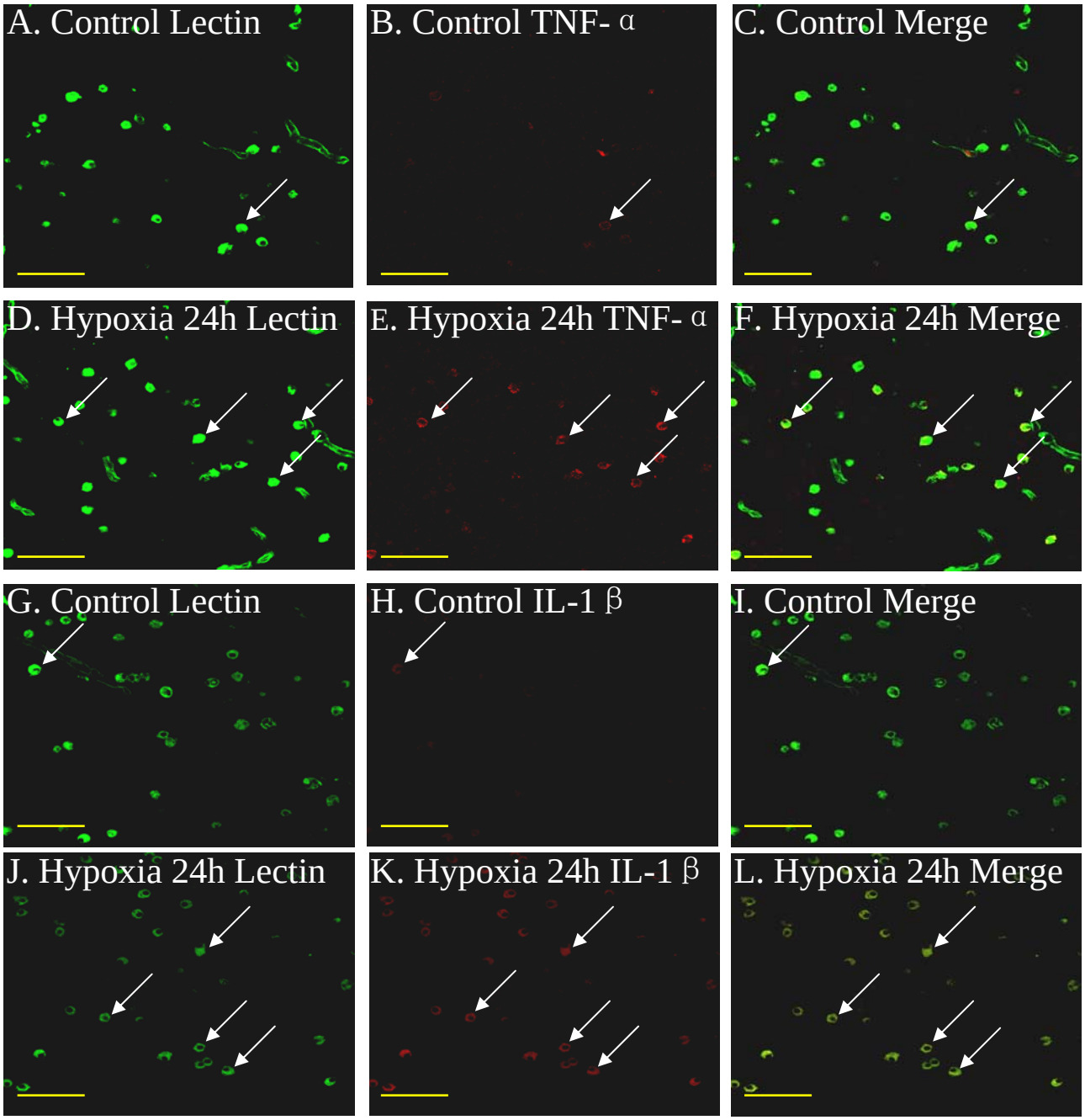
A. Control Lectin
B. Control TNF- α
C. Control Merge
D. Hypoxia 24h Lectin
E. Hypoxia 24h TNF- α
F. Hypoxia 24h Merge
G. Control Lectin
H. Control IL-1 β
I. Control Merge
J. Hypoxia 24h Lectin
K. Hypoxia 24h IL-1 β
L. Hypoxia 24h Merge

Fig.6

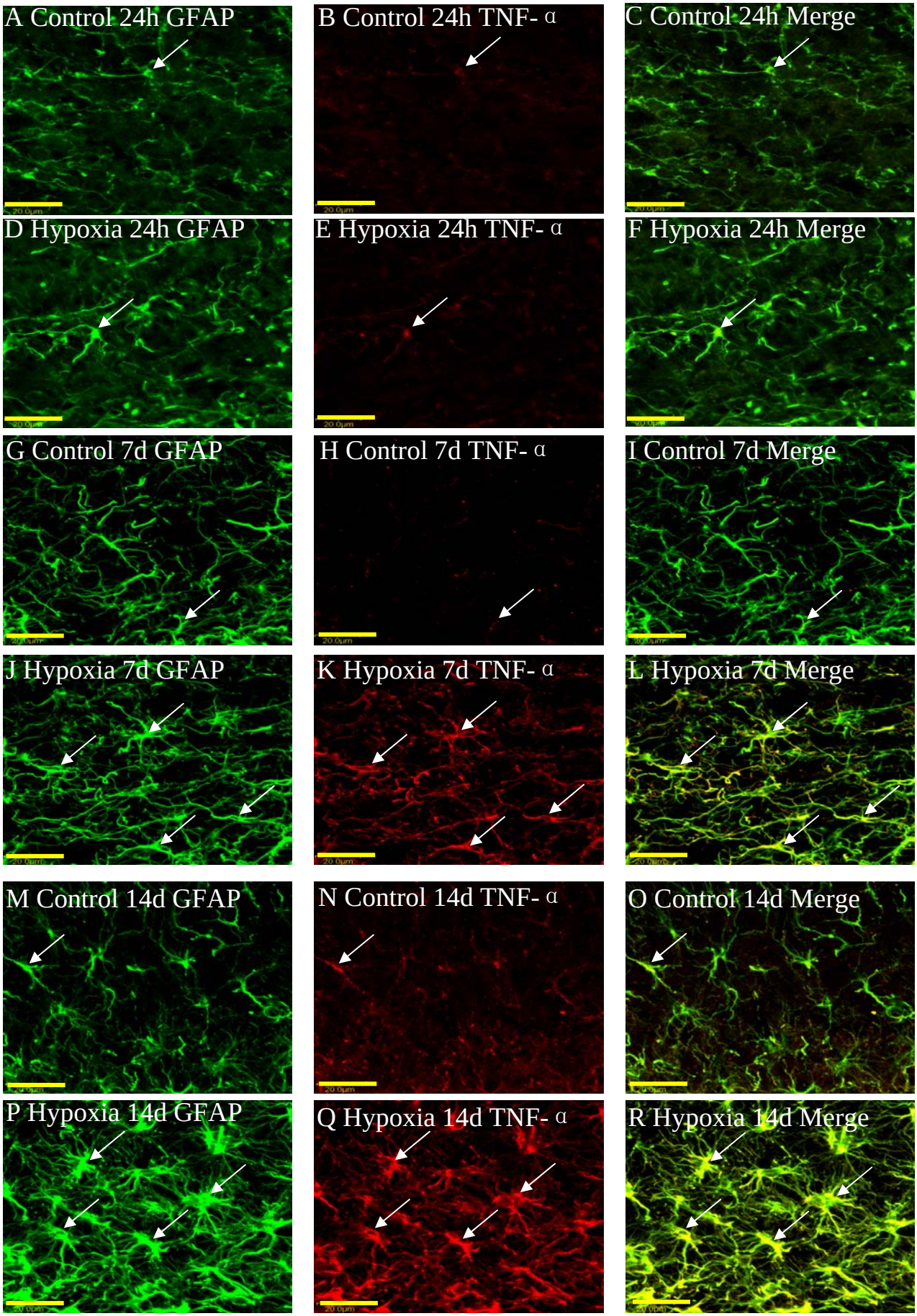
A Control 24h GFAP
B Control 24h TNF- α
C Control 24h Merge
D Hypoxia 24h GFAP
E Hypoxia 24h TNF- α
F Hypoxia 24h Merge
G Control 7d GFAP
H Control 7d TNF- α
I Control 7d Merge
J Hypoxia 7d GFAP
K Hypoxia 7d TNF- α
L Hypoxia 7d Merge
M Control 14d GFAP
N Control 14d TNF- α
O Control 14d Merge
P Hypoxia 14d GFAP
Q Hypoxia 14d TNF- α
R Hypoxia 14d Merge

Fig.7

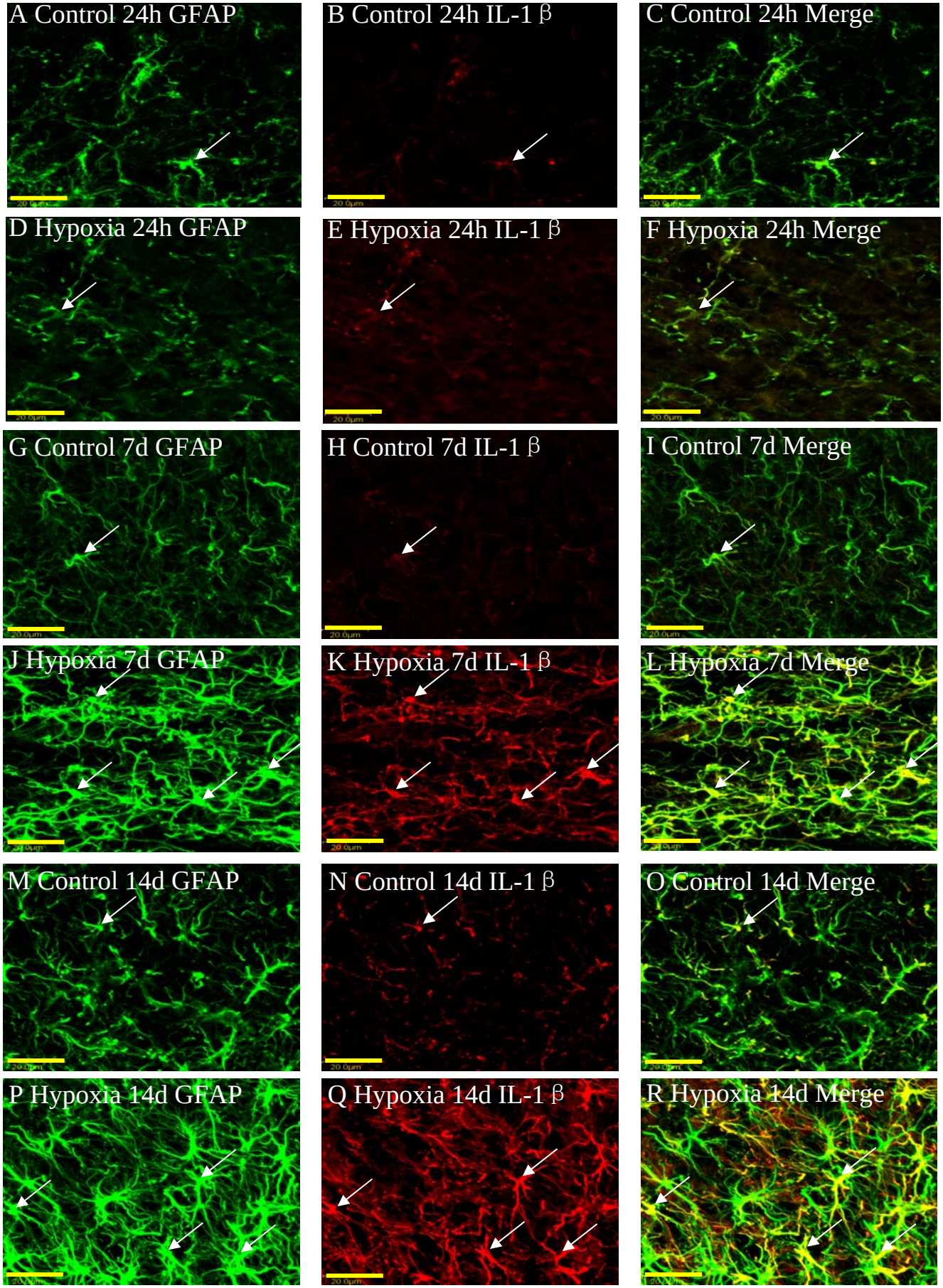
A Control 24h GFAP
B Control 24h IL-1 β
C Control 24h Merge
D Hypoxia 24h GFAP
E Hypoxia 24h IL-1 β
F Hypoxia 24h Merge
G Control 7d GFAP
H Control 7d IL-1 β
I Control 7d Merge
J Hypoxia 7d GFAP
K Hypoxia 7d IL-1 β
L Hypoxia 7d Merge
M Control 14d GFAP
N Control 14d IL-1 β
O Control 14d Merge
P Hypoxia 14d GFAP
Q Hypoxia 14d IL-1 β
R Hypoxia 14d Merge

Fig.8

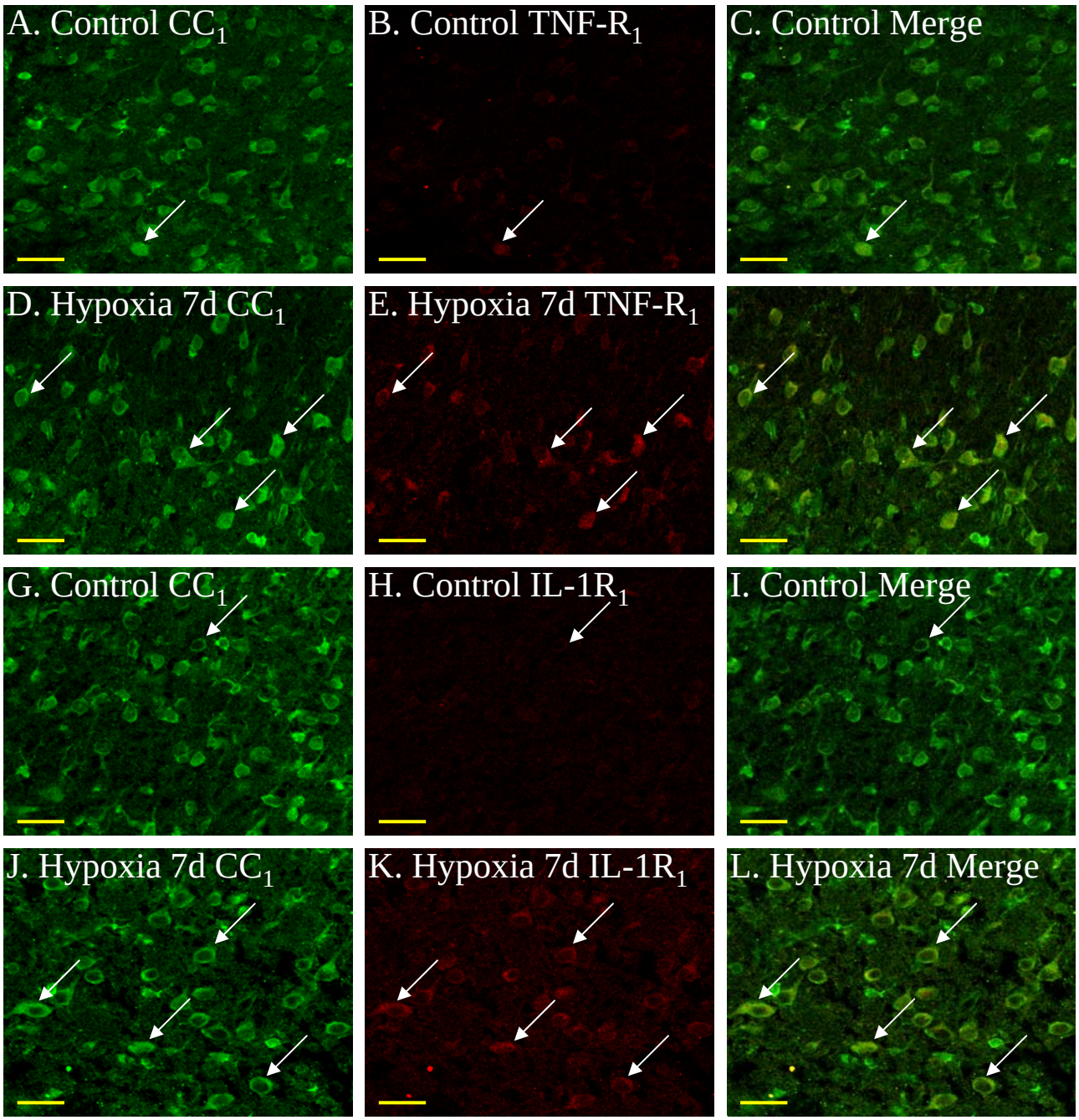
A. Control CC1
B. Control TNF-R1
C. Control Merge
D. Hypoxia 7d CC1
E. Hypoxia 7d TNF-R1
G. Control CC1
H. Control IL-1R1
I. Control Merge
J. Hypoxia 7d CC1
K. Hypoxia 7d IL-1R1
L. Hypoxia 7d Merge

Fig.9

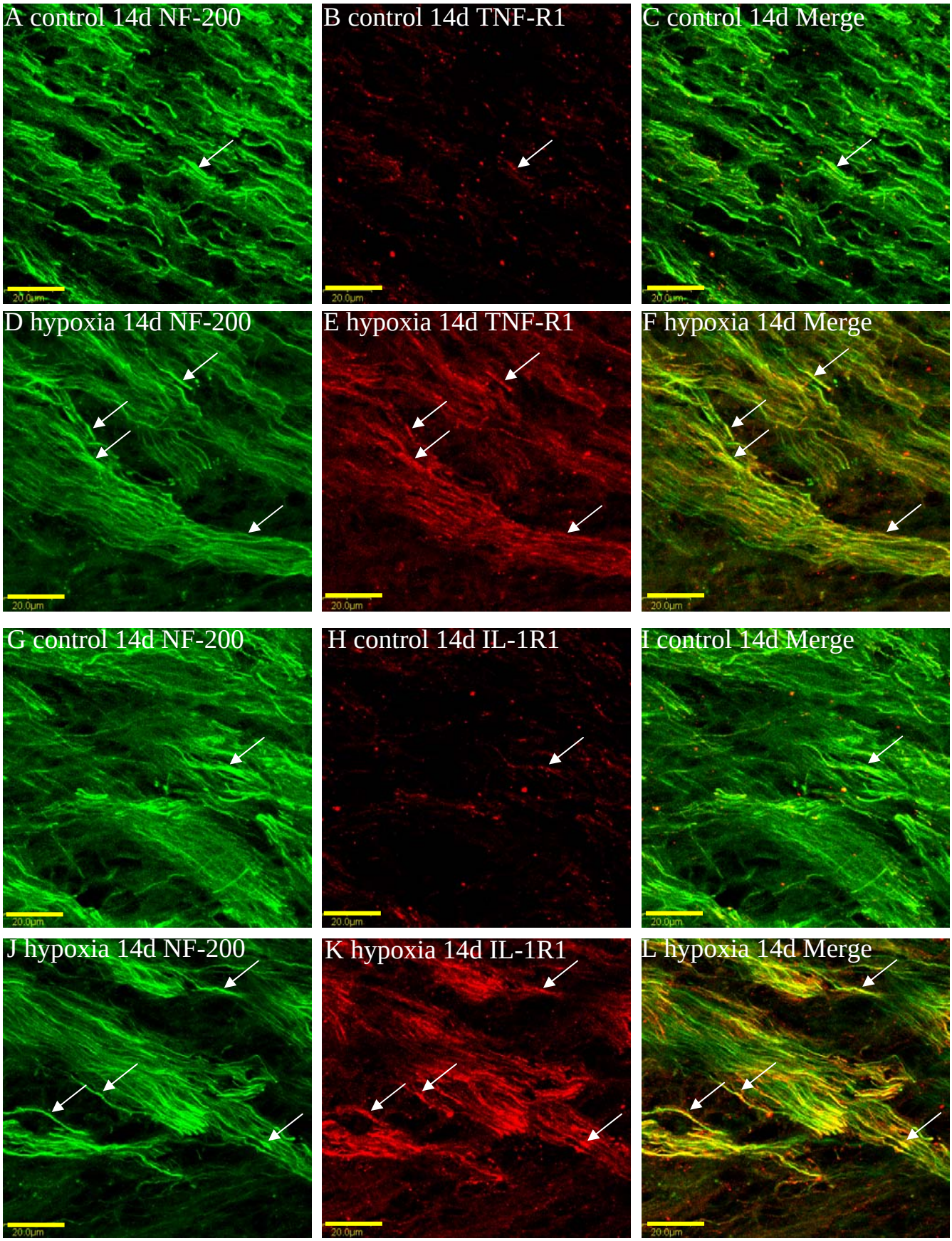
A control 14d NF-200
B control 14d TNF-R1
C control 14d Merge
D hypoxia 14d NF-200
E hypoxia 14d TNF-R1
F hypoxia 14d Merge
G control 14d NF-200
H control 14d IL-1R1
I control 14d Merge
J hypoxia 14d NF-200
K hypoxia 14d IL-1R1
L hypoxia 14d Merge

Fig.10

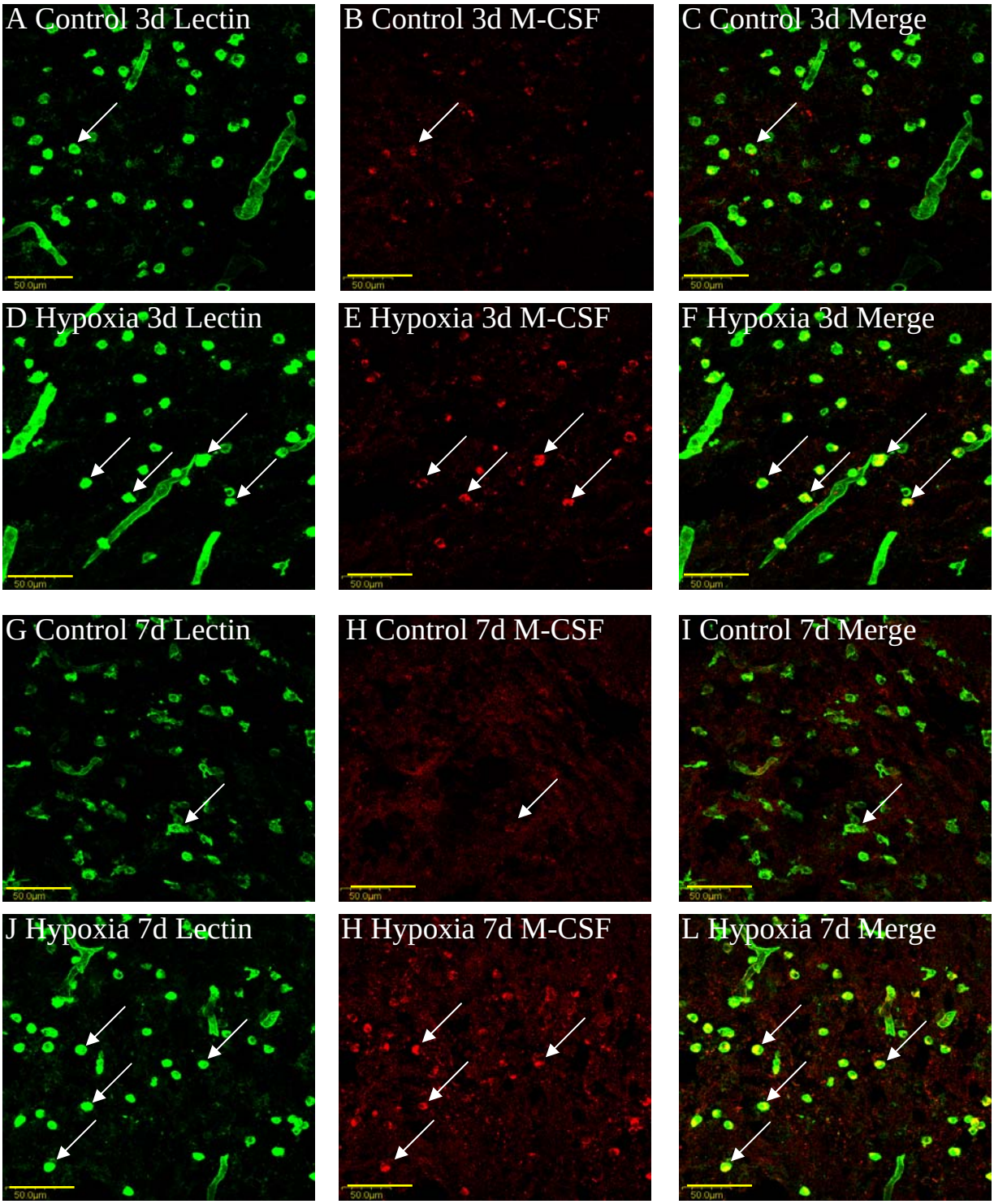
A Control 3d Lectin
B Control 3d M-CSF
C Control 3d Merge
D Hypoxia 3d Lectin
E Hypoxia 3d M-CSF
F Hypoxia 3d Merge
G Control 7d Lectin
H Control 7d M-CSF
I Control 7d Merge
J Hypoxia 7d Lectin
H Hypoxia 7d M-CSF
L Hypoxia 7d Merge

Fig.11

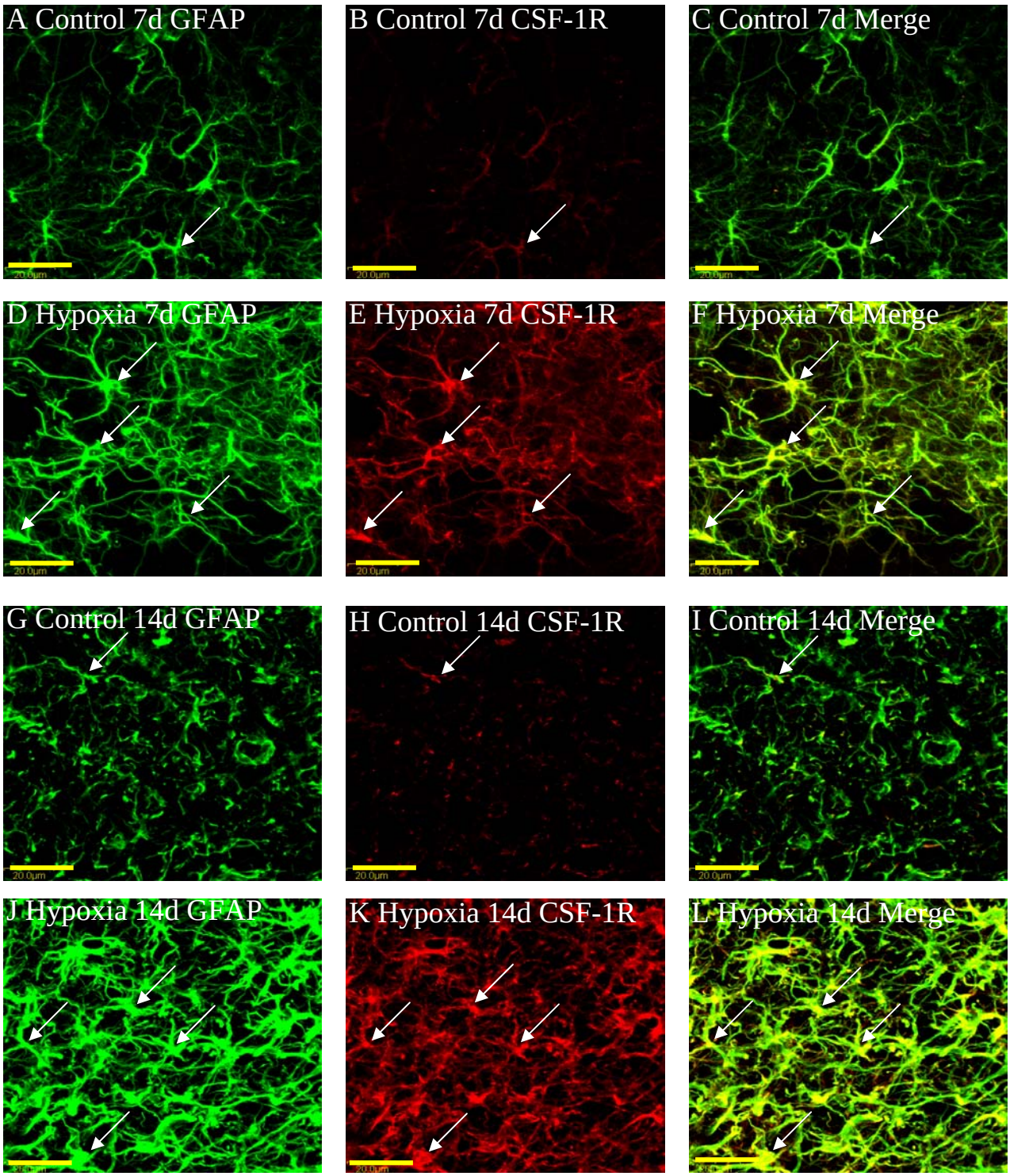
A Control 7d GFAP
B Control 7d CSF-1R
C Control 7d Merge
D Hypoxia 7d GFAP
E Hypoxia 7d CSF-1R
F Hypoxia 7d Merge
G Control 14d GFAP
H Control 14d CSF-1R
I Control 14d Merge
J Hypoxia 14d GFAP
K Hypoxia 14d CSF-1R
L Hypoxia 14d Merge

Fig.12

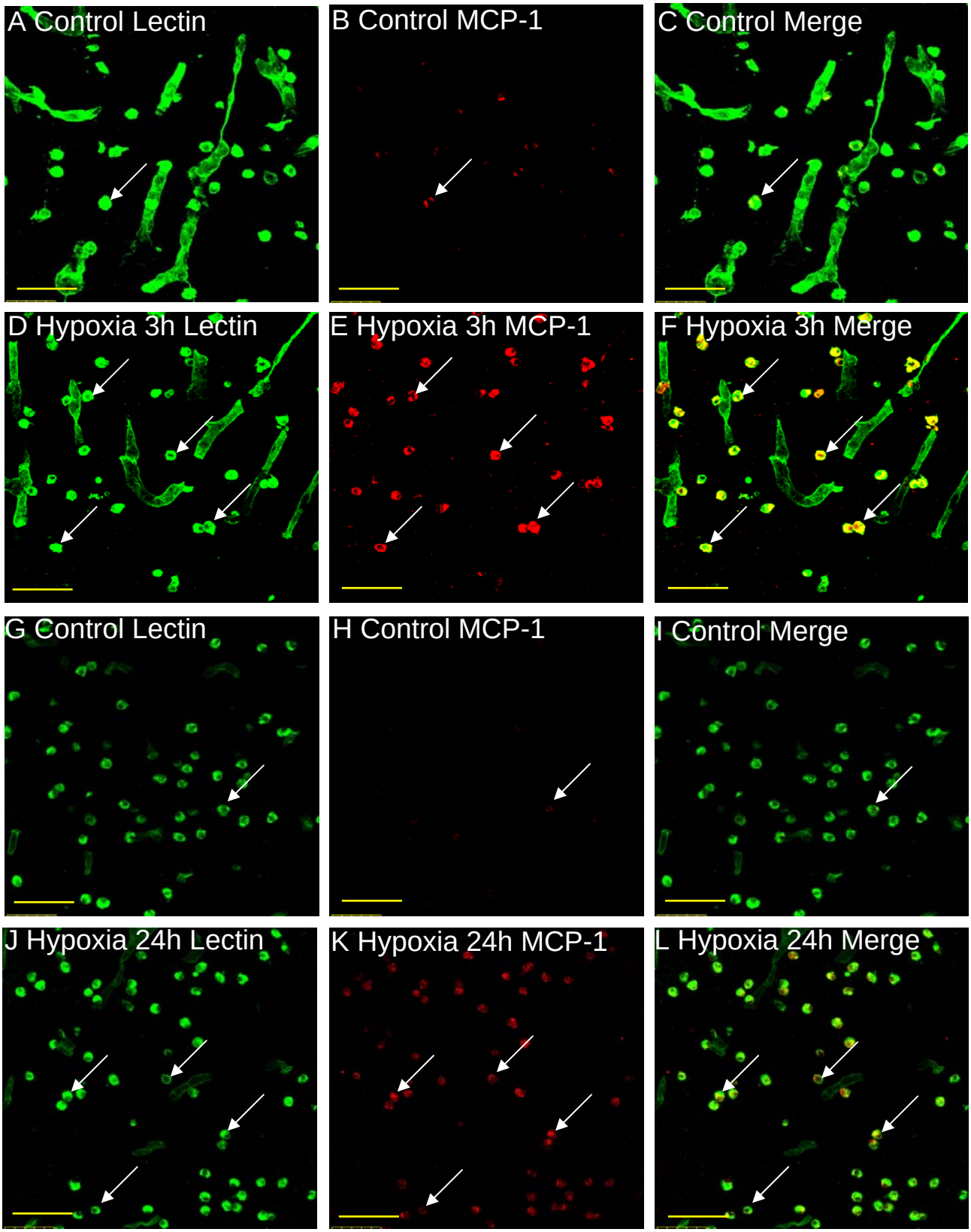
A Control Lectin
B Control MCP-1
C Control Merge
D Hypoxia 3h Lectin
E Hypoxia 3h MCP-1
F Hypoxia 3h Merge
G Control Lectin
H Control MCP-1
I Control Merge
J Hypoxia 24h Lectin
K Hypoxia 24h MCP-1
L Hypoxia 24h Merge

Fig.13

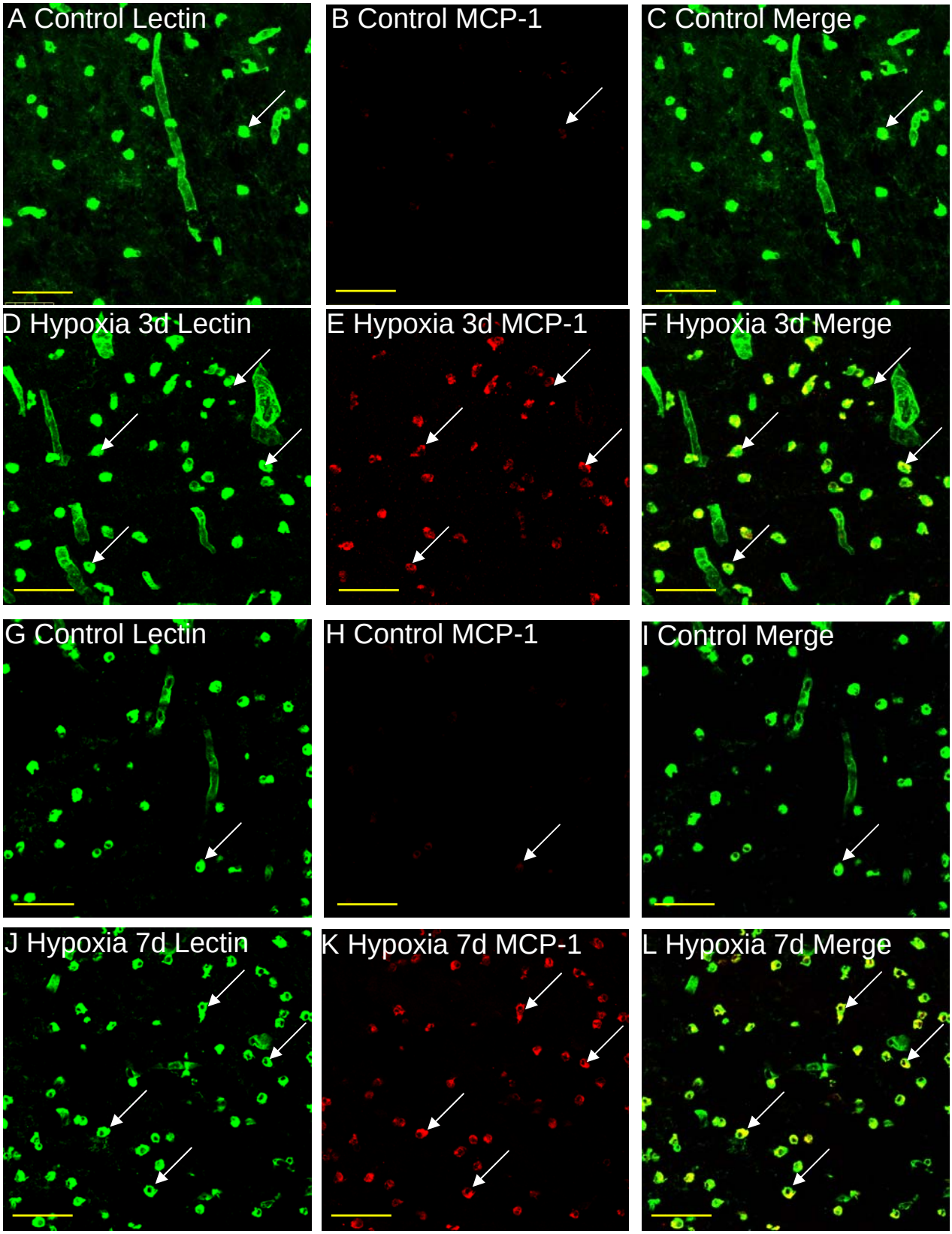
A Control Lectin
B Control MCP-1
C Control Merge
D Hypoxia 3d Lectin
E Hypoxia 3d MCP-1
F Hypoxia 3d Merge
G Control Lectin
H Control MCP-1
I Control Merge
J Hypoxia 7d Lectin
K Hypoxia 7d MCP-1
L Hypoxia 7d Merge

Fig.14

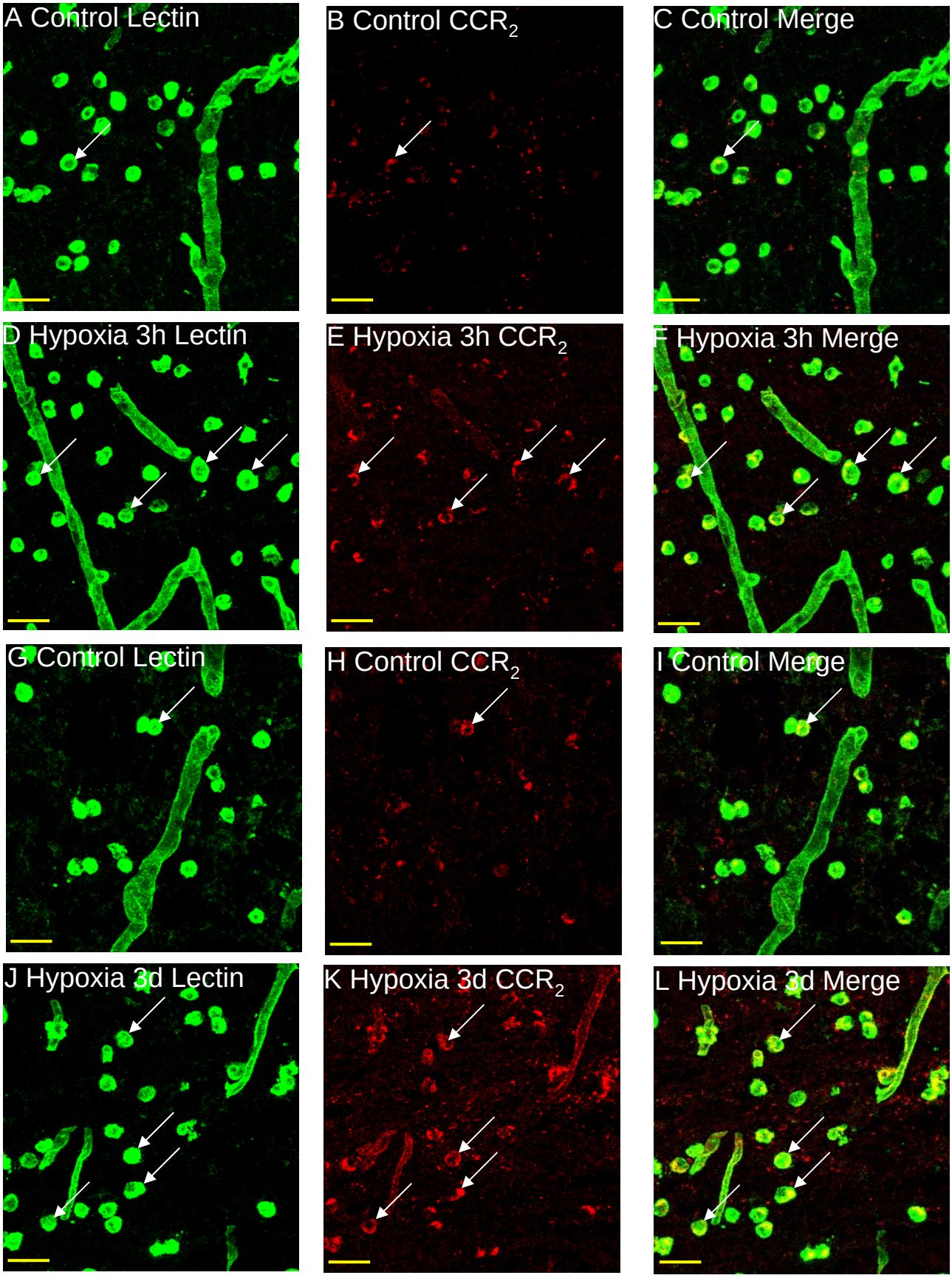
A Control Lectin
B Control CCR2
C Control Merge
D Hypoxia 3h Lectin
E Hypoxia 3h CCR2
F Hypoxia 3h Merge
G Control Lectin
H Control CCR2
I Control Merge
J Hypoxia 3d Lectin
K Hypoxia 3d CCR2
L Hypoxia 3d Merge

Fig.15

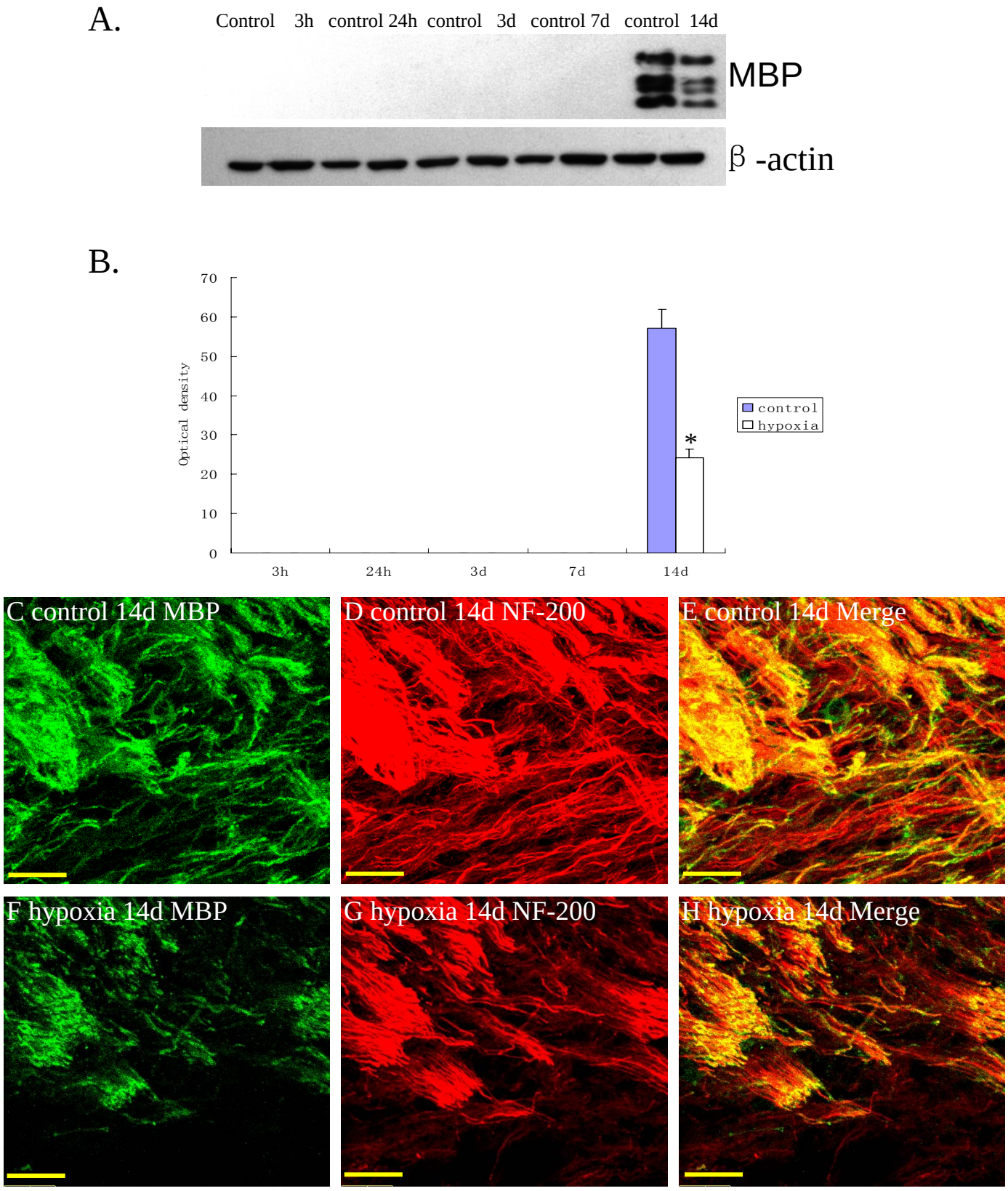
A.
Control
3h
control 24h
control
3d
control 7d
control
14d
MBP
β -actin
B.
Optical density
70
60
50
40
30
20
10
0
3h
24h
3d
7d
14d
control
hypoxia
*
C control 14d MBP
D control 14d NF-200
E control 14d Merge
F hypoxia 14d MBP
G hypoxia 14d NF-200
H hypoxia 14d Merge

Fig.16

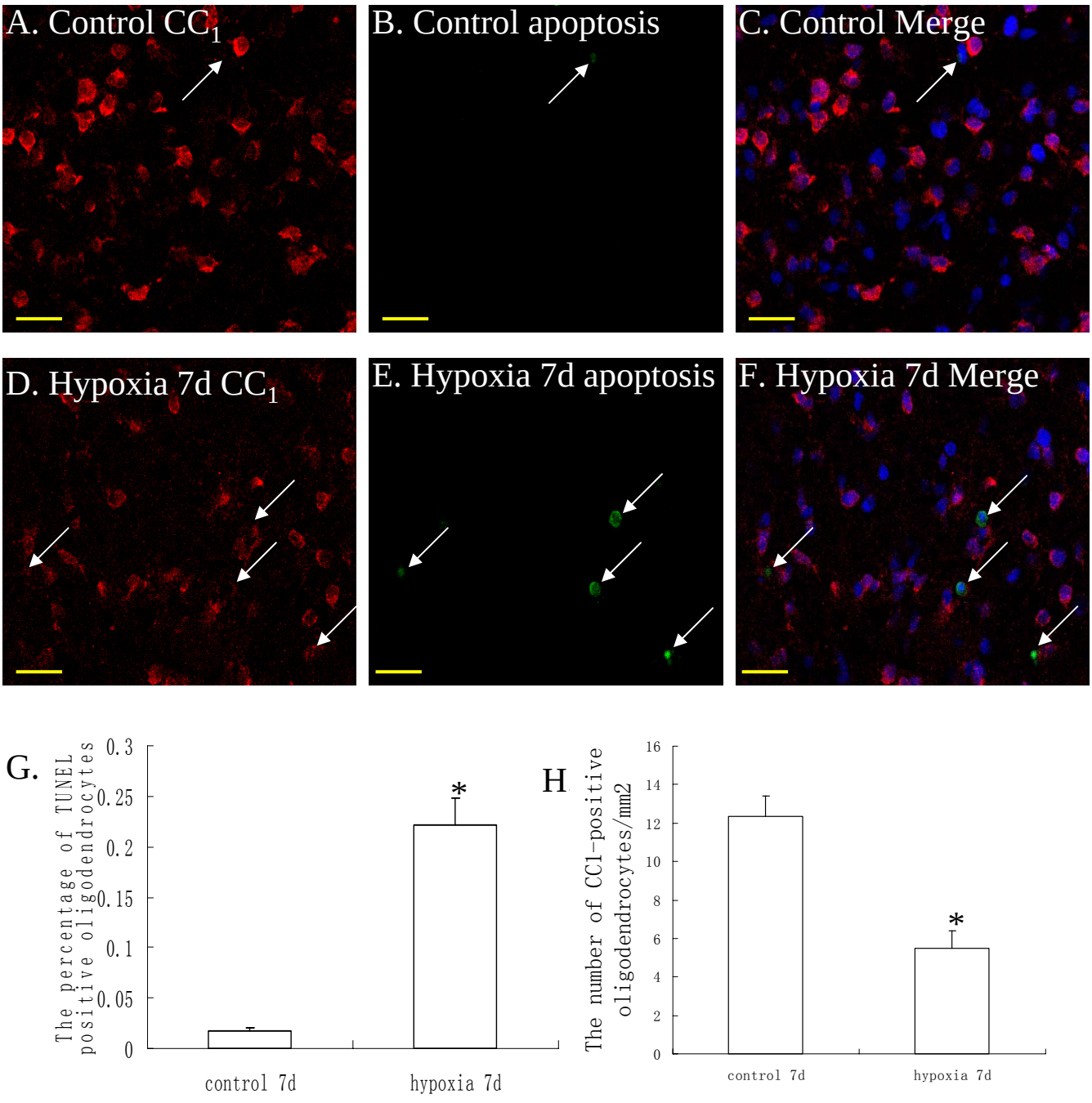
A. Control CC1
B. Control apoptosis
C. Control Merge
D. Hypoxia 7d CC1
E. Hypoxia 7d apoptosis
F. Hypoxia 7d Merge
G.
The percentage of TUNEL positive oligodendrocytes
0.3
0.25
0.2
0.15
0.1
0.05
0
*
control 7d
hypoxia 7d
H
The number of CC1-positive oligodendrocytes/mm2
16
14
12
10
8
6
4
2
0
*
control 7d
hypoxia 7d

Fig.17

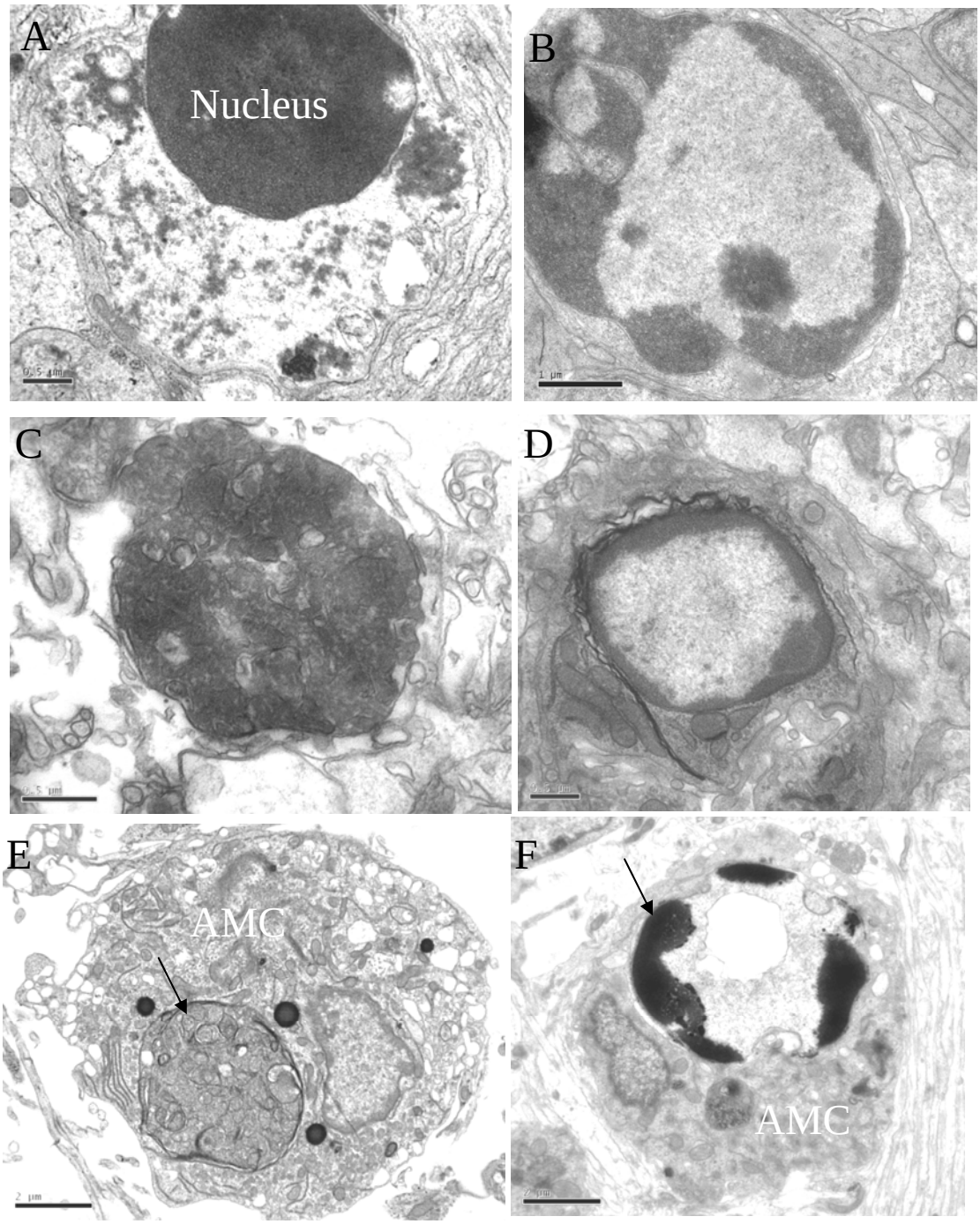

Fig.18

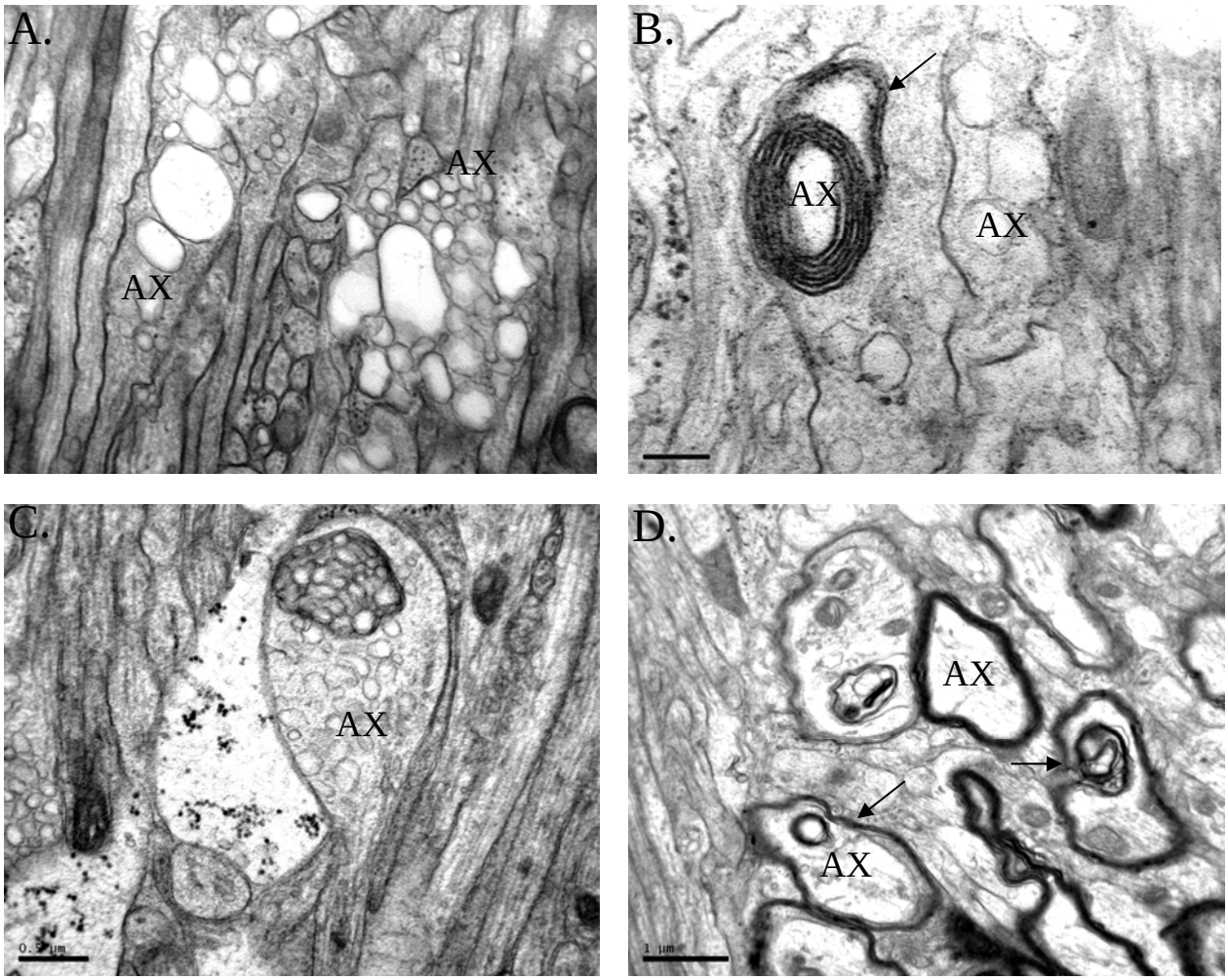

Fig. 19

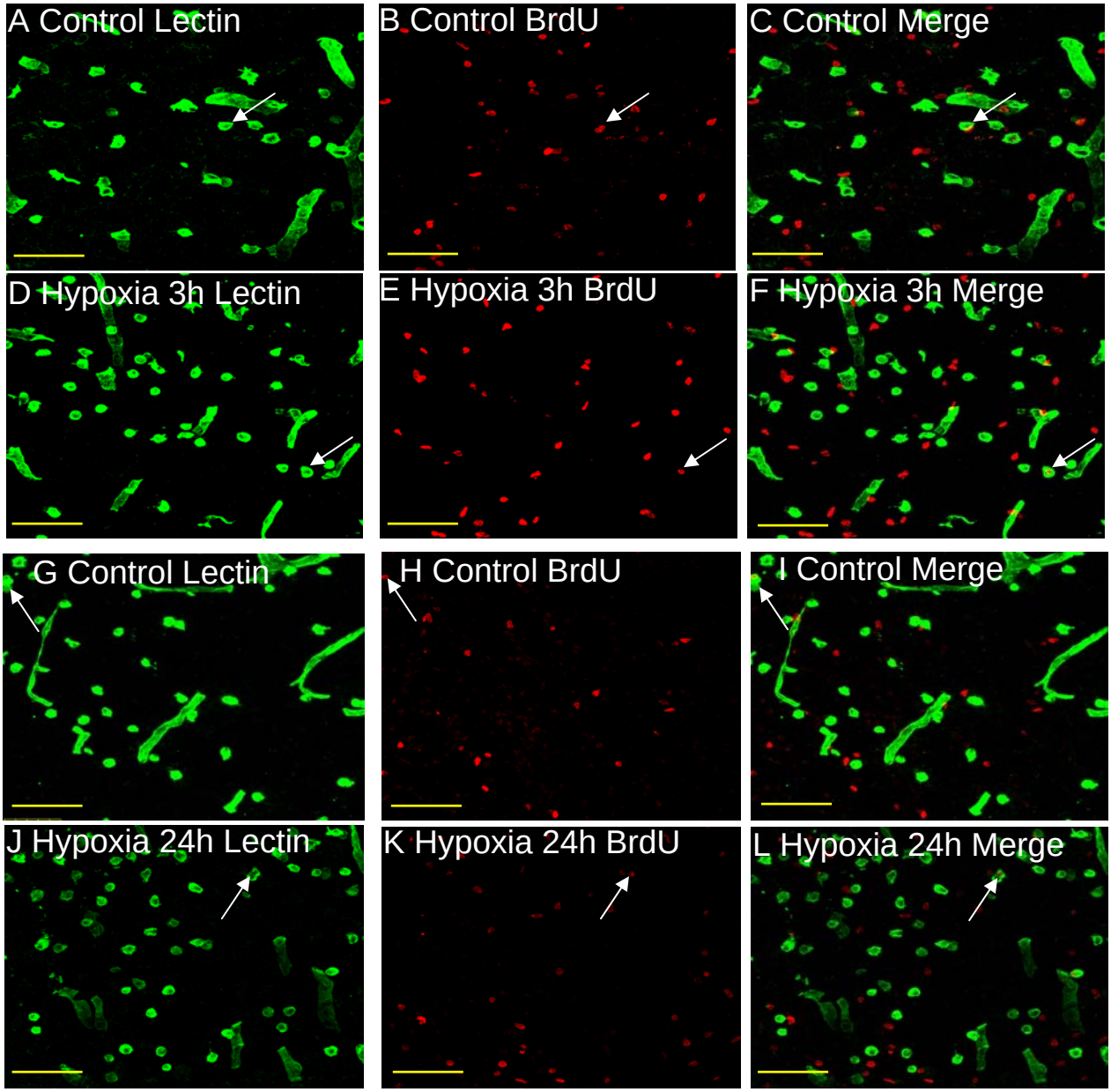
A Control Lectin
B Control BrdU
C Control Merge
D Hypoxia 3h Lectin
E Hypoxia 3h BrdU
F Hypoxia 3h Merge
G Control Lectin
H Control BrdU
I Control Merge
J Hypoxia 24h Lectin
K Hypoxia 24h BrdU
L Hypoxia 24h Merge

M.

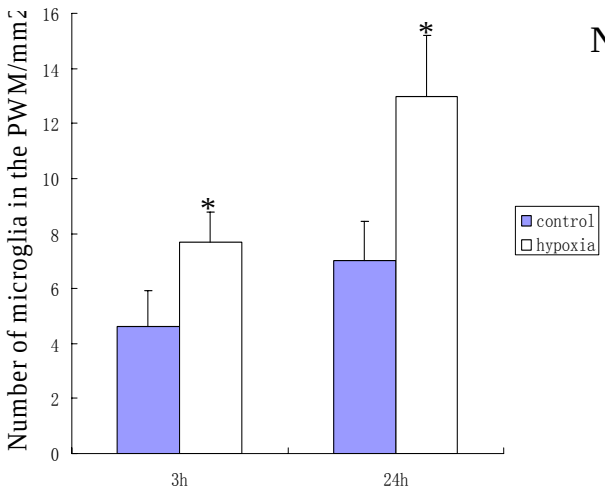
Number of microglia in the PWM/mm2
16
14
12
10
8
6
4
2
0
*
*
3h
24h
control
hypoxia

N.

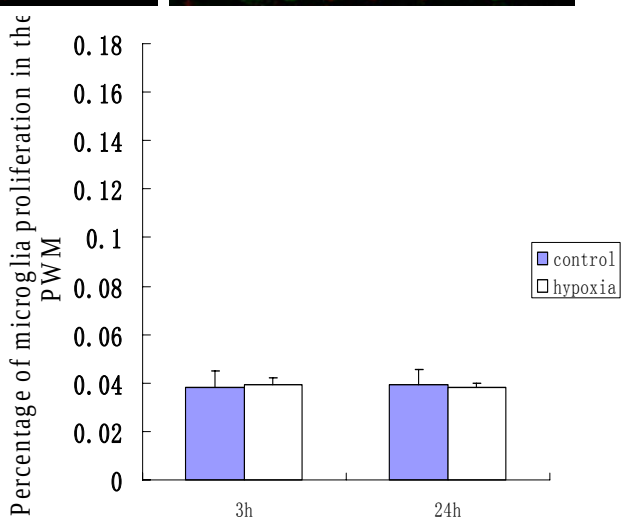
Percentage of microglia proliferation in the PWM
0.18
0.16
0.14
0.12
0.1
0.08
0.06
0.04
0.02
0
3h
24h
control
hypoxia

Fig.20

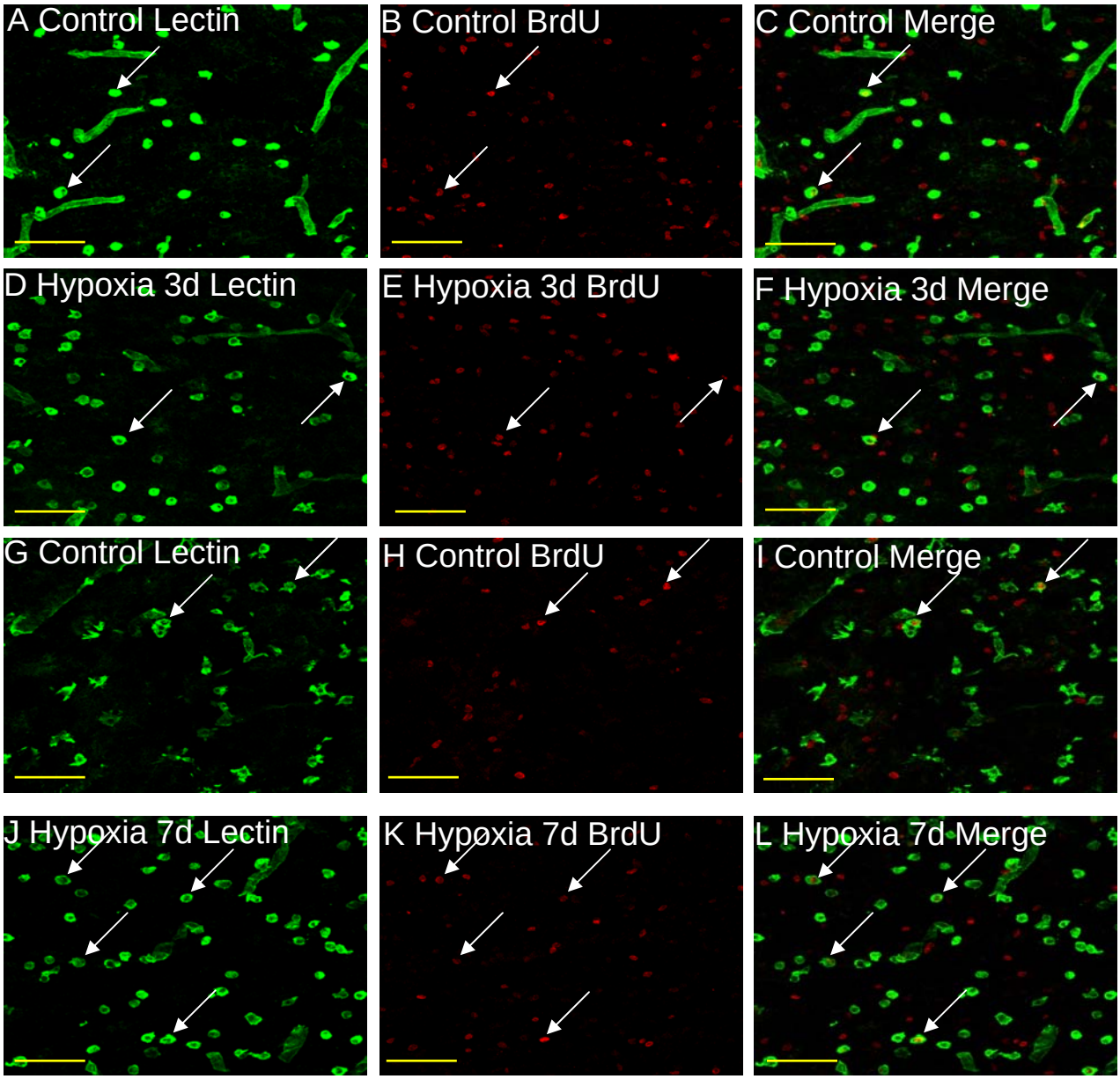
A Control Lectin
B Control BrdU
C Control Merge
D Hypoxia 3d Lectin
E Hypoxia 3d BrdU
F Hypoxia 3d Merge
G Control Lectin
H Control BrdU
I Control Merge
J Hypoxia 7d Lectin
K Hypoxia 7d BrdU
L Hypoxia 7d Merge

M.

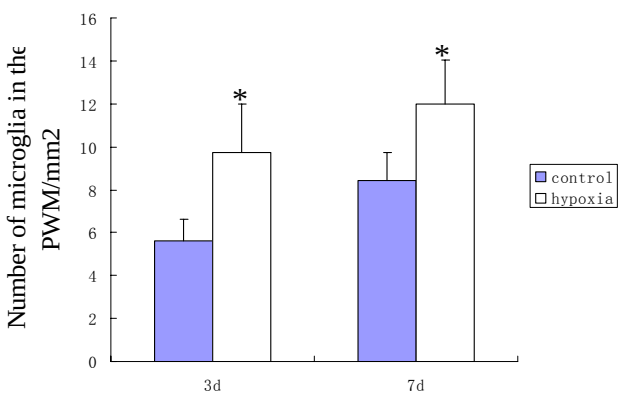
Number of microglia in the PWM/mm2
16
14
12
10
8
6
4
2
0
3d
7d
control
hypoxia

N.

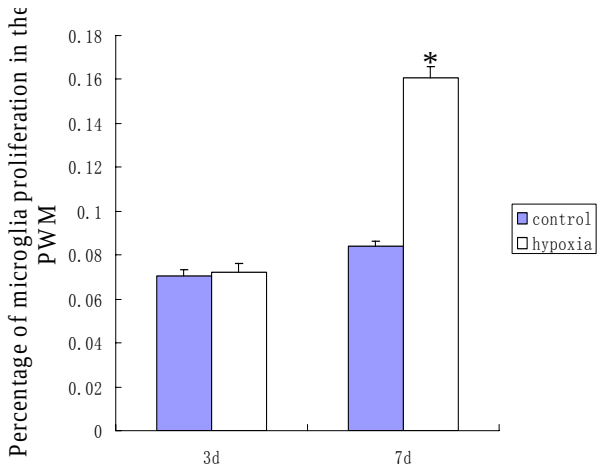
Percentage of microglia proliferation in the PWM
0.18
0.16
0.14
0.12
0.1
0.08
0.06
0.04
0.02
0
3d
7d
control
hypoxia

Fig.21

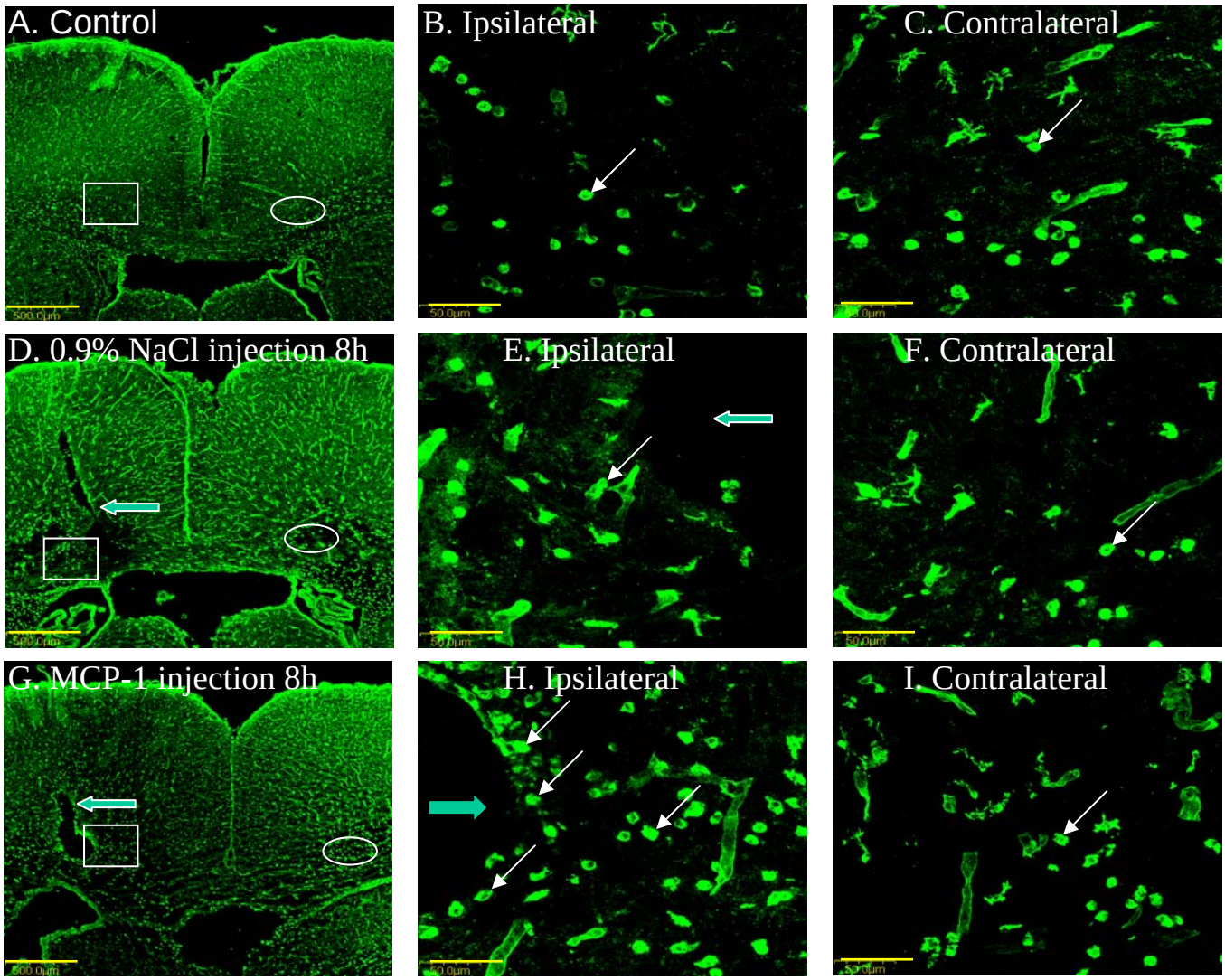
A. Control
B. Ipsilateral
C. Contralateral
D. 0.9% NaCl injection 8h
E. Ipsilateral
F. Contralateral
G. MCP-1 injection 8h
H. Ipsilateral
I. Contralateral

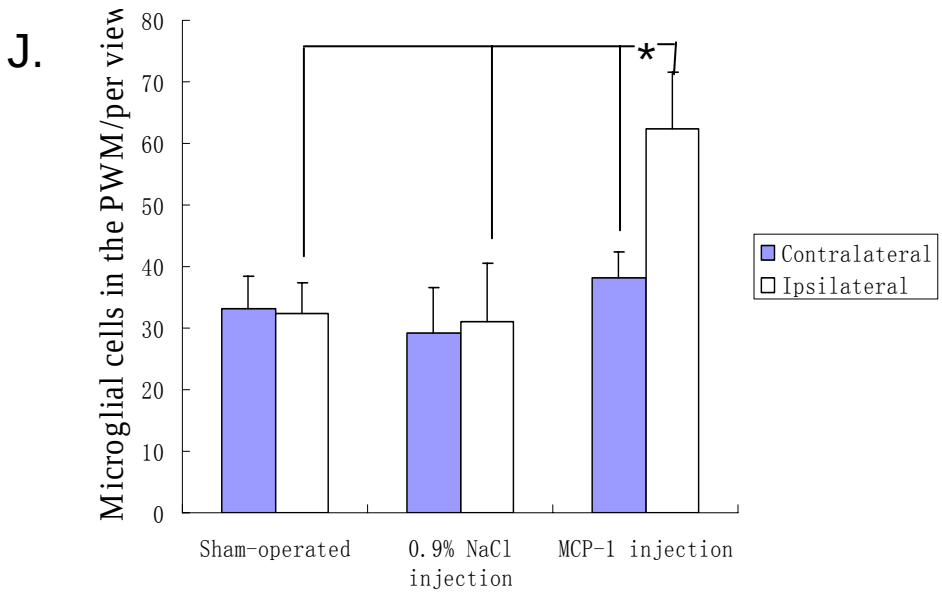
J.
Microglial cells in the PWM/per view
80
70
60
50
40
30
20
10
0
*
Sham-operated
0.9% NaCl injection
MCP-1 injection
Contralateral
Ipsilateral

Fig.22

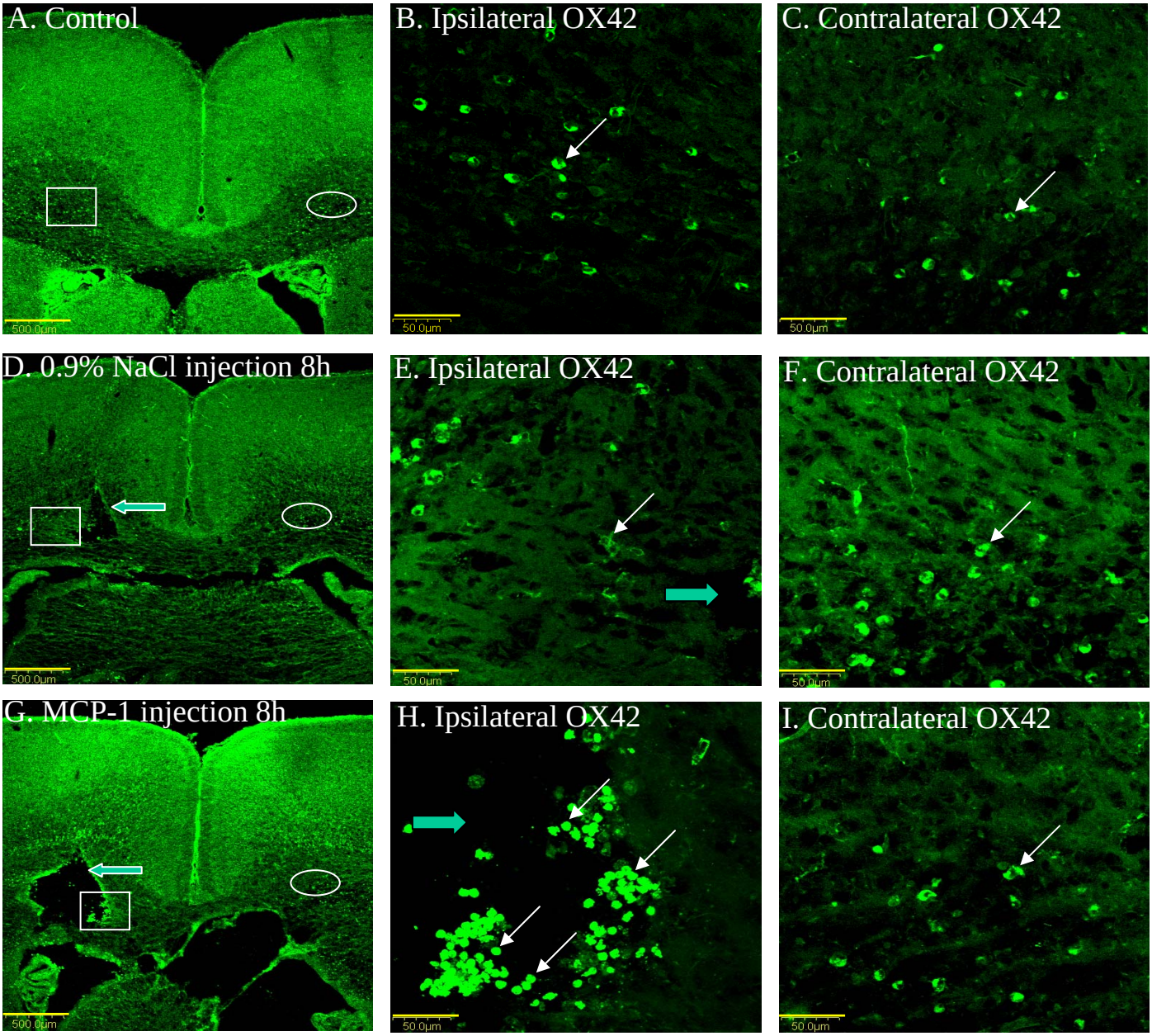
A. Control
B. Ipsilateral OX42
C. Contralateral OX42
D. 0.9% NaCl injection 8h
E. Ipsilateral OX42
F. Contralateral OX42
G. MCP-1 injection 8h
H. Ipsilateral OX42
I. Contralateral OX42
500.0μm
50.0μm

J.

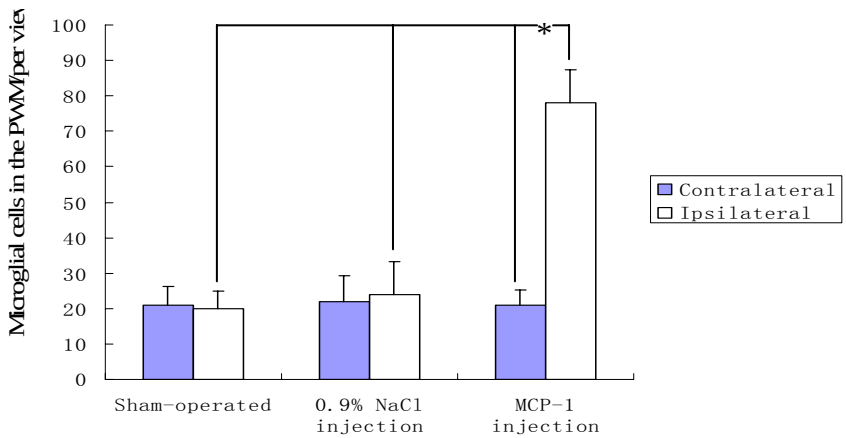
Microglial cells in the PWM per view
100
90
80
70
60
50
40
30
20
10
0
*
Contralateral
Ipsilateral
Sham-operated
0.9% NaCl injection
MCP-1 injection

Fig.23

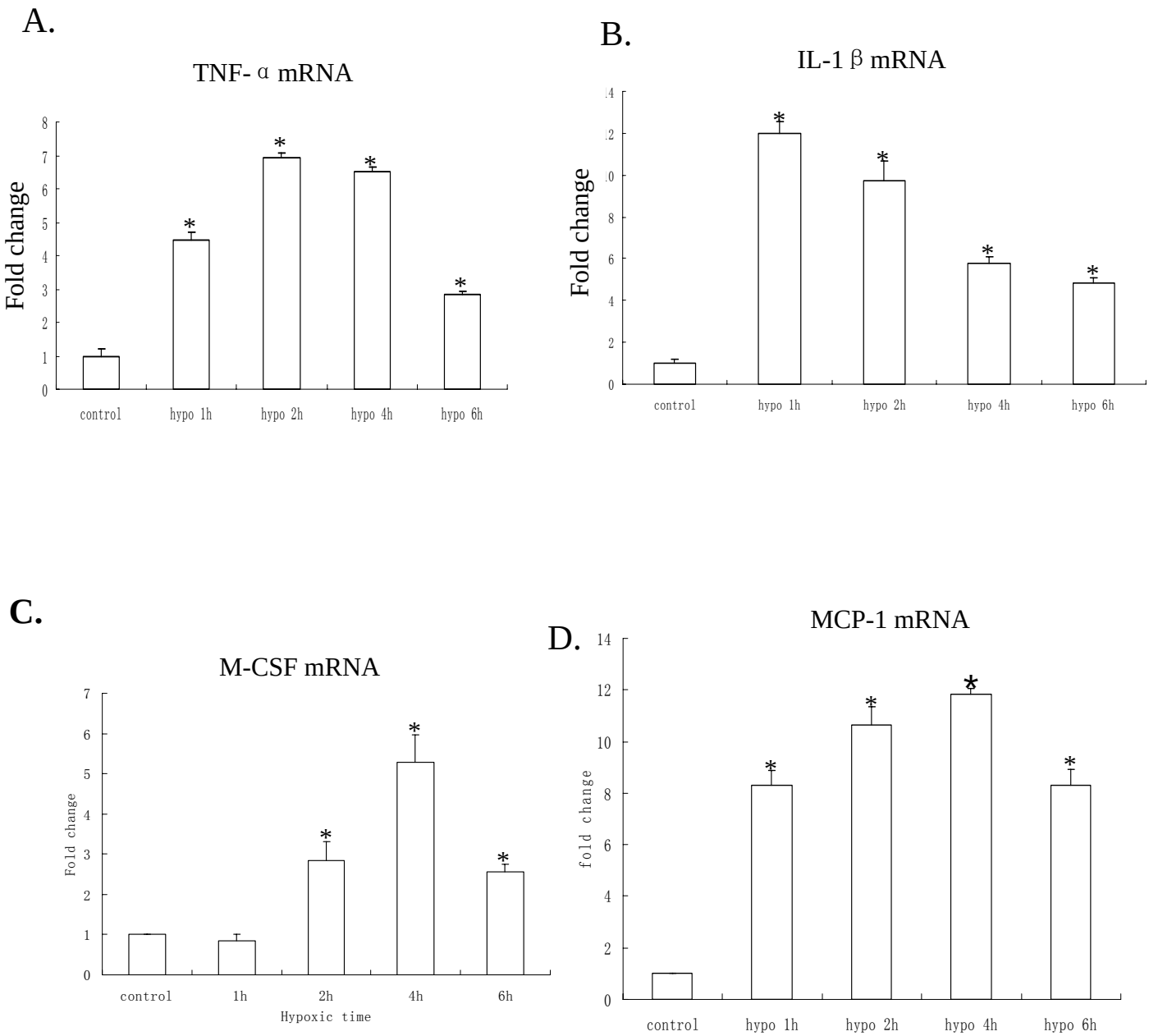
A.
TNF-α mRNA
Fold change
control
hypo 1h
hypo 2h
hypo 4h
hypo 6h
B.
IL-1β mRNA
Fold change
control
hypo 1h
hypo 2h
hypo 4h
hypo 6h
C.
M-CSF mRNA
Fold change
control
1h
2h
4h
6h
Hypoxic time
D.
MCP-1 mRNA
fold change
control
hypo 1h
hypo 2h
hypo 4h
hypo 6h

Fig.24

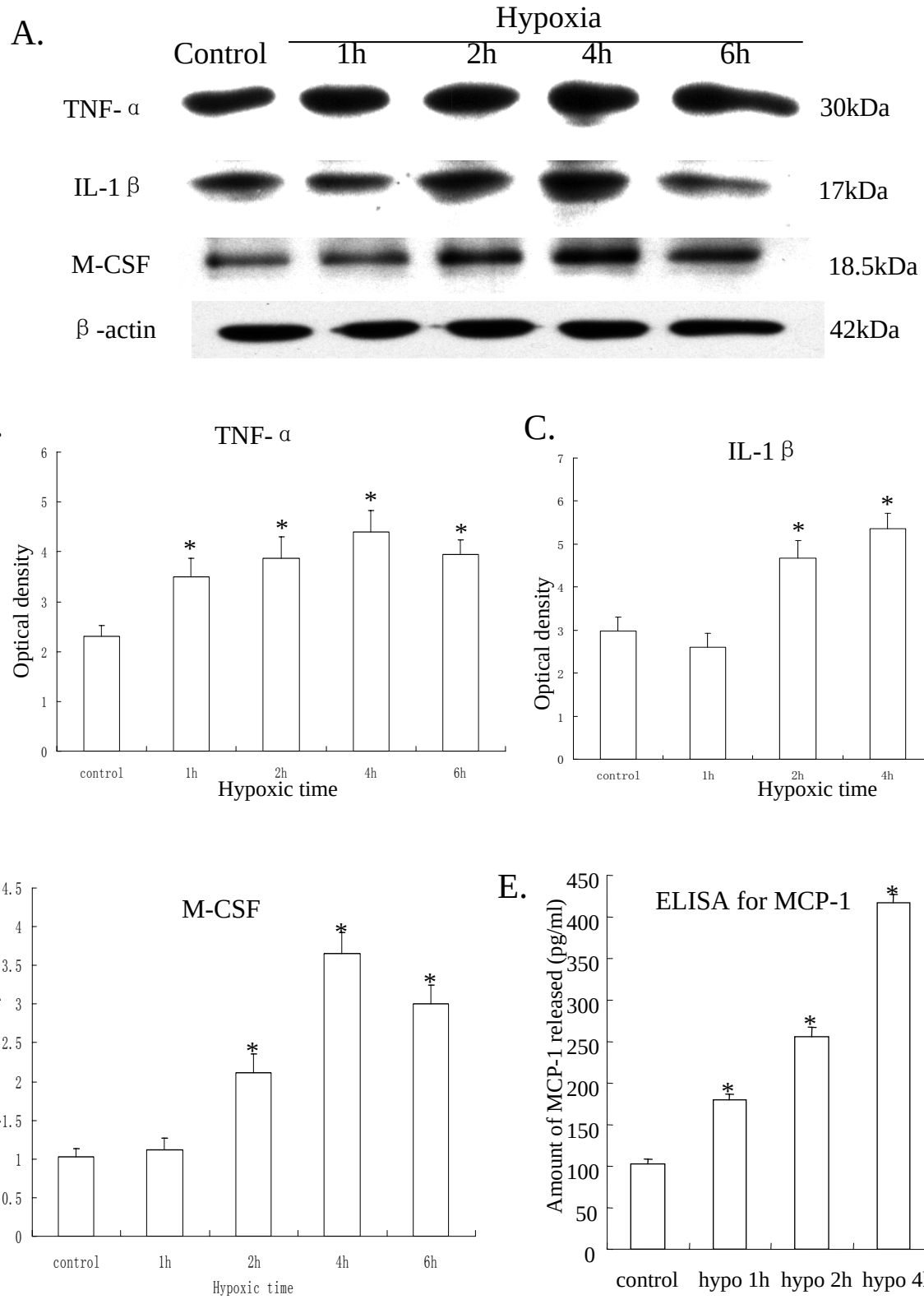
A.
Hypoxia
Control
1h
2h
4h
6h
TNF- α
30kDa
IL-1 β
17kDa
M-CSF
18.5kDa
β -actin
42kDa
B.
TNF- α
Optical density
control
1h
2h
4h
6h
Hypoxic time
C.
IL-1 β
Optical density
control
1h
2h
4h
6h
Hypoxic time
D.
M-CSF
Optical density
control
1h
2h
4h
6h
Hypoxic time
E.
ELISA for MCP-1
Amount of MCP-1 released (pg/ml)
control
hypo 1h
hypo 2h
hypo 4h
hypo 6h

Fig.25

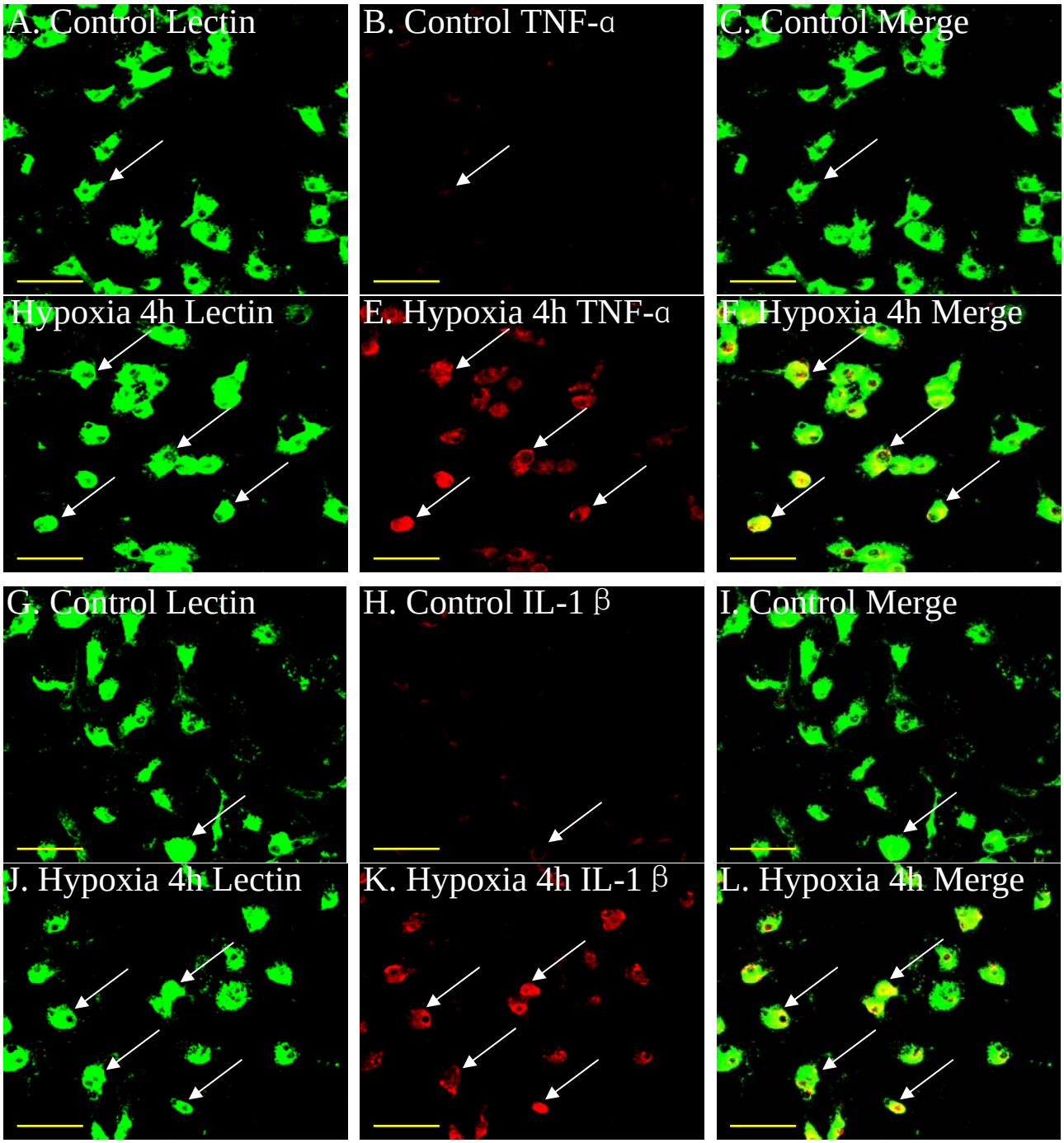
A. Control Lectin
B. Control TNF-α
C. Control Merge
Hypoxia 4h Lectin
E. Hypoxia 4h TNF-α
F. Hypoxia 4h Merge
G. Control Lectin
H. Control IL-1 β
I. Control Merge
J. Hypoxia 4h Lectin
K. Hypoxia 4h IL-1 β
L. Hypoxia 4h Merge

Fig.26

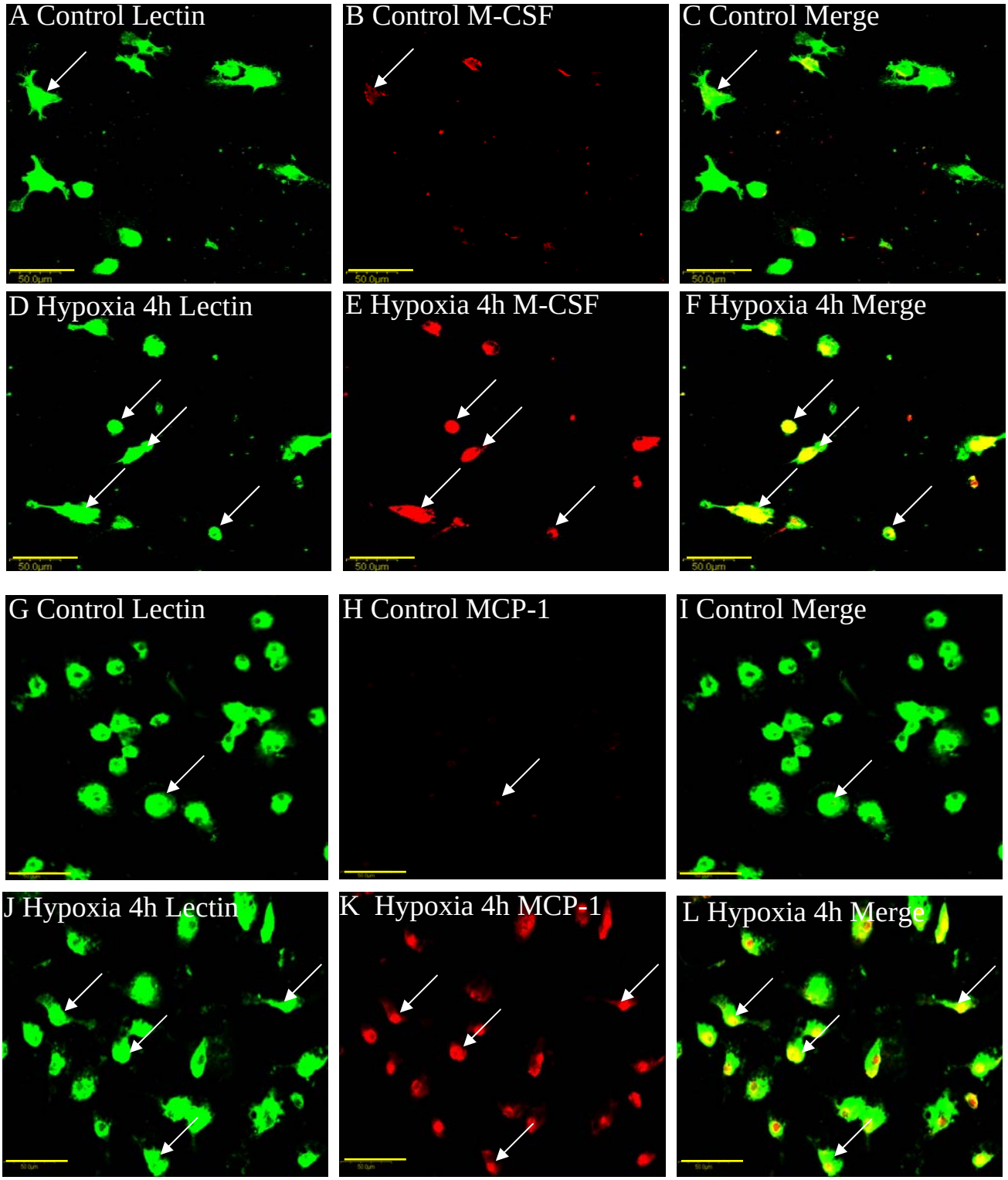
A Control Lectin
B Control M-CSF
C Control Merge
D Hypoxia 4h Lectin
E Hypoxia 4h M-CSF
F Hypoxia 4h Merge
G Control Lectin
H Control MCP-1
I Control Merge
J Hypoxia 4h Lectin
K Hypoxia 4h MCP-1
L Hypoxia 4h Merge

Fig.27

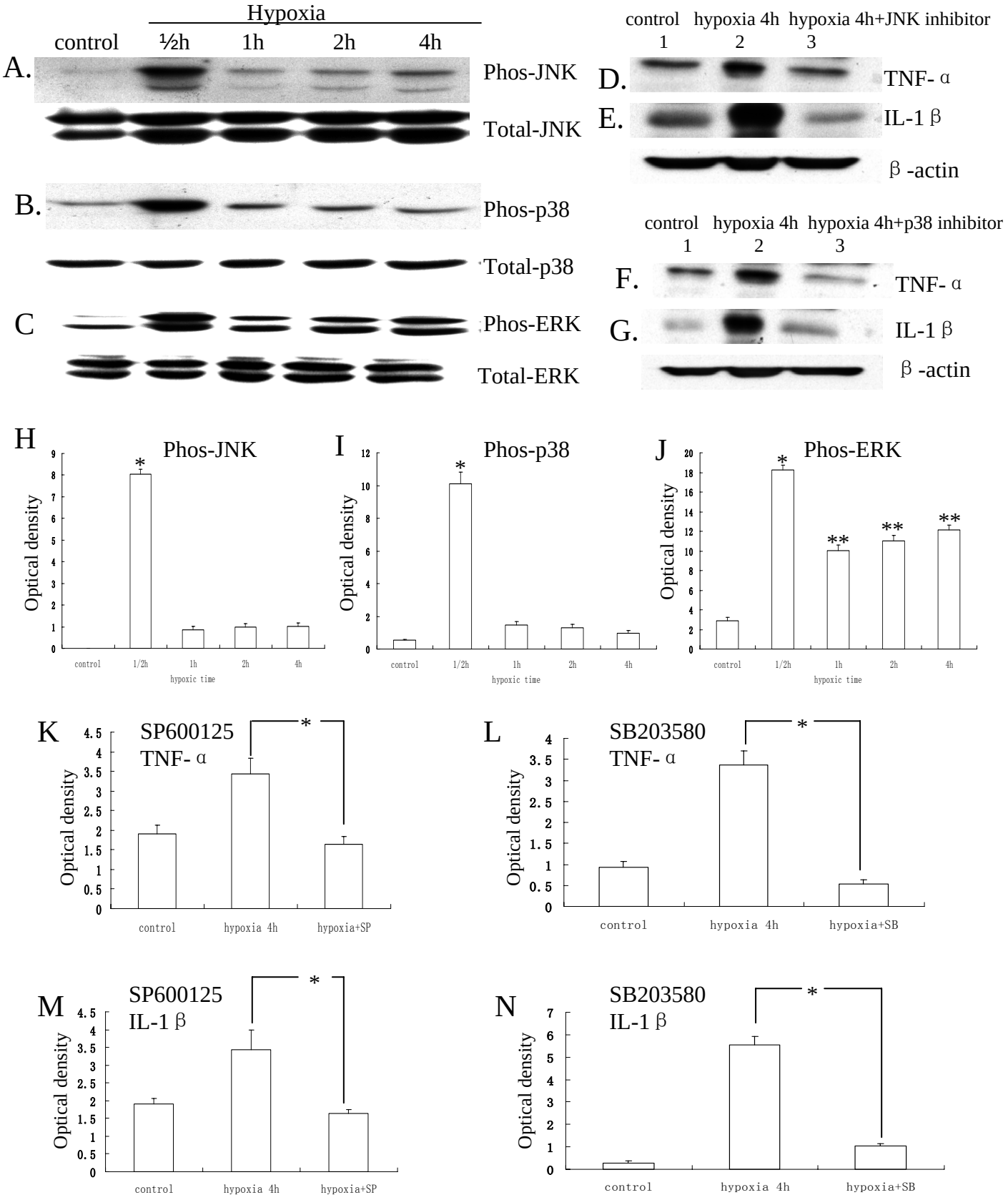
Hypoxia
control
½h
1h
2h
4h
A.
Phos-JNK
Total-JNK
B.
Phos-p38
Total-p38
C
Phos-ERK
Total-ERK
control
hypoxia 4h
hypoxia 4h+JNK inhibitor
1
2
3
D.
TNF- α
E.
IL-1 β
β -actin
control
hypoxia 4h
hypoxia 4h+p38 inhibitor
1
2
3
F.
TNF- α
G.
IL-1 β
β -actin
H
Phos-JNK
Optical density
control
1/2h
1h
2h
4h
hypoxic time
I
Phos-p38
Optical density
control
1/2h
1h
2h
4h
hypoxic time
J
Phos-ERK
Optical density
control
1/2h
1h
2h
4h
hypoxic time
K
SP600125
TNF- α
Optical density
control
hypoxia 4h
hypoxia+SP
L
SB203580
TNF- α
Optical density
control
hypoxia 4h
hypoxia+SB
M
SP600125
IL-1 β
Optical density
control
hypoxia 4h
hypoxia+SP
N
SB203580
IL-1 β
Optical density
control
hypoxia 4h
hypoxia+SB

Fig.28

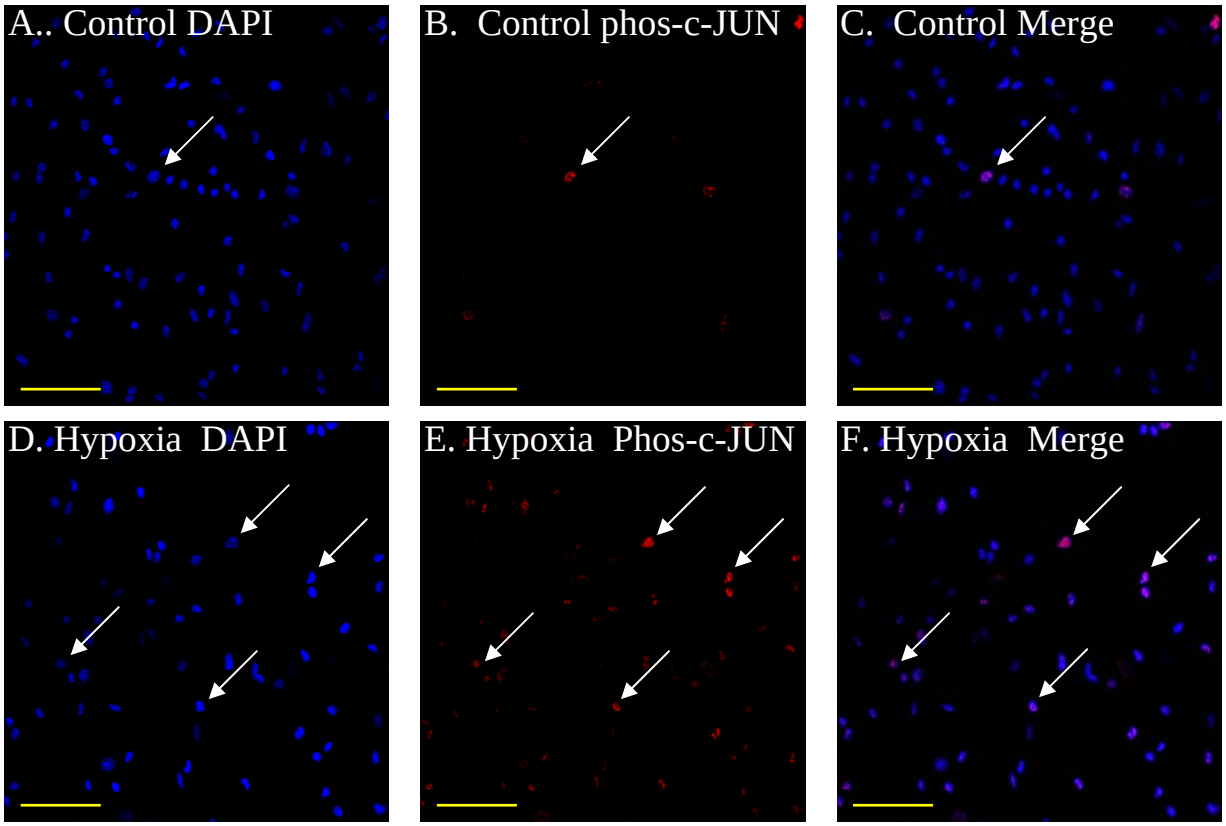
A.. Control DAPI
B. Control phos-c-JUN
C. Control Merge
D. Hypoxia DAPI
E. Hypoxia Phos-c-JUN
F. Hypoxia Merge

G.

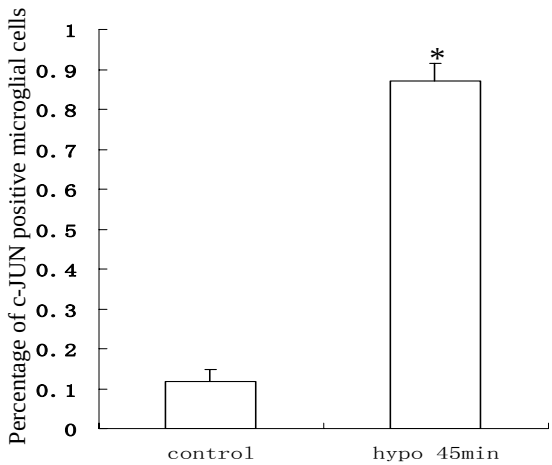
Percentage of c-JUN positive microglial cells
1
0.9
0.8
0.7
0.6
0.5
0.4
0.3
0.2
0.1
0
*
control
hypo 45min

Fig.29

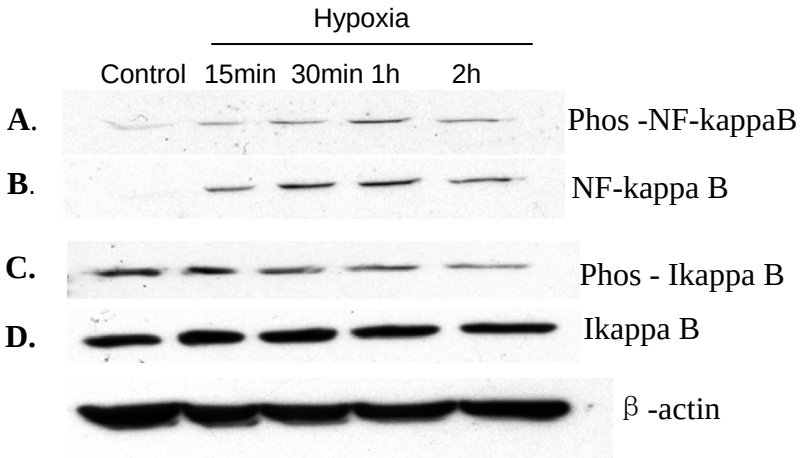
Hypoxia
Control 15min 30min 1h 2h
A.
Phos -NF-kappaB
B.
NF-kappa B
C.
Phos - Ikappa B
D.
Ikappa B
β -actin

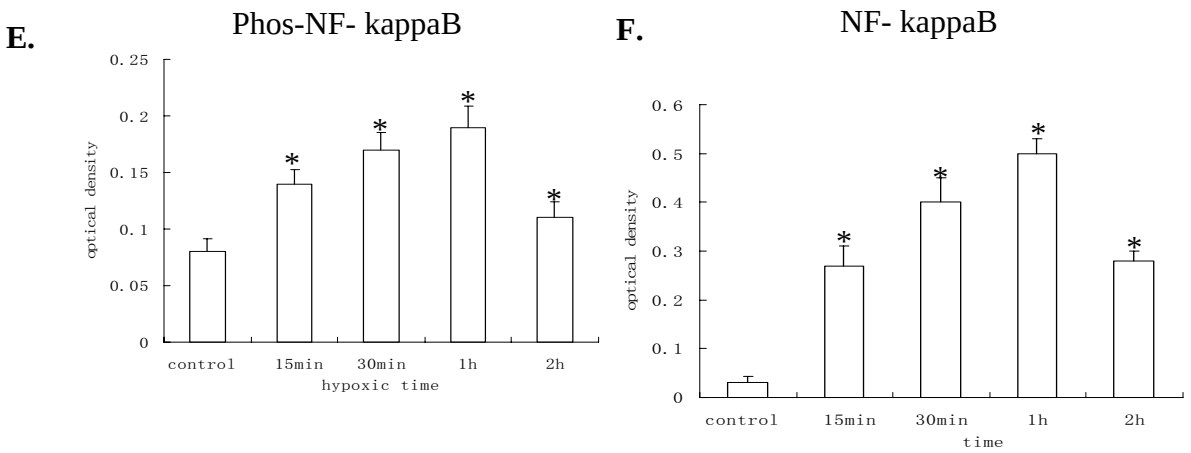
E.
Phos-NF- kappaB
optical density
control
15min
30min
1h
2h
hypoxic time
F.
NF- kappaB
optical density
control
15min
30min
1h
2h
time

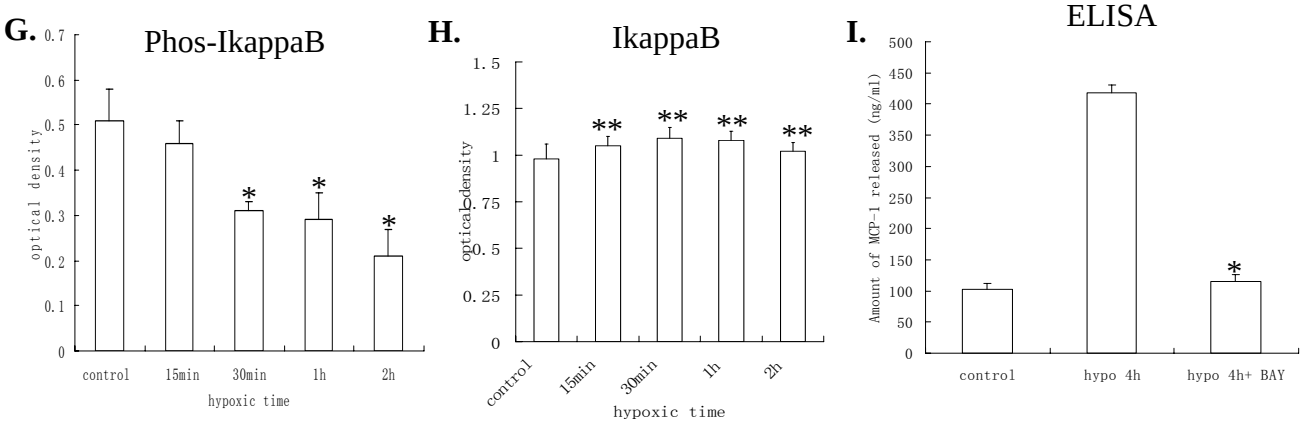
G.
Phos-IkappaB
optical density
control
15min
30min
1h
2h
hypoxic time
H.
IkappaB
optical density
control
15min
30min
1h
2h
hypoxic time
I.
ELISA
Amount of MCP-1 released (ng/ml)
control
hypo 4h
hypo 4h+ BAY

Fig.30

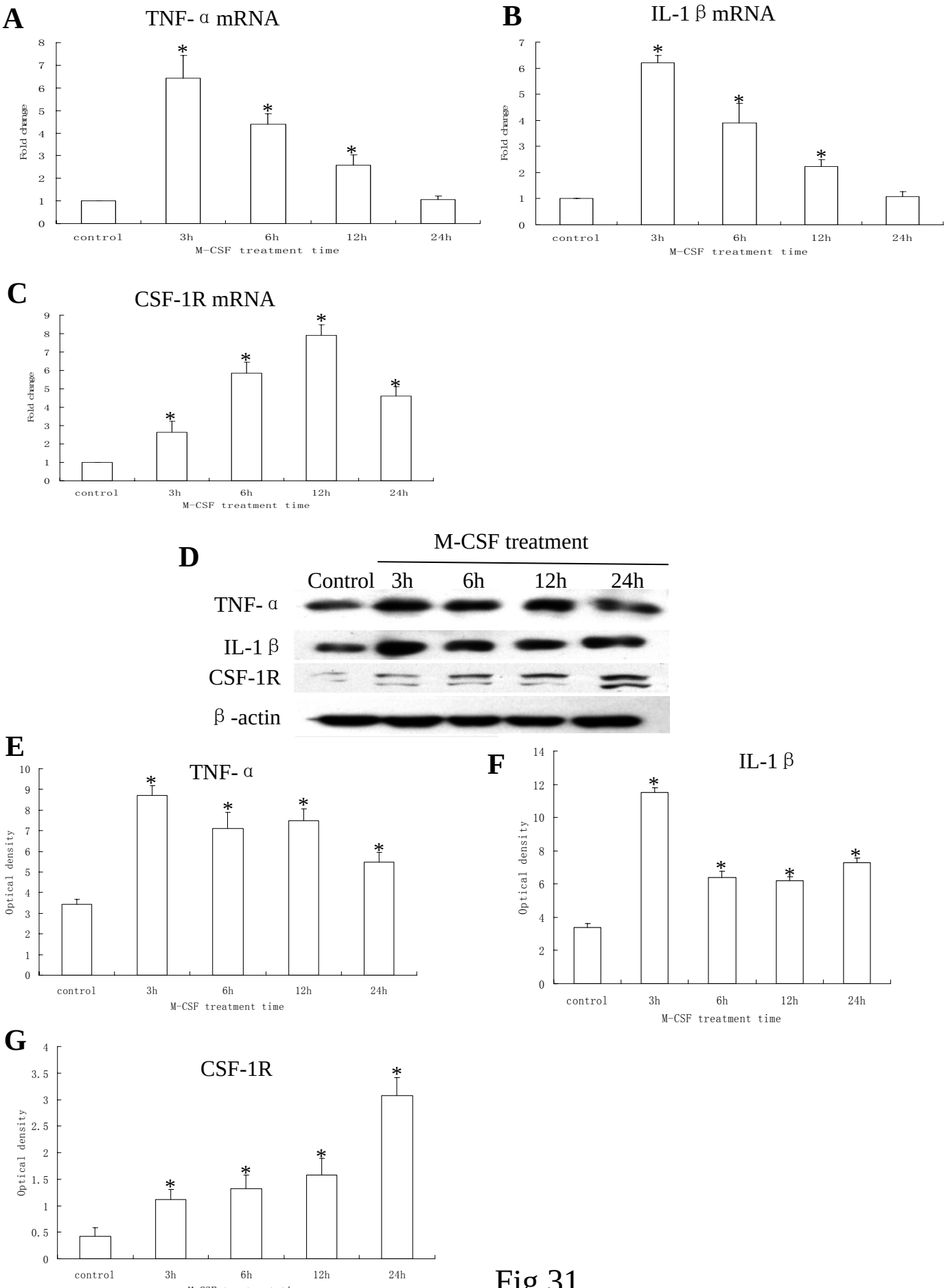
A
TNF- α mRNA
Fold change
control
3h
6h
12h
24h
M-CSF treatment time
B
IL-1 β mRNA
Fold change
control
3h
6h
12h
24h
M-CSF treatment time
C
CSF-1R mRNA
Fold change
control
3h
6h
12h
24h
M-CSF treatment time
D
M-CSF treatment
Control
3h
6h
12h
24h
TNF- α
IL-1 β
CSF-1R
β -actin
E
TNF- α
Optical density
control
3h
6h
12h
24h
M-CSF treatment time
F
IL-1 β
Optical density
control
3h
6h
12h
24h
M-CSF treatment time
G
CSF-1R
Optical density
control
3h
6h
12h
24h
M-CSF treatment time

Fig.31

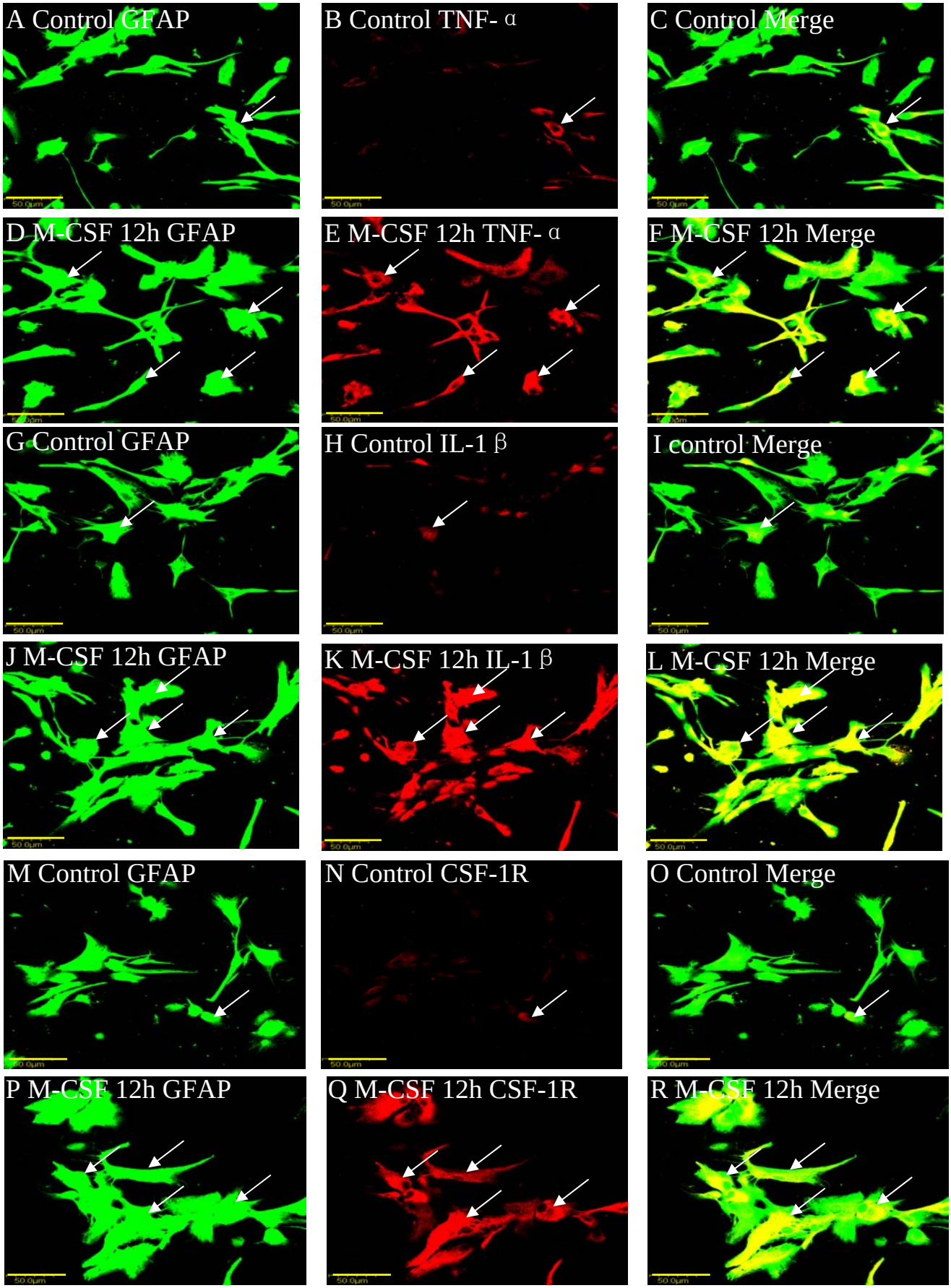
A Control GFAP
B Control TNF- α
C Control Merge
D M-CSF 12h GFAP
E M-CSF 12h TNF- α
F M-CSF 12h Merge
G Control GFAP
H Control IL-1 β
I control Merge
J M-CSF 12h GFAP
K M-CSF 12h IL-1 β
L M-CSF 12h Merge
M Control GFAP
N Control CSF-1R
O Control Merge
P M-CSF 12h GFAP
Q M-CSF 12h CSF-1R
R M-CSF 12h Merge

Fig.32

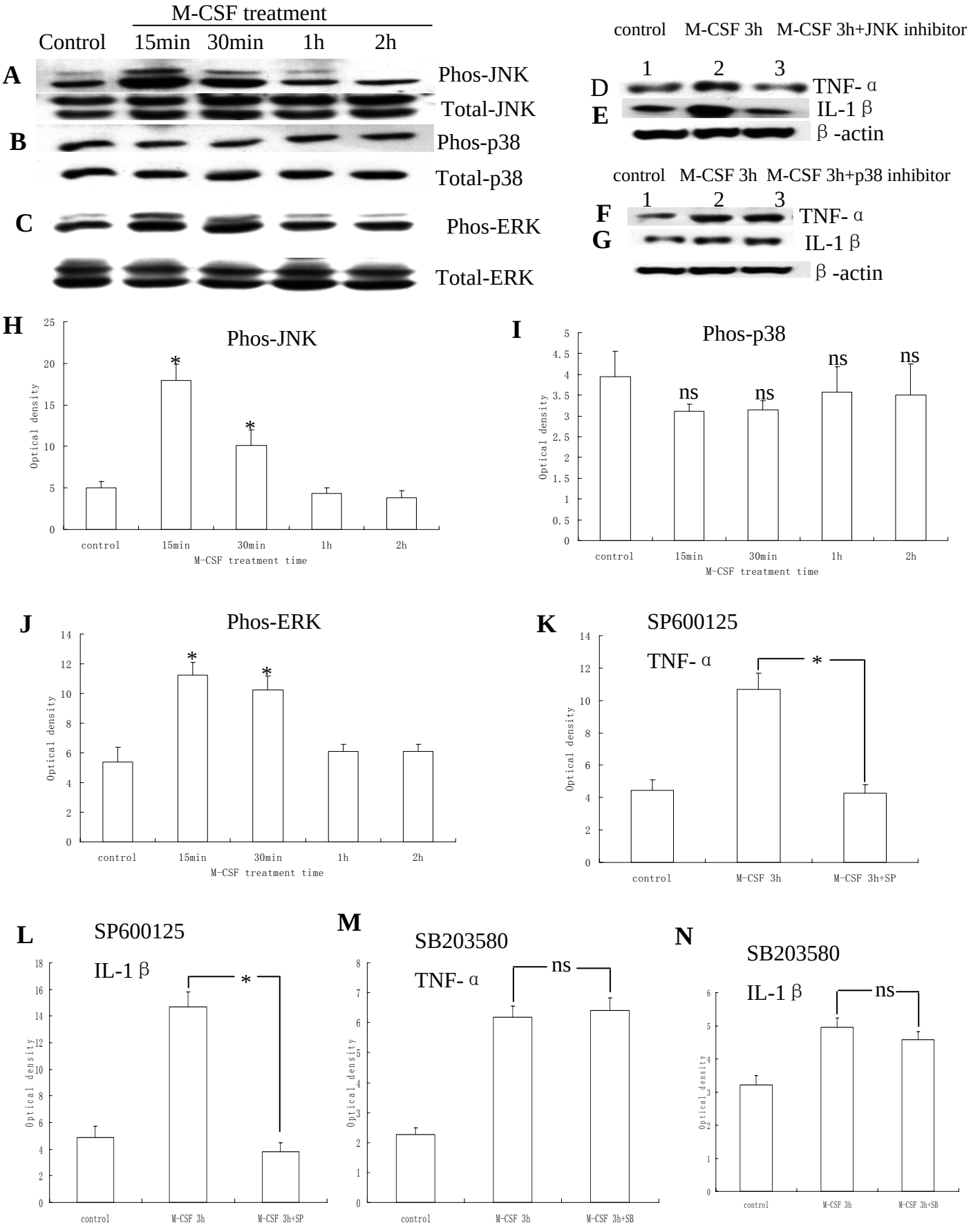
M-CSF treatment
Control
15min
30min
1h
2h
A
Phos-JNK
Total-JNK
B
Phos-p38
Total-p38
C
Phos-ERK
Total-ERK
control
M-CSF 3h
M-CSF 3h+JNK inhibitor
1
2
3
D
TNF- α
E
IL-1 β
β -actin
control
M-CSF 3h
M-CSF 3h+p38 inhibitor
1
2
3
F
TNF- α
G
IL-1 β
β -actin
H
Phos-JNK
Optical density
control
15min
30min
1h
2h
M-CSF treatment time
I
Phos-p38
ns
J
Phos-ERK
K
SP600125
TNF- α
M-CSF 3h
M-CSF 3h+SP
L
SP600125
IL-1 β
M
SB203580
TNF- α
M-CSF 3h+SB
N
SB203580
IL-1 β

Fig.33

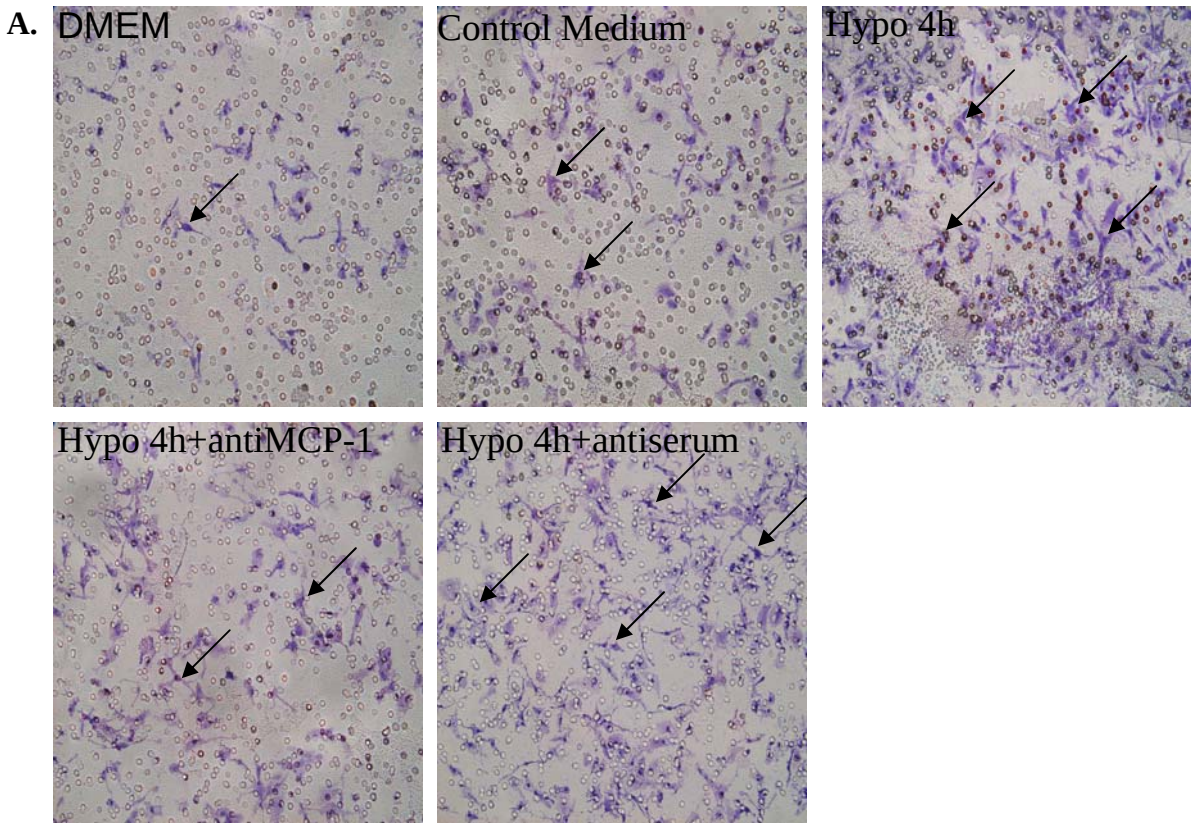
A.
DMEM
Control Medium
Hypo 4h
Hypo 4h+antiMCP-1
Hypo 4h+antiserum

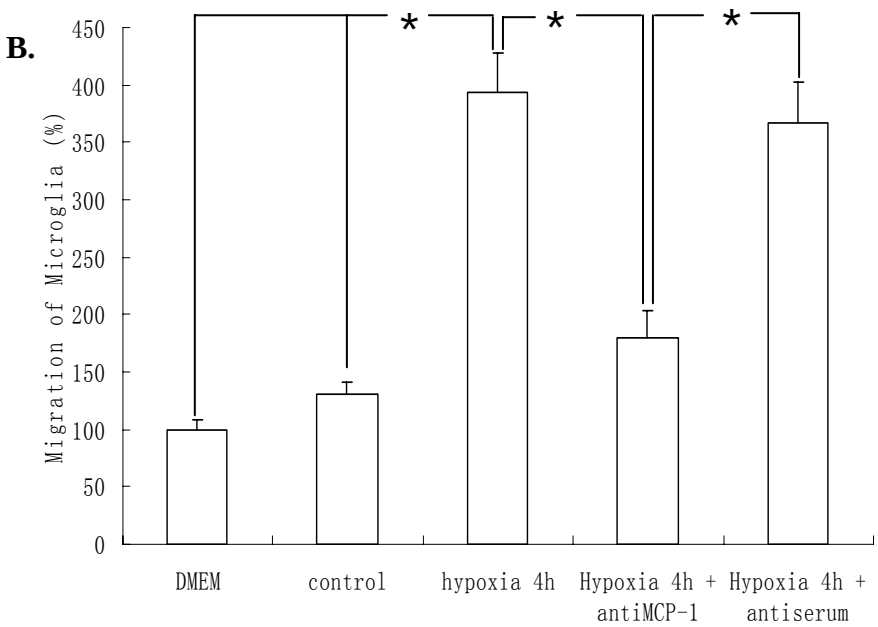
B.
Migration of Microglia (%)
450
400
350
300
250
200
150
100
50
0
*
*
*
DMEM
control
hypoxia 4h
Hypoxia 4h + antiMCP-1
Hypoxia 4h + antiserum

Fig.34